2019

Scalable Map Information Dissemination for Connected and Automated Vehicle Systems

S. M. Osman Gani
University of Central Florida

SCALABLE MAP INFORMATION DISSEMINATION FOR CONNECTED AND AUTOMATED VEHICLE SYSTEMS

by

S M OSMAN GANI
M.S. West Virginia University, 2015

A dissertation submitted in partial fulfillment of the requirements
for the degree of Doctor of Philosophy
in the Department of Electrical and Computer Engineering
in the College of Engineering and Computer Science
at the University of Central Florida
Orlando, Florida

Summer Term
2019

Major Professor: Yaser P. Fallah

ABSTRACT

Situational awareness in connected and automated vehicle (CAV) systems becomes particularly challenging in the presence of non-line of sight objects and/or objects beyond the sensing range of local onboard sensors. Despite the fact that fully autonomous driving requires the use of multiple redundant sensor systems, primarily including camera, radar, and LiDAR, the non-line of sight object detection problem still persists due to the inherent limitations of those sensing techniques. To tackle this challenge, the inter-vehicle communication system is envisioned that allows vehicles to exchange self-status updates aiming to extend their effective field of view and thus compensate for the limitations of the vehicle tracking subsystem that relies substantially on onboard sensing devices. Tracking capability in such systems can be further improved through the cooperative sharing of locally created map data instead of transmitting only self-update messages containing core basic safety message (BSM) data. In the cooperative sharing of safety messages, it is imperative to have a scalable communication protocol to ensure optimal use of the communication channel. This dissertation contributes to the analysis of the scalability issue in vehicle-to-everything (V2X) communication and then addresses the range issue of situational awareness in CAV systems by proposing a content-adaptive V2X communication architecture. To that end, we first analyze the BSM scheduling protocol standardized in the SAE J2945/1 and present large-scale scalability results obtained from a high-fidelity simulation platform to demonstrate the protocol's efficacy to

address the scalability issues in V2X communication. By employing a distributed opportunistic approach, the SAE J2945/1 congestion control algorithm keeps the overall offered channel load within an optimal operating range, while meeting the minimum tracking requirements set forth by upper-layer applications. This scheduling protocol allows event-triggered and vehicle-dynamics driven message transmits that further the situational awareness in a cooperative V2X context. Presented validation results of the congestion control algorithm include position tracking errors as the performance measure, with the age of communicated information as the evaluation measure. In addition, we examine the optimality of the default settings of the congestion control parameters. Comprehensive analysis and trade-off study of the control parameters reveal some areas of improvement to further the algorithm's efficacy. Motivated by the effectiveness of channel congestion control mechanism, we further investigate message content and length adaptations, together with transmit rate control. Reasonably, the content of the exchanged information has a significant impact on the map accuracy in cooperative driving systems. We investigate different content control schemes for a communication architecture aimed at map sharing and evaluate their performance in terms of position tracking error. This dissertation determines that message content should be concentrated to mapped objects that are located farther away from the sender to the edge of the local sensor range. This dissertation also finds that optimized combination of message length and transmit rate ensures the optimal channel utilization for cooperative vehicular communication, which in turn improves the situational awareness of the whole system.

This dissertation is dedicated to my parents who constantly supported me and helped me to become the person I am today.

ACKNOWLEDGMENTS

First, I would like to express my sincere gratitude to my advisor, Dr. Yaser P. Fallah, for his advice and guidance throughout the course of my research. His encouragement helped me to pursue my research, and to write this dissertation.

I would also like to thank my dissertation committee: Dr. Azadeh Vosoughi, Dr. Murat Yuksel, Dr. Mainak Chatterjee and Dr. Samiul Hasan, for their insightful feedback. I wish to acknowledge the Department of Electrical and Computer Engineering to give me the opportunity to pursue my Ph.D. degree in such a research-oriented and academically vibrant environment. I am also thankful to the members of my research group for all the help and assistance during my research at UCF.

Finally, I would like to thank my parents who have been always there for me, providing unconditional and endless love, motivation and support throughout my life.

TABLE OF CONTENTS

LIST OF FIGURES

LIST OF TABLES

LIST OF ACRONYMS

BSM	Basic Safety Message
CAV	Connected and Automated Vehicle
CBP	Channel Busy Percentage
CSMA/CA	Carrier Sense Multiple Access/ Collision Avoidance
DSRC	Dedicated Short Range Communication
IA	Information Age
ITT	Inter Transmit Time
MAC	Medium Access Control
PER	Packet Error Ratio
PTE	Position Tracking Error
RSS	Received Signal Strength
SINR	Signal to Interference and Noise Ratio
V2I	Vehicle-to-Infrastructure
V2V	Vehicle-to-Vehicle
V2X	Vehicle-to-Everything
VANET	Vehicular Ad hoc Network
WAVE	Wireless Access in Vehicular Environments

CHAPTER 1: INTRODUCTION

Automated driving systems heavily rely on a wide range of onboard sensors to better perceive the surrounding driving context and to take optimal driving decisions. To complement the detection mechanism of local sensing, dedicated short range communications (DSRC) technology is introduced which facilitates communication among neighboring vehicles, roadside traffic control systems, and networked mobile devices carried by pedestrians [1]. V2X-enabled onboard units operating in the DSRC band can communicate with neighboring entities that are beyond the reach of local sensing devices. In this way participating vehicles in cooperative intelligent transportation systems (ITS) can achieve a sweeping perception of their surroundings by combining the communicated and locally sensed objects into a situational awareness map. This locally constructed map can then be fed to higher-level vehicle safety applications including, but not limited to, long-range trajectory planning, crash avoidance strategy [1], conflict resolution at traffic intersections [2] [3], vehicle re-routing [4]. The performance of these applications can be significantly improved by the cooperative exchange of the locally constructed situational awareness map information with neighboring vehicles.

In its fundamental form, inter-vehicle communications allow vehicles to exchange periodic update messages containing vehicle status information which are called Basic Safety Messages [5] (BSMs) in the United States and Cooperative Awareness Messages [6] (CAMs) in Europe. The

update messages typically contain information collected by the global navigation satellite system (GNSS) receiver of the vehicle. These include position information, speed and heading, and optionally, some path history data of the sender vehicle. A richer set of information can be exchanged if data from local sensing devices are combined with the positional data. Data collected by the local sensing devices such as radars, LiDARs or cameras can provide a vehicle with information about its surroundings, and sharing this information with neighboring vehicles can benefit the whole cooperative automated driving system. However, the inclusion of all locally aggregated information may not always be possible because of the limited capacity of the communication channel. In vehicular ad hoc networks (VANETs), the communication medium becomes congested due to an increase in the traffic density or an increase in the offered data load. For a given network density, the offered load on the channel is a function of message length, message generation rate, transmit power or a combination of these parameters. A seamless communication requires these parameters to be regulated in such a way that the channel congestion can be avoided; otherwise, information cannot be shared in a timely fashion, which is essentially one of the main objectives of cooperative vehicle safety communication. Furthermore, the content of the exchanged messages must deliver useful information to the intended recipients because the effectiveness of the overall map of a networked vehicular system not only depends on the quality of the communication channel but also the usefulness of the disseminated information.

Considering the capacity of the communication channel, it is imperative to have demonstrated evidence that the communication system can scale as the number of participating vehicles increases, prior to large scale deployment of V2X technology. To that end, a BSM scheduling mech-

anism regulating inter-transmit interval and transmit power is standardized in the SAE J2945/1 that outlines an adaptive upper layer message rate control mechanism as a function of vehicle dynamics and estimated tracking error, and a transmit power control approach as a function of instantaneous channel busy measurement. In this dissertation, we demonstrate the potency of the congestion control mechanism through the scheduling of core BSM update messages, by focusing on the performance evaluation of the SAE J2945/1 congestion control algorithm. We also provide additional analysis to further the efficacy of the algorithm, in light of an extensive trade-off study of the algorithm's control parameters. In the process, we develop and validate a high fidelity simulation platform for realistic simulations of inherently dynamic vehicular environments. We recognize that the validation of V2X communication framework requires numerous test cases to be evaluated to ensure its robustness. Understandably, evaluation and validation of upper layer safety applications greatly depend on the performance of the underlying DSRC network. However, it is very difficult, if not impossible, to evaluate application performance under different DSRC communication conditions and in particular at a large scale. As a result, researchers resort to the simulation of DSRC networks to determine possible issues that may exist for application performance. In this dissertation, we describe how connected vehicle applications can be simulated, with an emphasis on high fidelity but efficient simulation of underlying DSRC networks. Different approaches to simulation of DSRC are summarized and the sub-frame based method, which has widespread use, is discussed in detail. We present several enhancements to widely used discrete event simulators (such as ns-3) to enable sub-frame level simulation of DSRC. The resulting simulator is evaluated and shown to be accurate when comparing to results from field tests. In addition to sub-frame

level processing, which mostly concerns how wireless frames are processed in a node, the channel propagation model is also discussed. The channel model stages and components are described and its use in the simulator is also explained. In this dissertation, we first establish the efficacy of channel congestion control mechanism using a high fidelity sub-frame level DSRC simulation platform and then seek to extend its applicability to a content-adaptive cooperative communication paradigm to further the benefits of envisioned vehicle safety applications.

1.1 V2X Simulation Platform

Cooperative vehicle safety applications use Dedicated Short-Range Communications (DSRC) technology to disseminate safety-critical or traffic information [7] [8] [9]. Active safety applications are arguably the most important connected vehicle applications. Given the criticality of safety applications, it is imperative to extensively research and test the applications before deployment. However, the dynamic nature of (DSRC) communication networks and vehicular traffic, and a multitude of factors that affect each make it prohibitively expensive, and technically infeasible to conduct field tests for all possible communication and traffic scenarios. In particular, the nature of safety applications and rarity of events is such that large scale tests with hundreds of vehicles are usually very difficult, if not impossible. Even small scale tests of the application under all communication possibilities may not be feasible. Given the difficulties of field trials, researchers generally resort to simulation to examine and verify the performance of safety applications. Simulation efforts generally target three different aspects of DSRC based safety applications: communication

network, vehicle traffic and movement, and safety algorithms. While safety algorithms can often be exactly implemented in simulators, the communication network and traffic aspects have to be modeled and simulated at lower fidelity. As a result, it becomes vital to ensure that the simulation tools are precise enough and credible.

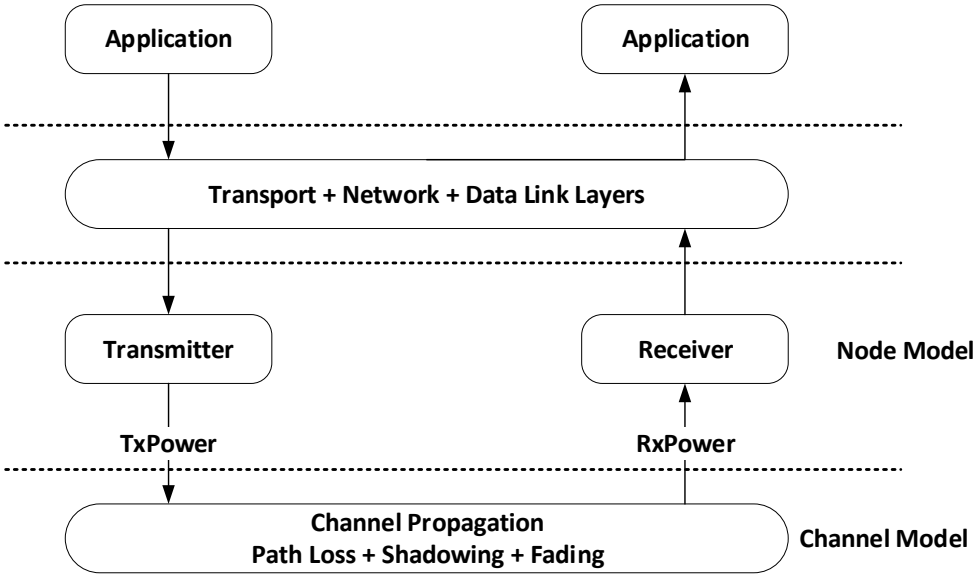

Figure 1.1: Functional diagram of V2X communication layers.

Simulation of wireless communication networks requires modeling different layers of the protocol stack (Figure 1.1), in addition to the behavior of the wireless medium. While most protocol behaviors can be exactly implemented according to the standard, some details at the lower layers have to be abstracted. Modeling of the wireless medium, i.e., channel propagation behavior, is also a challenging task and exact reconstruction of what goes on in the physical wireless environment is generally impossible. As a result, there are numerous approaches to modeling and abstracting the behavior of different layers and channel models.

Overall, the simulation of wireless networks requires developing models for nodes and the wireless channel. Node models should in general take into account transmitter and receiver behavior, while channel models describe the signal loss and deformation between each pair of nodes. Therefore, we describe the node model and channel model separately in this dissertation. It should be noted that the node model details will depend on how detailed the channel model is.

Some of the recent works on simulation of DSRC focused on adapting existing popular network simulators such as ns-2 and ns-3. Chen et al. in [10] [11] addressed the shortcomings of the simplistic physical layer (PHY) and medium access control (MAC) implementations of ns-2. In their work, the authors separated PHY and MAC layer implementations in such a way that functionalities of the network components are placed in their respective layers, improving ns-2 simulation accuracy. The simplistic approach of carrier sensing in ns-2 was also enhanced by integrating a "NoiseMonitor" to keep track of all interferences at a transceiver. The work in [10] also introduced an SINR based reception criteria, that determined whether a frame is successfully received or not. In [12] the authors have extensively investigated, using their 802.11 testbed, the details of the physical layer capture effect by explaining various capture scenarios. Based on that study [13], [14] proposed some modifications of the 802.11 PHY in QualNet [15]. Papanastasiou, Mittag et al. [16], [17] developed a detailed PHY model (PhySim-Wifi) based on ns-3 in an effort to incorporate DSRC based vehicular communication to the simulator. Instead of using a frame that is defined solely by the length field of the frame, PhySim-Wifi emulates the physical bits of the frame by transforming a randomly generated bit sequence equal to the size of the length field into complex time-domain samples as per IEEE 802.11 standard. Although PhySim models a real-

istic WiFi PHY by considering bitwise processing of the signal, the trade-offs here are the higher memory and computational requirements.

Another DSRC simulation component demanding higher realism is the wireless propagation behavior which is affected by the characteristics of electromagnetic signals. The strength of electromagnetic signal attenuates as it travels through the medium (air) from the sender to the receiver. Signal strength weakens in the presence of obstructing elements such as buildings and large trees. Furthermore, radio signals are also influenced by some natural phenomena [18] [19]. Reflection occurs when a propagating signal encounters a surface which is much greater than its wavelength. Usually, buildings, walls, or even ground can be reflectors of signals. Diffraction occurs when irregular-shaped objects are on the signal path, and several copies of the signal are produced from the irregular sharp edges of the blocking objects. Different copies will have different amplitudes and phases and will arrive at the receiver at different times. Scattering happens when the signal hits objects that are smaller than the signal wavelength and the original signal splits into several ones. Considering these natural phenomena that deteriorate wireless signals, three types of modeling are required to approximate the channel losses: large-scale deterministic path loss, shadowing or large-scale fading, and small-scale fading.

Different measurement campaigns have been established and numerous scenarios were investigated concerning various surrounding environments of VANETs to identify the aforementioned parameters of vehicular channels based on both channel sounder devices and RSSI-based measurements. In [20], two different path-loss models are proposed for inter-vehicle communication channels for three different environments: rural, highway, and urban. In that work, the measurement

framework was set up at 5.9 GHz, using a channel sounder at the transmitter side which generated a multi-tone signal and one receiver. A two-ray model with a zero mean log-normal shadowing is derived as a rough path-loss model for both rural and highway environments for distances larger than 32 meters. For the urban scenario, a general log-distance model with a zero mean log-normal shadowing is recommended. The path-loss exponent of 1.61 is calculated based on their measured dataset. Path-loss, power delay profile and delay Doppler spectrum analysis in highway, rural, urban and suburban environments were investigated using channel sounder in [21] [22] [23] [24]. Measurements were performed over the 240 MHz band around 5.2 GHz central frequency. Two GPS-equipped trucks were employed as transmitter and receiver. The most important characteristic of all of their measurement scenarios is the dominant line-of-sight (LOS) between transmitter and receiver. Log-distance model plus a zero-mean log-normal shadowing is proposed for highway, urban, and suburban environments. The parameters are evaluated for the measured data using the least mean square error curve fitting method. Due to the low density of scatterers, which leads to a dominant LOS plus a ground reflection, two-ray is found to be the best matching path-loss model in the rural environment. The validity of the models is claimed for distances greater than 10 and 20 meters for log-distance and two-ray, respectively. Nakagami-m and Weibull distributions were proposed in [24] [25] to model the small scale fading in a highway scenario based on the MIMO car-to-car measurements at 5.3 GHz. In [26] two different obstruction modes are proposed as NLOS and obstructed LOS (OLOS) based on the type of obstacle between transmitter and receiver. Three different log-distance path-loss models are then derived for LOS, OLOS, and NLOS cases from a measurement data using LUND channel sounders. Rayleigh and Rician fading mod-

els have been proposed for V2V channels with realistic non-isotropic scatterers in [27] and [28]. A novel method with higher precision for Rayleigh parameter computation was investigated in [27] while Rician envelope level crossing rate and average fade duration are investigated in [28]. A Rician geometry-based stochastic fading model has been proposed for wideband multiple-input multiple-output (MIMO) V2V channels in [29] and a method for inter-carrier interference (ICI) cancellation is proposed based on this model. In [30], fading statistics are analyzed in four environments: highway, motorway, urban and suburban. Two vehicles, one transmitter equipped with a 5.2 GHz signal generator and one receiver equipped with a network analyzer were used for data collection. It is claimed that urban and suburban environments have the same behavior, in terms of small-scale fading, as motorway and highway scenarios, respectively. Rician, Rayleigh, Gaussian, and Nakagami-m distributions were examined and the Rician channel model was found to be the best match in all scenarios based on the least mean absolute error method which was reasoned by dominant LOS in all measurements. The log-normal model was offered to be used for shadowing in all scenarios. It should be mentioned that flat fading assumption for vehicular channels is insupportable for DSRC-based networks [31], [32]. Therefore, due to the frequency selective nature of DSRC channel fading, whereas RSSI values represent the effect of total channel attenuation through energy measurement, their use is best limited to path-loss, shadowing, and fading analysis [32], [33]. Authors in [34] [35] [36] [37] considered the intermediate vehicles between transmitter and receiver as dynamic obstacles and added them to static obstacles, like buildings, in the path-loss model calculations. The results indicate that path-loss of the vehicular channel, packet delivery ratio (PDR), latency, and jitter completely depends on the presence of LOS. Two

vehicles - one transmitter and one receiver, were equipped with NEC LinkBird-MX which is a DSRC platform working based on IEEE 802.11p on 5.9 GHz frequency. RSSI and PDR values were logged in different measurement scenarios. The results supported the two-ray as the best fitted path-loss model in the presence of LOS for highway, suburban, and urban areas. Empirical RSSI values from a measurement campaign in the freeway environment, divided into ten-meter bins, were used to find the best fitted fading distribution in [33]. Nakagami-m distribution is proposed as an appropriate fit based on the cumulative distribution function (CDF) matching approach. Reported values of shape parameter m for Nakagami-m distribution lies between 1 to 1.8 for distances less than 100 meters, and 0.7 to 1 beyond it. Therefore, the behavior of Nakagami-m distribution is dominantly similar to Rician and Rayleigh for distances below and above 100 meters, respectively. In another effort [38], path-loss and fading were analyzed for the suburban environment based on two RSSI datasets collected from two vehicles as a transmitter-receiver pair. A dual-slope log-distance path-loss model, plus a zero-mean log-normal shadowing, is suggested to model large-scale power attenuation. Different path-loss exponents and shadowing standard deviations for distances under and above 100 meters are calculated using regression methods. Small-scale fading is modeled using Nakagami-m distribution. The first dataset tends toward Rician and Rayleigh distributions for distances under and above 70 meters, respectively. The other dataset has the same behavior pattern except that the transition point is around 90 meters. A similar approach is taken to derive the log-distance path-loss and zero mean log-normal shadowing parameters from RSSI measurements in highway and rural environments in [38], [39]. Due to the fewer number of obstacles, the critical distance for slope change in the path-loss model is reported much closer

to the first Fresnel zone. Moreover, shadowing standard deviations of rural and highway environments are also less than shadowing standard deviation of the suburban environment of [37], [38]. RSSI-based measurements with a single transmitter-receiver pair of vehicles in motorway, rural and urban environments have been utilized to identify the best fading model for vehicular scenarios in [39], [40]. Dual-slope log-distance path-loss with a zero mean log-normal shadowing and Nakagami-m fading models are derived as the best match for large- and small-scale received power variations, respectively. Nakagami-m distribution is also selected to model the small-scale fading of the vehicle-to-vehicle (V2V) channel based on the RSSI measurements in a highway and an open-sky area [40], [41]. The results propose greater values of Nakagami-m shape parameter m for open-sky in comparison with the highway. A simulation-based study of IEEE 802.11p also takes Nakagami-m fading to model the vehicular networks channel in [42]. A suburban scenario is simulated in OPNET with a modified physical layer model that has a Nakagami-m fading model included. They found the best value for shape parameter m, as a function of separation distance and relative velocity of transmitter and receiver.

In [43], the authors studied the shadowing impact of trucks as obstacles and found that an average of additional 12-13 dB losses is added in the presence of a truck. Diverse TX antennas were also used to find the best antenna location to model the shadowing loss for such obstacles. Authors in [44] emphasize on the importance of the vehicle type in overall vehicle shadowing distribution. The authors argued that using the prior knowledge of vehicle type distribution, field observations in the presence of obstacles can be reproduced in simulation. In [45], the authors investigated the limitation of log-normal and unit disk models in realistic V2X settings and proposed a match-

ing mechanism for log-normal model parameter tuning based on vehicle density and a correlation model to account for the evolution of the link characteristics over time. In [46], the authors studied a field RSS dataset to model a composite channel propagation loss. The large-scale dataset consists of RSS samples from a controlled highway like scenario; however, the proposed methodology works for separation distances where packet loss ratio is minimal. Most of the RSS-based measurement campaigns reported in the literature either consists of a smaller set of transmitting entities or collected in a controlled environment. As a result, corresponding datasets fail to capture many driving and topological scenarios from real-world roadways. This work investigates RSS samples collected from real-world driving scenarios and models the propagation behavior to better realize the V2X communication channel.

1.2 Scalable V2X Communication for Connected Automated Driving

Smart vehicles outfitted with sensors like radar, LiDAR or cameras can collect a variety of positional and surroundings data to provide situational awareness to the automated driving system. The collected information can then be combined with the map (in the form of vehicle position update and additional neighbor data) information exchanged over the communication channel to construct a localized map. Figure 1.2 illustrates how a host vehicle (HV) sees its surroundings in a roadway. In such a map data exchange based communication approach, a map radius is defined for the HV to focus on a particular area of interest that it deems critical from a safety perspective. Therefore, HV tracks only those RVs that are in its map radius. In cooperative vehicle communications, vehicles

maintain a local map by combining data from various local sensors and incoming safety beacons from surrounding vehicles. This local map helps a vehicle to maintain up-to-date knowledge about its surroundings. Since the local map contains information about all the neighboring vehicles, communicating the full map is limited by the capacity of the wireless medium.

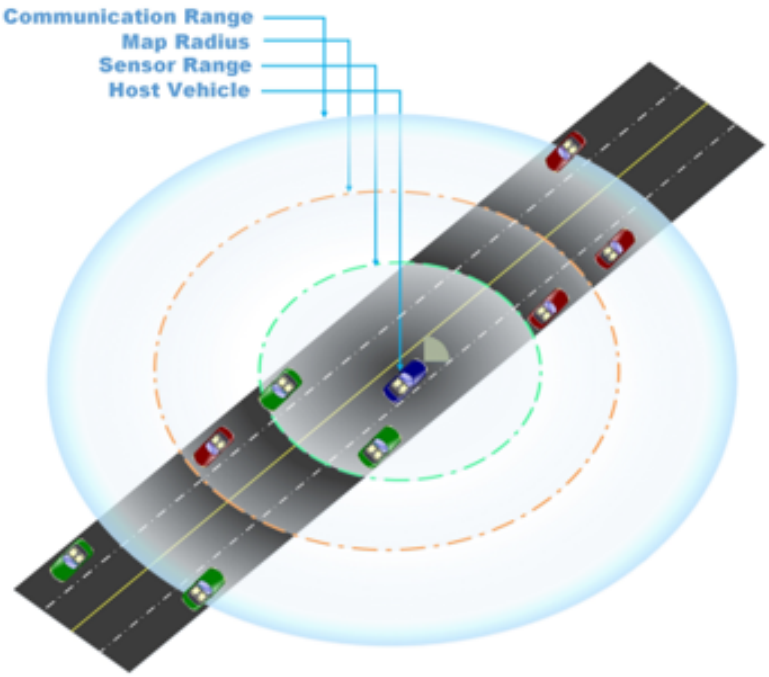

Figure 1.2: Host vehicle's perspective of the situational awareness map

In heavy traffic environments, with a high number of transmitting V2X entities, the communication channel suffers congestion due to rising interference and channel contention [47]. The conventional approach to handle interference in the IEEE 802.11p standard (PHY standard for DSRC) is to use Carrier-Sense Multiple Access with Collision Avoidance (CSMA/CA) as the medium access protocol [48]. In CSMA/CA, when a node (or vehicle) has a packet (i.e., BSM)

to transmit it first listens to the channel. If the channel is deemed idle or unoccupied, it transmits the packet. Otherwise, the node waits for a random back-off time before transmitting the packet. While this mechanism reduces the chances of packet collisions, it does not avoid it entirely. In large and dense V2V networks, the performance of safety applications may therefore unnecessarily suffer if all vehicles send their BSMs at the same high transmission rate and transmit power. The consequent high packet losses affect V2V situational awareness and make it difficult to predict a vehicle's movement or recognize an imminent crash in a timely manner. Hence, mitigating channel congestion has been widely studied to address the challenge of scalability and to make safety applications robust.

Channel congestion in DSRC can be regulated by adapting a number of transmit parameters, e.g., message length, transmit rate, transmit power, and data rate. Various congestion control algorithms have been proposed in the literature that adapts these transmit parameters in combination or separately. The authors of [49] proposed a scalable communication method where a subject vehicle adjusts its BSM generation rate depending on the estimated tracking accuracy of the vehicle from the perspective of the neighboring vehicles. The sender also adapts the transmit power based on the observed channel load to curb channel congestion. In [50], a congestion control algorithm called Linear Message Rate Integrated Control (LIMERIC) based on linear message rate adaptation has been outlined which converges to a desired channel utilization level. In [51], the authors enhanced LIMERIC algorithm to control transmit power by mapping message rate through a predefined monotonic transmit rate-power function. Rate-adaptive congestion control based on observed channel load is also studied in [52]. In [53], the authors presented an analysis

of the distribution of inter-packet receptions to determine the optimized transmit parameters and proposed a joint transmit power/rate control approach for a targeted awareness distance. In this approach, transmit power is selected based on the awareness distance while the transmit rate is adapted based on channel load. In [54], the authors proposed a content-centric medium access control (MAC) scheme that provides a mechanism through which the limited wireless bandwidth is adaptively allocated to the information objects based on the number of requests for them. This approach also allocates bandwidth for the participating network entities based on the timeliness and completeness of the information they possess about a given requested region. In [55], the authors proposed an awareness framework for vehicle safety applications where a joint transmit rate/power control algorithm adapts the awareness quality as a function of the awareness range. In [56], the authors provided a congestion control algorithm based on transmit power control that separately targets two different groups of vehicles, using two different transmit powers. The high power transmits are for farther vehicles as well as for the closer vehicles, while the low power transmits are only for closer ones. The authors also presented results of a hybrid variant that uses a combination of transmit power and transmit rate control. In [57], the authors proposed a machine learning-based congestion control algorithm to mitigate channel congestion at road intersections. Using a k-means algorithm to identify the vehicle clusters in the aggregated data at intersections, the congestion control unit determines a set of transmit and MAC parameters for each cluster. Determined transmit parameters are disseminated to the stopped (awaiting) vehicles at an intersection using road-side units (RSUs). The SAE J2945/1 [58] standardized a scalable BSM scheduling methodology based on the channel congestion level and the estimated vehicle density. In this algo-

rithm, BSMs are transmitted depending on the vehicle dynamics and the estimated vehicle density in a predetermined radius of the sender vehicle. It also adapts transmit power as a function of the observed channel load. The decentralized congestion control (DCC) algorithm standardized by the European Telecommunications Standards Institute (ETSI) [59] considers channel load as the feedback input to regulate the message rate. Depending on the observed load on the channel, the algorithm switches to one of three possible states: relaxed, active and restrictive. Each of these states has its own transmit rate and power setting. In [60], the authors proposed a distributed congestion control approach based on a modified CSMA/CA mechanism of the MAC layer that adjusts the contention window size considering the priority of the user data. A scalable and cooperative MAC protocol for VANETs is also proposed in [61] where a time-slot reservation policy is introduced for upcoming channel demand in DSRC networks. This policy helps the scalability issue in dense traffic scenarios. In [62], the authors provided a detailed survey of the adaptive beaconing approaches suggested to date by classifying them based on their underlying design approaches.

Local dynamic map (LDM) is being standardized by ETSI which aggregates data locally in a subject vehicle [63, 64]. LDM contains real-world data of four different types: (1) permanent map data provided by map data supplier, (2) transient static data, e.g., speed limit signs, (3) transient dynamic data, e.g., weather advisory, and (4) highly dynamic data, e.g. CAMs. LDM is essentially a database that locally serves queries from the safety applications, but it does not share local information with neighboring vehicles. In [65], a general vehicle communication framework has been proposed where each vehicle creates a multi-resolution map based on the information collected by its local sensing devices as well as the information extracted from the awareness-map broadcast

by other vehicles within its communication range. To tackle the scalability problem of such a map sharing scheme, a message length and content control strategy have been presented to adapt the size and content of the exchanged messages based on locally observable network performance metrics. In this approach, message size is adapted by considering the offered load on the communication channel. After determining the message length, contents (neighboring vehicle information to disseminate) are selected based on their distance to the sender vehicle where mapped objects at a closer distance get a higher priority over farther objects. Given the well-known issue of scalability in DSRC networks reported in [49, 50, 53, 66, 67], when BSMs are used, it is clear that any exchange of sensory information among the connected vehicles has to consider the limited capacity of the network. This limitation of channel capacity poses a major challenge here since sensory information in automated driving applications are usually much richer than what is included in the periodically exchanged BSMs. A new method about message content control and message length adaptation was proposed in an earlier work [65]. However, the issue of adapting the rate of message generation and its trade-off with controlling the message length had not been considered. Also, the distance aspect of the included message objects on map accuracy had not been investigated in [65], where semantic-less maps are considered in the form of multi-resolution map representation. This multi-resolution map was created by transforming point cloud data to map format similar to [54]. A method of adding the multi-resolution maps to object maps was presented in [65], giving higher priority to detected objects and then using the remaining capacity to deliver the multi-resolution map data. In general, since the semantic-less maps are expected to be static, we can assume that some stored information from these maps can be preloaded into the

vehicle and frequent communication of those objects will not be necessary. It is expected that only a small differential between stored maps and sensed static semantic-less maps exist and will be represented as a multi-resolution map as described in [65]. We can simply consider such differentials as an object and encode them in the smallest resolution, and then treat it as another object in the object map. Also, note that the object map information that is being shared and discussed in this dissertation is used to augment and extend a vehicle's view of its environment and is not a replacement for point cloud-style immediate maps of the surrounding.

1.3 Organization of the Dissertation

The first major contribution of this dissertation is to validate and analyze the channel congestion control mechanism standardized in SAE J2915/1 and elaborate on the optimality of the congestion control algorithm to identify potential room for improvements to further its efficacy. The second major contribution is to extend the safety benefit of channel congestion mechanism through a content-adaptive map information dissemination architecture, aiming at improving map accuracy in connected automated driving systems.

In Chapter 2 we discuss the development of high fidelity and efficient simulation platform for evaluating connected vehicle applications. Modeling techniques for deriving realistic V2X channel from large scale RSS dataset is provided and validated. Factors, ranging from vehicle density to relative position of transmitting vehicles to the presence of blockers, are considered in the modeling stage. Enhancement of DSRC based receiver model in the popular ns-3 simulator is outlined, where

empirical results from prototype V2V devices were utilized to align the receiver behavior with the IEEE 802.11 PHY specifications. The developed simulation platform is then used to validate the channel congestion control algorithm standardized in SAE J2945/1 and outlined in Chapter 3.

In Chapter 3 we present large scale simulation results to validate the effectiveness of the channel congestion control algorithm standardized in SAE J2945/1. The results are obtained for real-world mobility scenarios using channel models calibrated to the vehicular environment the mobility traces are generated from. We further analyze the optimality of the current parameter settings of the CC algorithm. With a thorough trade-off study, we seek to identify potential areas of improvement to further the algorithm's safety benefit.

In Chapter 4, motivated by the channel congestion control validation results presented in Chapter 3, we provide a content-adaptive map information dissemination approach to extend situational awareness beyond the sensing range of on-board sensors like cameras, radars, and LiDARs. The idea is to leverage the availability of rich local sensor data and exchange that information with the immediate neighborhood. The issue of scalability in such a cooperative communication paradigm is discussed to find that optimal combination of length and transmit interval can significantly improve the tracking accuracy of the whole system. We also provide insights into the inclusion priority of the map objects in the communicated messages, which can be used as a guideline for map information dissemination based cooperative safety applications. And finally, we conclude in Chapter 5 with a list of research areas for future work.

Table 1.1 lists several terms and definitions that will be later used within the dissertation.

Table 1.1: Terms and Definitions

BSM	Basic Safety Message (BSM) contains position information data like latitude, longitude, speed, heading
RSS	Received Signal Strength (RSS) is the received power in dBm associated with a received packet over the air
CBP	Channel busy percentage (CBP) is the fraction of time the communication channel is sensed busy by the onboard network device during a predefined time interval (100 milliseconds)
PER	Packet Error Ratio (PER) is the ratio of missed BSMs to the total number of transmitted BSMs for each sender-receiver distance
PTE	Position Tracking Error (PTE) is the difference between current position estimate of a transmitting vehicle and the estimate of that vehicle at a receiver (based on received BSM) at a given time
IA	Information Age (IA) quantifies the time difference between the timestamp of contained data in a received BSM and the current time

CHAPTER 2: EFFICIENT AND HIGH FIDELITY SIMULATION PLATFORM FOR V2X COMMUNICATION

[1]Generally, computationally inexpensive yet realistic simulation platforms are desired for large scale evaluation experiments for V2X safety applications. As a result, many of the popular network simulators such as ns-2, ns-3, OMNET, etc., use frame level simulation of channel effect. The propagation model is also abstracted in most cases to formulas that try to recreate the impact of large scale channel loss, shadowing and fading on an entire frame. Some simulators allow for employing of ray tracing and more granular modeling of the propagation loss (e.g., OPNET allows both approaches). Nevertheless, such detailed propagation models are computationally costly. In this chapter, we detail the approach taken by ns-3 (an open-source simulator widely used by academic and industry researchers) and present the corrections that we have made to ns-3 based on DSRC field tests, to derive a higher fidelity sub-frame level simulator, which remains computationally efficient. We also outline a modeling technique for V2X propagation calibration using large scale field RSS data.

[1]The work presented in this chapter is based on the following publications: [1] S. M. O. Gani, A. Tahmasbi-Sarvestani, M. Fanaei, and Y. P. Fallah, "High fidelity DSRC receiver model for ns-3 simulation using large-scale field data," in the proceedings of 2016 IEEE Wireless Communications and Networking Conference, April 2016. [2] Y. P. Fallah and S. M. O. Gani, "Efficient and High Fidelity DSRC Simulation," Cham:Springer International Publishing, 2019

2.1 DSRC Physical Layer Modeling

ns-3 [68] was chosen as the base simulation platform in this work which is a discrete event simulator for internet systems and widely used in the wireless research community. Since any simulation-based evaluation process demands an accurate implementation of the underlying models, we calibrated ns-3 to fine-tune the DSRC physical layer (PHY) model to better align it with the PHY specifications outlined in IEEE 802.11 standard [69]. The calibration includes the adoption of frame capture features and empirical error rate models for the detection and decoding of OFDM frames. The calibration significantly enhanced the simulator to reflect the observations from DSRC hardware experiments [70].

2.1.1 OFDM Frame Modeling

Any OFDM frame in 802.11p can be divided into three key components: PLCP preamble, PLCP header and data bits [69]. The PLCP preamble is a sequence of training symbols that marks the start of an OFDM frame. The training symbols are known to both the transmitter and the receiver. Therefore, when a signal with a power level greater than the receiver sensitivity arrives at the receiver, a preamble detection mechanism is triggered. This mechanism essentially synchronizes the receiver with the transmitter for upcoming data bits that are contained in the payload of the frame. The SIGNAL field is included in the PLCP header which specifies the bit rate and length information of the payload. In 802.11p, the durations of the preamble and PLCP header are 32

microseconds and 8 microseconds long, respectively. Since bit-level processing of OFDM frames is computationally expensive, in our DSRC PHY model, we combine the preamble and PLCP header into the first key component of a frame and loosely refer to it as "preamble". We will use "payload" to collectively refer to the data bits. The resulting OFDM frame can then be considered as a two-part entity as illustrated in Fig. 2.1.

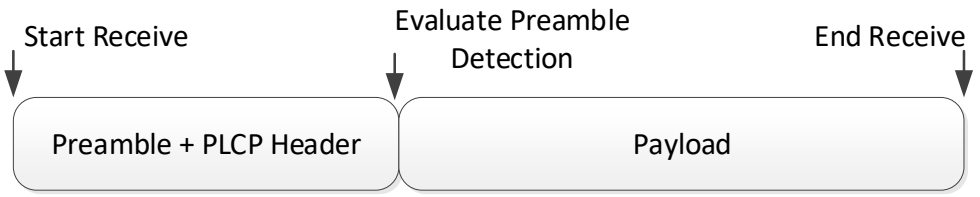

Figure 2.1: Key components of an OFDM frame along with associated action events.

2.1.2 Interference Modeling

To accommodate physical carrier sensing and energy detection, and to model impact of interference on signal decoding, the receiver model needs to keep track of cumulative interference by maintaining a list of all signals that are currently present in the medium. This list is populated by adding the incoming signal which can be described by the received power (*RxPower*), and the start and end time of a signal that has just arrived at the receiver, assuming that the *RxPower* does not vary over the frame lifetime. This interference list helps calculate instantaneous cumulative interference by simply summing up all signals that are active at that time instance. Also, the calculation of signal-to-interference-and-noise ratio (SINR) is possible for individual signals, which is

frequently used for checking reception probability and making a decision about the continuation of current reception or switching to frame capture. The determination of SINR for a signal of interest is required for various frame detection and decoding steps. For example, the arrival of a new signal during the reception of another signal requires an SINR check to decide whether the newer frame should be captured or not. To accommodate the calculation of SINR for any signal, a subroutine is needed which returns the total interference caused by signals that overlap with the signal of interest. During the SINR calculation, the noise floor and noise figure are also considered. The noise floor is a measure of all unwanted background noise present in the system. In general, thermal noise is modeled as $N_t = KTB$, where K is Boltzmann constant, T is the temperature in Kelvin, and B is the signal bandwidth in Hz. Noise figure, NF, is a measure of degradation of SNR caused by the components in the radio signal chain, for a given bandwidth. Therefore, the total noise floor is calculated by

$$noisefloor = NF * N_t \tag{2.1}$$

SINR of signal i is then calculated as follows:

$$SINR_i = \frac{RxPower_i}{noise\ floor + \sum_{j=\ signal\ overlaps\ with\ i} RxPower_j} \tag{2.2}$$

Where $RxPower_i$ and $RxPower_j$ are in Watts. An example showing SINR computations for a signal of interest (in red color) at different instance of time is illustrated in Figure 2.2.

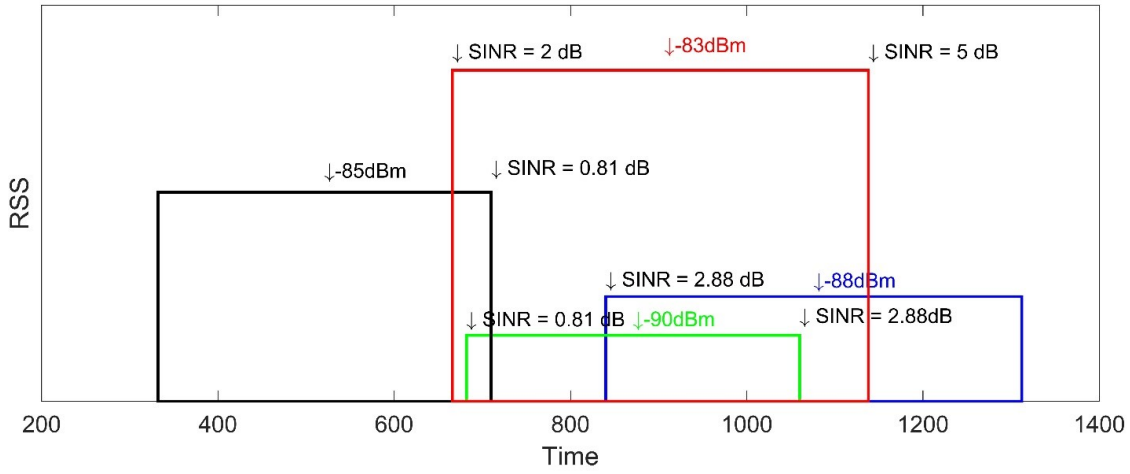

Figure 2.2: An example SINR computation for a signal of interest (in red color) at different instances of time

2.1.3 DSRC Receiver Modeling

An incoming OFDM frame is processed based on the instantaneous PHY state. A DSRC PHY can be in one of the four following possible states at a given time: transmit (TX), receive (RX), idle (IDLE) and busy (CCA_BUSY). If the PHY is in TX state, the signal is ignored and does not require any processing. If the PHY state is in RX or CCA_BUSY, a receiver sensitivity (r_{th}) is used to trigger an RX event. If the total energy (e) on the communication channel exceeds r_{th}, the detection of the preamble training symbols begins. At the end of preamble (40 microseconds) duration, the SINR of the receiving signal is evaluated to determine a successful preamble detection. A *Frame Success Rate vs. SINR* relationship curve is used for the evaluation. If a preamble is successfully detected, the receiver is deemed to be in sync with the signal and further processing of the receiving frame can advance. A payload decoding probability is evaluated when the last bit

of the frame is received. Similar to preamble detection, an empirical *Frame Success Rate vs. SINR* curve is used to determine if the frame can be successfully decoded.

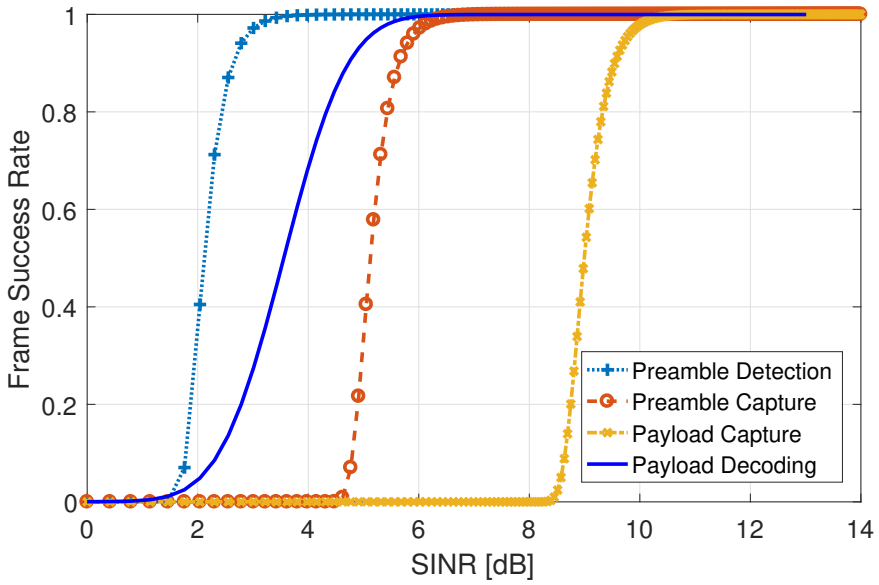

Figure 2.3: SINR versus frame success probability for preamble detection and capture, and payload decoding and capture.

The processing of an incoming signal becomes complex when the PHY is in RX state, i.e., the receiver is either already locked to a signal or is in the preamble detection stage. Simplistic modeling of DSRC receiver would drop an incoming (colliding) signal when the receiver is in RX state. However, field experiments, as reported in [71] [70], suggest that the frame capture mechanism kicks in in such scenarios. The radio chipsets in real-world DSRC devices try to capture the stronger signal when multiple signals overlap in time. This is called *frame capture* which, based on the arrival times of the colliding frames, can be further divided into two classes, preamble capture, and payload capture. Preamble capture occurs when a second signal arrives at

the receiving antenna when its radio is in the detection phase of an existing potential OFDM signal. SINR of the first signal is compared to determine if its strength can result in a successful preamble detection. If so, the receiver continues the detection of the first signal. If the SINR evaluation does not favor the first signal, the SINR of the second signal is evaluated for a possible preamble detection. In the payload capture case, the arrival of the second signal happens after successful preamble detection of the first signal, resulting in a signal overlap in time during the payload part of the first signal. Similar to preamble capture, the SINR of the first signal is evaluated to determine if its reception can advance. The receiver continues with the first signal if SINR is deemed sufficient for a successful frame decode. Otherwise, SINR of the second signal is evaluated to determine if the receiver needs to switch to that signal. The *Frame Success Rate vs. SINR* probabilities for preamble detection, preamble capture, payload capture, and payload decoding are graphed in Fig. 2.3.

Enhanced DSRC receiver model with the tweaks mentioned above provides a high-fidelity simulation platform to evaluate upper layer algorithms with higher accuracy. The calibrated PHY model is validated against the large-scale field dataset reported in [70]. CBP and PER plots, as illustrated in Fig. 2.4, evidently suggest that the results from the calibrated PHY model are in good agreement with the field observations.

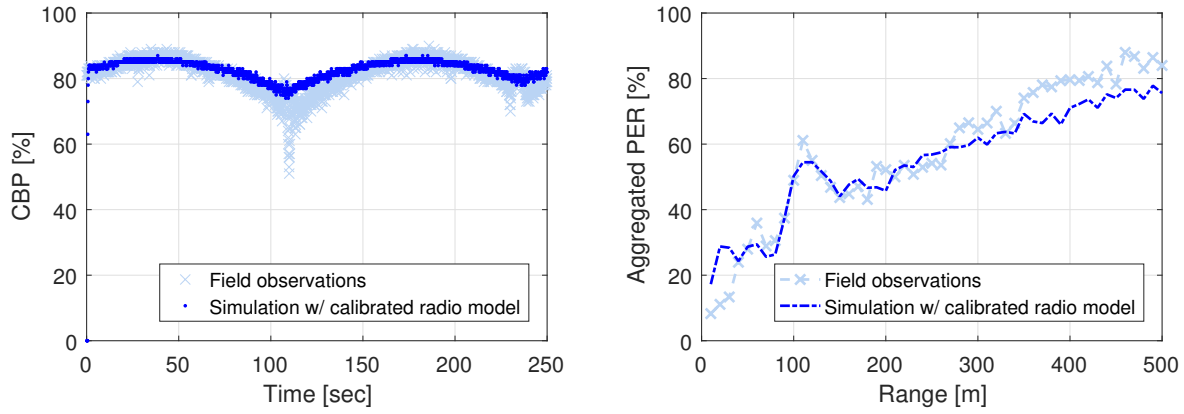

(a) (b)

Figure 2.4: Validation of calibrated DSRC radio model (a) CBP of field dataset versus simulation results (b) PER of field dataset versus simulation results

2.2 Realistic V2X Channel Modeling

Characterization of the naturally dynamic V2X channel is particularly challenging due to immensely diverse environments typical vehicular networks operate in. Driving context in such networks ranges from rural highways to multi-lane freeways to urban grids. Successful deployment of V2X solutions demands accurate modeling of channel propagation for validating different network protocols. To that end, several channel characterization datasets are reported in the literature using different measurement approaches. While a channel sounder based approach can analyze channel behavior at a significant degree of details, this approach may suffer from limited dataset size due to the complex setup of the associated data collecting apparatus. A cost-effective measurement approach is to equip a number of vehicles with off-the-shelf prototype on-board V2X

units and drive along the region of interest to collect received signal strength data for a variety of driving conditions. However, this approach also has limitations of its own. Off-the-shelf V2X units log RSS information only for successfully decoded packets, which essentially place a hard threshold on the received RSS information. The measurement, therefore, results in a dataset that is censored below the receiver sensitivity threshold. Despite this limitation, this approach is used by several measurement campaigns aiming at collecting V2X characterization data. Furthermore, ease of equipment setup makes this approach an ideal candidate for a large scale measurement drive in real-world driving environments.

Using prototype V2X onboard units, Crash Avoidance Metrics Partners (CAMP LLC) Vehicle Safety Communications 6 (VSC6) Consortium measured a dense freeway stretch and a four-way suburban intersection to collect RSS samples for characterizing the DSRC band. A total of ten vehicles (sedans of different auto makes) were used in the data collection campaign. The total dataset consists of multi-day RSS measurements sampled from different times of the day. Dashboard-mounted GoPro® cameras were used to capture traffic conditions during data collection runs. Each vehicle was equipped with DSRC On-Board Equipment (OBE) and Global Positioning System (GPS) devices that were connected to a roof-mounted omnidirectional shark-fin antenna (Figure 2.5). Transmit power was set to 20 dBm and over the air packet size was 139 bytes. The 10 MHz channel in the frequency range of 5855 MHz - 5865 MHz of the DSRC band (Channel 172) was measured. The GPS devices were providing position and time information to the OBEs. The OBEs were logging relevant items for the transmitted and received Basic Safety Messages (BSMs) [5] such as timestamp, transmit power, RSS, latitude, longitude, speed, heading,

and message sequence number. The GPS data is used to determine the sender-receiver separation distances and for accurate positioning of the transmitting and receiving vehicles. The time-stamped OBE logs come in handy for separating time-spanned samples from the whole data set collected over multiple days from a variety of traffic conditions. We observed variation in RSS samples depending on the traffic congestion present at the time of sampling. We used the reference data from Caltrans PeMS ([72]) to map the time-stamped logs from freeway measurement to different traffic densities. The details of density-level filtering are provided in a later section.

Figure 2.5: Equipment setup as shown was identical in all vehicles under test

2.2.1 Large Scale RSS Measurement

As part of the large-scale data collection campaign conducted by CAMP LLC Vehicle Safety Communications 6 (VSC6) Consortium, RSS samples were collected using a set of DSRC-equipped

cars from a 3.5-kilometer section of the I-405 freeway in Orange County, California. The stretch between the I-405/I-605/SR-22 and I-405/SR-22 junctions is chosen due to the relative flatness and straightness of the freeway segment. This part of the freeway has 16 lanes of traffic consisting of 8 lanes in each direction, including 2 High Occupancy Vehicle (HOV) lanes in each direction, as shown in Figure 2.6. The roadside environment is characterized by open fields on one side and noise barrier on the other, and by a median barrier separating the traffics in each direction (approximately 1.45 meters high). A variety of driving patterns were used to capture the randomness of vehicular settings in typical freeway scenarios. RSS samples were measured with cars driving in the same direction (convoy) and opposite direction (encounter). The dataset is comprised of measurements from different times of the day to obtain RSS samples for different traffic densities.

(a) Highlighted stretch of the I-405 Freeway in Orange County, CA is chosen as our region of interest for freeway RSS measurement. Source: Google Inc ©

(b) 4-way Intersection of Beach Boulevard and Westminster Avenue in Orange County, CA. Source: Google Inc ©

Figure 2.6: RSS measurement sites for freeway and intersection region of interest (ROI)

To characterize V2X channel in suburban intersections, a representative of the typical 4-way intersections (the intersection of Beach Boulevard and Westminster Avenue in Orange County,

CA) was selected to collect RSS samples from different legs of the intersection. Using a variety of driving patterns, e.g., intersection-encounter and midblock-encounter, channel characteristics of radio links for different sender-receiver separations were captured.

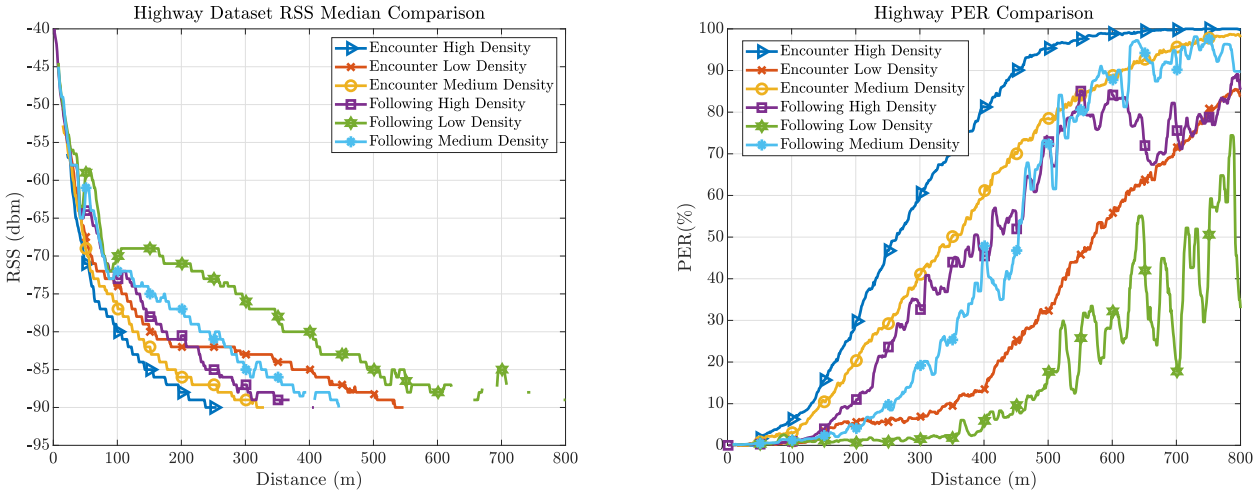

Figure 2.7: Analysis of highway datasets led to clustering the data for different traffic levels. We can observe the difference of the median between different clusters and the effect of vehicle density on PER. Median values are calculated considering the ratio of the lost packet. Median of samples with PER values higher than 50% cannot be calculated.

2.2.2 Freeway RSS Analysis

This subsection provides insight into the channel propagation characteristics of the freeway RSS dataset, focusing on dominant channel loss factors that affect the communication link behavior.

RSS and Travel Direction. As mentioned earlier, the measured freeway-stretch has a median barrier with a height closer to the heights of vehicles under study. Therefore, we reasonably assume

that measurements of vehicles driving in the same direction and opposite direction have characteristically different RSS pattern. Opposite direction links usually lack a prominent LOS for a longer period. Also, the relative speed is greater for communicating pair traveling in the opposite direction which may influence the fading characteristics of the corresponding links. This RSS dependency on relative travel direction is further corroborated by the median curves shown in Figure 2.7. Based on the above analysis of the RSS dependency on travel direction and vehicle density, required channel propagation models for the I-405 freeway dataset can be classified as shown in Figure 2.8.

RSS and Traffic Density. It is commonly understood that RSS has a direct relationship with density around the link, the higher the density the greater the propagation loss. This loss in signal strength can be attributed to the blockage amount the existing traffic density, in the form of physical dimension and orientation of the vehicles relative to communicating pair, may introduce to the communication link. Owing to this fact, we categorized the freeway RSS dataset considering the traffic density present at the time of measurement. Traffic density data is obtained from publicly available Caltrans PeMS data by calculating whether the communicating vehicle pairs are in opposite lane having a barrier in between or in the same direction of the highway. Traffic density calculation is shown in (2.4).

$$d_i = \frac{q}{v} \tag{2.3}$$

$$d = \sum \frac{d_i}{n} \tag{2.4}$$

where q, v, n, d_i are vehicle flow, average speed, number of lanes and density of vehicles over lane i respectively. The freeway dataset is divided into six clusters as shown in Table 2.1. While the RSS data can be separated into more clusters, the cost for doing so would decrease the number of samples per cluster and eventually result in noisy estimation.

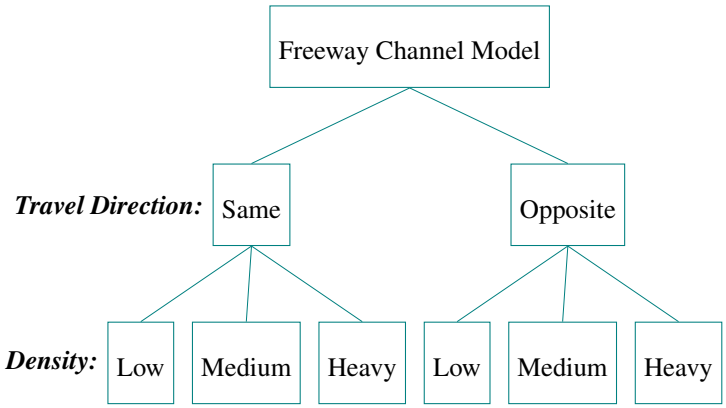

Figure 2.8: Freeway channel model classification - the density ranges defining the density levels shown here are provided in Table 2.1.

Table 2.1: Highway Dataset Clusters (density in veh/mile/lane)

Travel Direction	Density Level	Density (veh/mile/lane)	Travel Direction	Density Level	Density (veh/mile/lane)
Encounter	Low	$\leq$10	Following	Low	$\leq$10
	Medium	(10 - 20)		Medium	(10 - 20)
	Heavy	$\geq$ 30		Heavy	$\geq$ 30

2.2.3 Intersection RSS Analysis

A number of channel loss factors are identified from the observations on RSS samples collected from intersection driving scenarios. Since the loop-sensor data was not available for the intersection we measured RSS data from, we assumed no distinction based on traffic density. This assumption is further supported by the observation we made from the dataset by plotting them for different time segments of the day, which showed no evidence of time-dependency (and in turn, density dependency) of the RSS dataset.

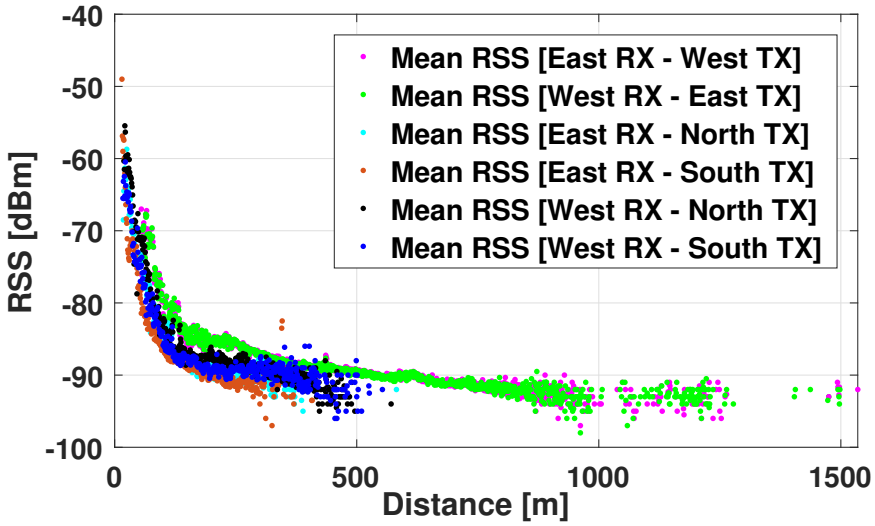

Figure 2.9: RSS vs. distance for TX-RX pair on same road and intersecting roads.

Same Road vs. Intersecting Road. From the field data we observed that, for a given TX-RX separation distance, signal strength significantly differs based on the relative position of the TX-RX pair. Signal levels are typically higher for the links on the same road while links on intersecting

roads show lower RSS due to the NLOS nature of such links. As a result, the same road evidently shows extended range compared to intersecting roads, as illustrated in Fig. 2.9.

Same Leg LOS vs. Different Leg LOS. The same leg LOS occurs when the TX-RX link is obstructed on the same leg. Different leg LOS occurs when the sender and receiver are located on different legs of the intersection. This can occur in two cases: when the sender-receiver pair is on the same road but different legs; or, if the pair is on intersecting roads but still has a direct LOS due to the opening of the intersection box. Fig. 2.10 shows RSS samples for the case where the TX-RX pair is on intersecting roads. Higher RSS values are observed when at least one of the vehicles of the communicating pair is closer to the intersection box. If a polygon can be defined comprised of the corners of four building-blocks located on the four corners of the intersection, then any link intersecting that polygon can be considered as LOS. The higher RSS values around the corners are essentially representing these different leg LOS cases. Figure 2.11 shows the median RSS and associated PER of LOS and NLOS links.

Based on our observations on the RSS variation due to relative sender-receiver distance, we classified the RSS samples into three broad categories: the same leg LOS, different leg LOS (across leg or intersecting leg) and NLOS. Figure 2.12 graphs the relative position of these three classes of TX-RX links. And overall required intersection models to capture channel loss behavior in the intersection can be classified as shown in Figure 2.13.

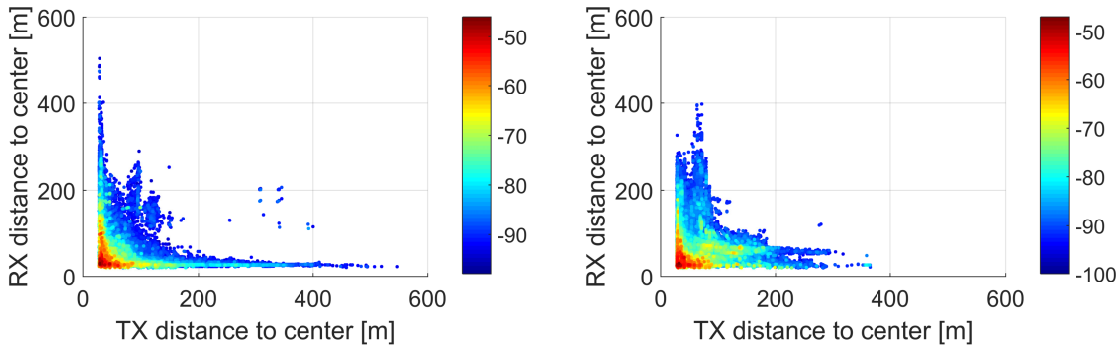

(a) South RX-West TX

(b) South RX-East TX

(c) North RX-West TX

(d) North RX-East TX

Figure 2.10: RSS vs Distance-to-Center of the intersection box for sender-receiver pair on intersecting roads.

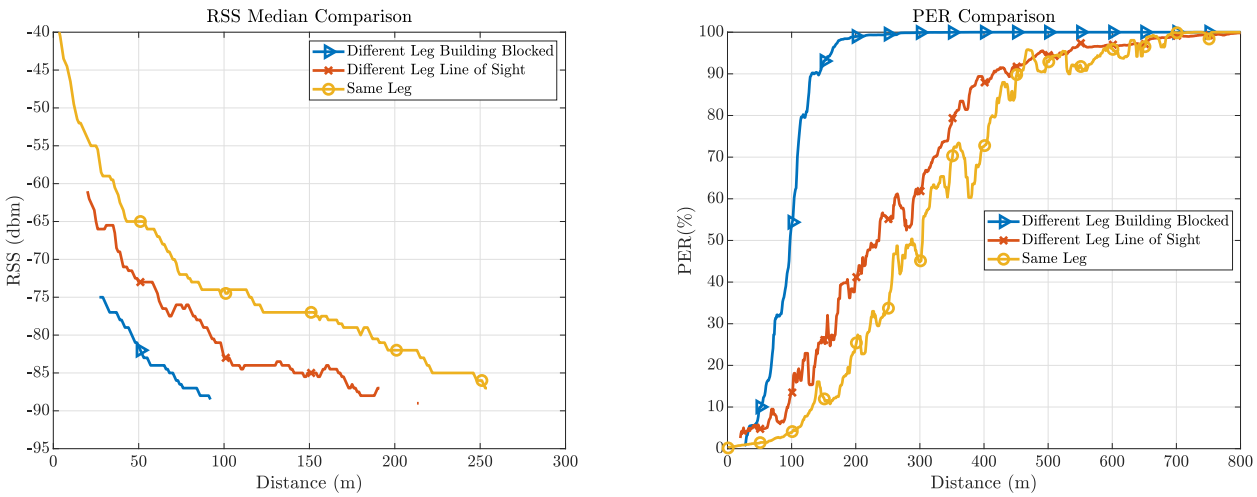

Figure 2.11: RSS Median vs. Distance based on selected scenarios for clustering data.

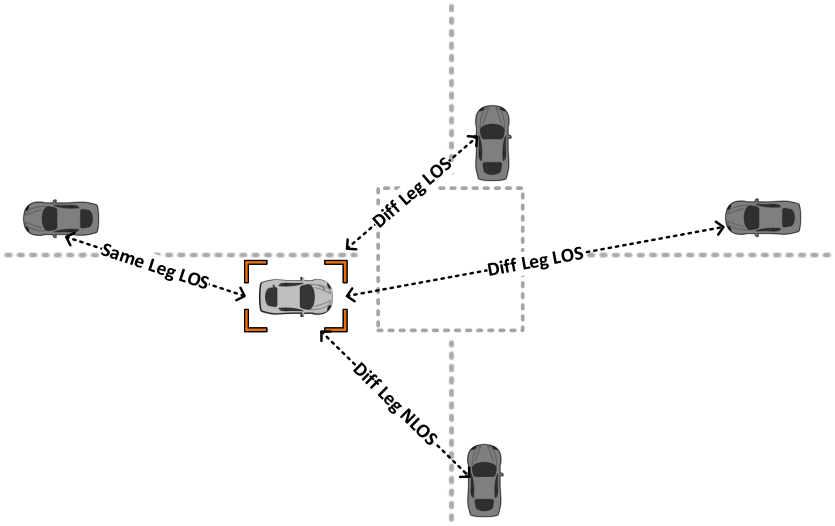

Figure 2.12: Orientation of communication links based on relative positions of the sender and receiver

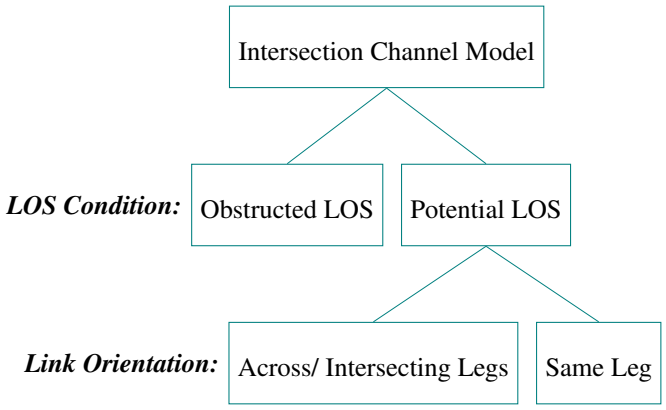

Figure 2.13: Intersection model classification

2.2.4 V2X Channel Propagation Loss Modeling

2.2.4.1 Modeling Approach: Big Picture

The overall flow of the channel propagation modeling can be explained by the steps illustrated in Figure 2.14. As can be seen, after filtering the dataset into different categories based on the insights discussed above, identical methodologies are applied to estimate model parameters for both freeway and intersection channel propagation behavior.

Considering the natural phenomena that deteriorate signals, three models are required to approximate the channel losses: large-scale path loss, shadowing or large-scale fading, and small-scale fading. The logarithmic representation of received signal strength at an arbitrary transmitter-receiver separation distance d can be written as:

$$P_r(d) = P_t - L_{LS}(d) + g_{(P,dB)} + S_\sigma \tag{2.5}$$

where P_t is the transmission power in dB, L_{LS} (d) is the deterministic path-loss at distance d, $g_{(P,dB)}$ is the small-scale fading, and S_σ is the zero-mean shadowing with standard deviation of σ. Large-scale path loss describes the deterministic signal attenuation at a specific distance. Shadowing, in vehicular communications, occurs when the direct path of the propagating signal is obstructed by large objects. Vehicular networks are very dynamic in nature, and thus, shadowing may change rapidly over time, especially in urban settings. Small-scale fading, sometimes referred to as just fading, captures the signal strength changes due to vehicle movements. All these models collectively describe a wireless channel. We can rewrite (2.5) by assuming that the components governing the distribution of RSS samples at a given distance are a composite of a deterministic and a non-deterministic (combining the effects of shadowing and multi-path fading) function. The non-deterministic function is a member of distribution family $\mathcal{M}$. (2.6) and (2.7) are defining the general setting of our modeling technique.

$$X_d = Y_d + \gamma_d \tag{2.6}$$

$$Y_d \sim M(\theta_d) \tag{2.7}$$

where random variable Y at distance d is sampled from distribution $\mathcal{M}$ parameterized on θ. γ_d is the deterministic function acting as a bias at distance d.

In the next few sections, we elaborate on the challenges (and assumptions) of model estimation from a censored dataset and then provide derivation techniques for deterministic large scale path loss and stochastic fading models for such datasets.

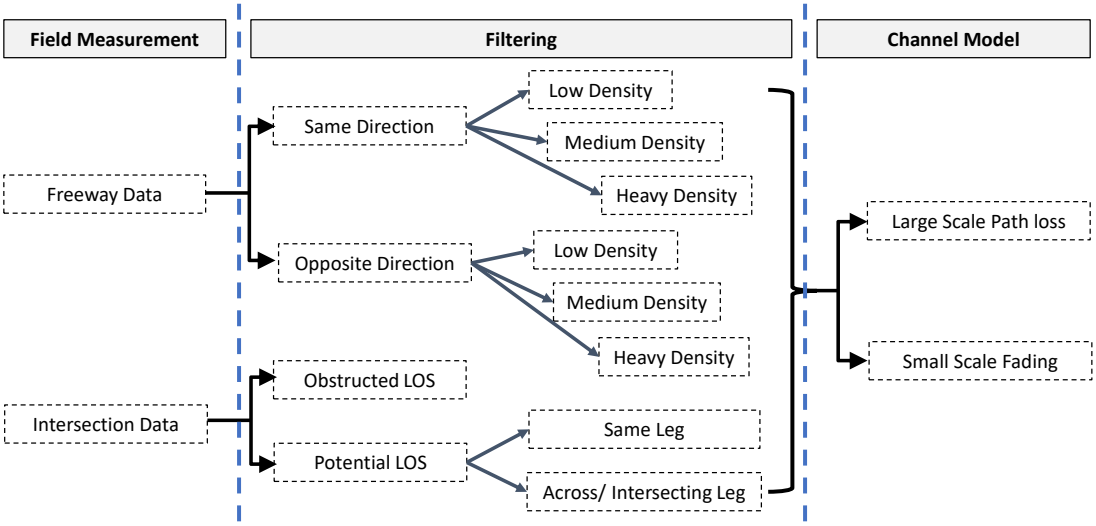

Figure 2.14: Channel propagation modeling steps: from measurement to filtering to modeling. After dataset is classified based on the identified channel loss factors, a parameter estimation technique is used for both freeway and intersection loss models.

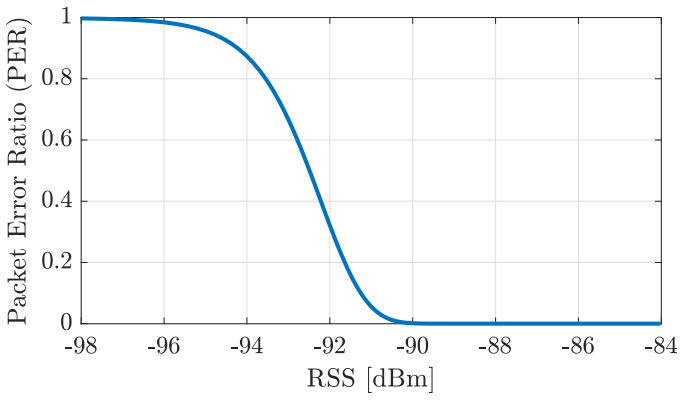

Figure 2.15: RSS versus packet error ratio (PER): all packets having Rx power above -90 dBm are considered successfully received, assuming zero interference from other transmitting vehicles and a noise floor of -98 dBm.

2.2.4.2 Censored RSS Dataset and PER Assumption

Censored data is inherent in the RSS dataset obtained using off-the-shelf DSRC radio devices. Here, censoring occurs due to the operating receiver sensitivity level of the DSRC devices and the decodability of the received messages. RSS samples are only logged if the received signals are above the receiver sensitivity and corresponding messages are successfully decoded. A message's decodability depends on its signal-to-interference-plus-noise ratio (SINR). In this dataset, we assume that the lost messages are due to signal attenuation rather than signal collisions as the number of transmitting vehicles is relatively low. Therefore, we assume no interference from other transmitting vehicles and the thermal noise is determined to be approximate -98 dBm for a 10 MHz channel in 5.9 GHz band. An empirical SINR-versus-PER curve is derived from DSRC hardware experiments in [73], which can be transformed into the RSS-vs-PER curve as shown in Figure 2.15, assuming zero interference from transmitting vehicles. In our model derivations, we use this packet error model to determine the portion of RSS samples that were not correctly decoded and thus, considered missing in the RSS dataset.

2.2.4.3 Large Scale Path Loss Estimation

From the measured data, it is observed that the relationship between RSS and sender-receiver separation distance closely resembles the structure of widely reported two-ray ground reflection

path loss [74] [75]. Therefore, we assume that model for estimating the large scale path loss component, which can be formulated as follows:

$$\gamma(d;\alpha,\varepsilon_r) = 10 * \alpha * \log(4\pi\frac{d}{\lambda}|1+\Gamma_{\perp}e^{i\phi}|^{-1}) \tag{2.8}$$

where α is the path loss exponent, ε_r is a fixed unit-less constant dependent on the reflection medium, and $\lambda = \frac{c}{f}$ is the wavelength of the corresponding transmitted signal with central frequency of f that is propagating in the environment with the speed of c. In the above equation, the reflection coefficient $\Gamma_{\perp}$ can be found as:

$$\Gamma_{\perp} = \frac{\sin\theta - \sqrt{\varepsilon_r - \cos^2\theta}}{\sin\theta + \sqrt{\varepsilon_r - \cos^2\theta}} \tag{2.9}$$

where $\sin\theta = \frac{h_t+h_r}{d_{ref}}$ and $\cos\theta = \frac{d}{d_{ref}}$, with $d_{ref} = \sqrt{d^2+(h_t+h_r)^2}$, are dependent on h_t and h_r which are the heights of the transmitter and receiver antennas, respectively. Furthermore, the phase difference of the two interfering rays, ϕ, can be found as:

$$\phi = 2\pi * \frac{d_{los} - d_{ref}}{\lambda} \tag{2.10}$$

where $d_{los} = \sqrt{d^2+(h_t-h_r)^2}$.

By applying the assumptions made in [46] about the fading parameters having minimal variation compared to path loss and considering (2.6), we can remove the fading component by sub-

tracting the expected value of RSS random variables at neighboring distances. Therefore (2.11) holds true.

$$\begin{aligned} E(X|d_2) - E(X|d_1) &\approx \gamma(d_2;\alpha,\varepsilon_r) - \gamma(d_1;\alpha,\varepsilon_r) \\ &= 10 * \alpha * \log(\frac{d_1}{d_2} * \left|\frac{1+\Gamma_{\perp,d_2} e^{i\phi_{d_2}}}{1+\Gamma_{\perp,d_1} e^{i\phi_{d_1}}}\right|) \end{aligned} \tag{2.11}$$

Although using (2.11) for any arbitrary pair of distinct distances should theoretically yield to an identical value of ε_r, the obtained value may vary for each pair of distances due to the empirical data imperfection. Therefore, statistical mode of the distribution of obtained ε_r values is chosen as the best approximation of the actual value. A similar method is used to determine the value of α which can be derived using Equation (2.11), and using the same reasoning as ε_r, statistical mode of the distribution of obtained values of α is selected as the most accurate approximation of the actual value.

Having different PER values at neighboring distances due to path loss makes estimation of expectation equivalent to estimating the full distribution. Hence, estimating path loss according to (2.11) is only valid when packet loss is minimal. In order to avoid the packet loss problem we can use (2.12). $\dot{p}$ is an arbitrary probability value preferably close to 0.5. Choosing $\dot{p}$ close to 0 or 1 leads to increased presence of noise in percentile estimation.

$$F_X^{-1}(\dot{p};d_2) - F_X^{-1}(\dot{p};d_1) = \gamma(d_2;\alpha,\varepsilon_r) - \gamma(d_1;\alpha,\varepsilon_r) \tag{2.12}$$

Since $F^{-1}(\dot{p}, d_i)$ cannot be estimated for values less than $p_e^{d_i}$, value of $\dot{p}$ should be selected with respect to the following condition.

$$\dot{p} \geq max(p_e^{d_2}, p_e^{d_1}) \tag{2.13}$$

Having samples from $\hat{X}$ rather than X, we can use Eq. (2.14):

$$F^{-1}_{\hat{X}_{d_2}}(p_{d_2}) - F^{-1}_{\hat{X}_{d_1}}(p_{d_1}) = \gamma(d_2; \alpha, \varepsilon_r) - \gamma(d_1; \alpha, \varepsilon_r) \tag{2.14}$$

where

$$p_{d_i} := \frac{\dot{p} - p_e^{d_i}}{1 - p_e^{d_i}} \tag{2.15}$$

we can estimate the path loss with the aforementioned method in case PER is greater than zero and changing with a high rate in a neighborhood as path loss can have a prominent effect in variation of PER.

2.2.4.4 Small Scale Fading Estimation

By removing large scale path loss, we can estimate the fading distribution parameters over the distance. Assuming fading parameters are more consistent over the distance, we expect to observe smoother parameter variations over distance by removing large scale path loss. This property will become handy in cases where the estimation becomes noisy due to a small sample set and additionally will help us in parameter initialization during the optimization process.

To estimate the distribution of RSS, given the distance between transceivers, we have constructed two cost functions. It is crucial for the cost functions introduced to incorporate the em-

pirical PER value. The first cost function is inspired by the conventional Maximum Likelihood Estimator with respect to PER value. We refer to such a method as Censored Maximum A Posteriori (CMAP). The cost function consists of two terms: the first is log-likelihood and the second is an auxiliary regularization term. First, we will discuss the details about the log-likelihood term and explain why a second term might be a necessity for the optimization process.

2.2.4.5 Maximum Likelihood Estimator for Left Censored Samples

Log likelihood is a well-known loss function for estimating distributions from observations. While likelihood function is usually derived from Bayesian framework and often introduced as the log of such probability in order to simplify calculations, it is worth mentioning that log likelihood can also be interpreted as the total number of bits required to describe a set of samples based on a model assuming that the coding scheme is based on minimum length prefix coding [76]. Eq. (2.16) is the log-likelihood function with regards to target distribution family $\mathcal{M}$ parameterized on θ.

$$\mathcal{L}(\theta|y) = \sum_{y_i \in y} \log(f(y_i;\theta)) \tag{2.16}$$

Since the samples are censored, using the loss function defined at Eq.2.16 is not valid. We need to redefine the loss function while considering the censoring function. The sample set likelihood should be maximum with regards to a distribution after being affected by the censoring function. PDF of the observed samples given censoring function according to underlying distribution family

is shown in Eq. (2.17).

$$\hat{f}(y;\theta,\mathcal{E},\gamma) = \frac{f(y;\theta)\mathcal{E}(y+\gamma)}{\int \mathcal{E}(x+\gamma)f(x;\theta)dx} \tag{2.17}$$

where $\hat{f}$ is the PDF corresponding to distribution family $\hat{\mathcal{M}}$, and therefore the defined log-likelihood over $\mathcal{M}$ is as follows:

$$\hat{\mathcal{L}}(\theta|y) = \sum_{y_i \in y} \log(\hat{f}(y_i;\theta)). \tag{2.18}$$

Eq. (2.18) is the result of incorporating the error model.

Using the PER information, we can set a constraint on the parameter space to ensure that the censored distribution has the same PER measure. (2.19) is the function used for the constrained optimization.

$$\pi(\theta;y) = 1 - \int_{-\infty}^{\infty} f(y;\theta)\mathcal{E}(y+pl)dy \tag{2.19}$$

$$\underset{\theta}{\operatorname{argmax}}\, \hat{\mathcal{L}}(\theta|y) \; s.t. \; \pi(\theta;y) = p_e \tag{2.20}$$

Since calculation of $\pi(\theta;y)$ might not be analytically feasible, we simplify the problem by introducing an alternative error model, $\hat{\mathcal{E}}$, shown in (2.21), and modify the sample set accordingly.

$$\hat{\mathcal{E}}(x) = \mathbb{I}(x > t) \tag{2.21}$$

where t is an arbitrary value such that the error model outputs at values above t are close to 1. Consequently, $\hat{p_e}$ can be recalculated as (2.22).

$$\hat{p_e} = \int_{-\infty}^{t} f(y;\hat{\theta})d(y) \tag{2.22}$$

Having the new error model we can remove samples below the threshold from the sample set. Eq. (2.23) is the constraint with regards to the new error model. the new sample set is defined as Eq. (2.24). As t increases we omit the noise on censored density estimation; on the other hand, removing samples from the data set increases the variance in error of estimation.

$$t = F^{-1}(\hat{p}_e; \theta) \tag{2.23}$$

$$\hat{y} = \{y | y \geq t\} \tag{2.24}$$

The modified log likelihood function is sufficient for correctly estimating the censored distribution parameters since it implicitly incorporate Eq. (2.23).

2.2.5 Freeway Model Validation

Figure 2.16 shows the validation results of channel modeling for the freeway dataset.

2.2.6 Intersection Model Validation

Figure 2.17 shows the intersection model validation results as well as the model parameters as a function of sender-receiver separation distance.

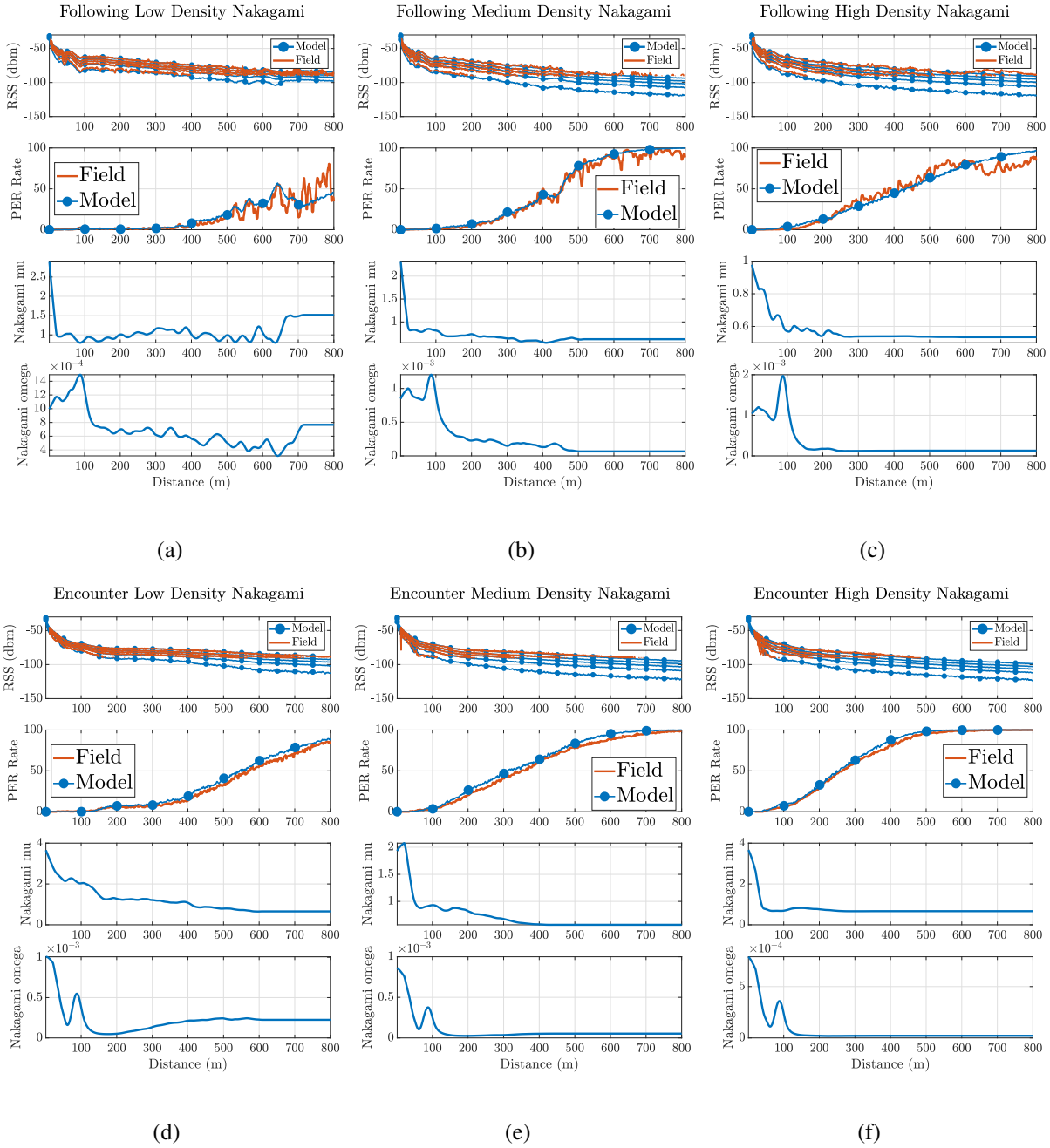

Figure 2.16: Freeway channel modeling validation: first row is the RSS percentiles for each scenario, second row is the PER and the last two rows are corresponding parameters for fading distributions. Nakagami distribution family was selected for fading modeling.

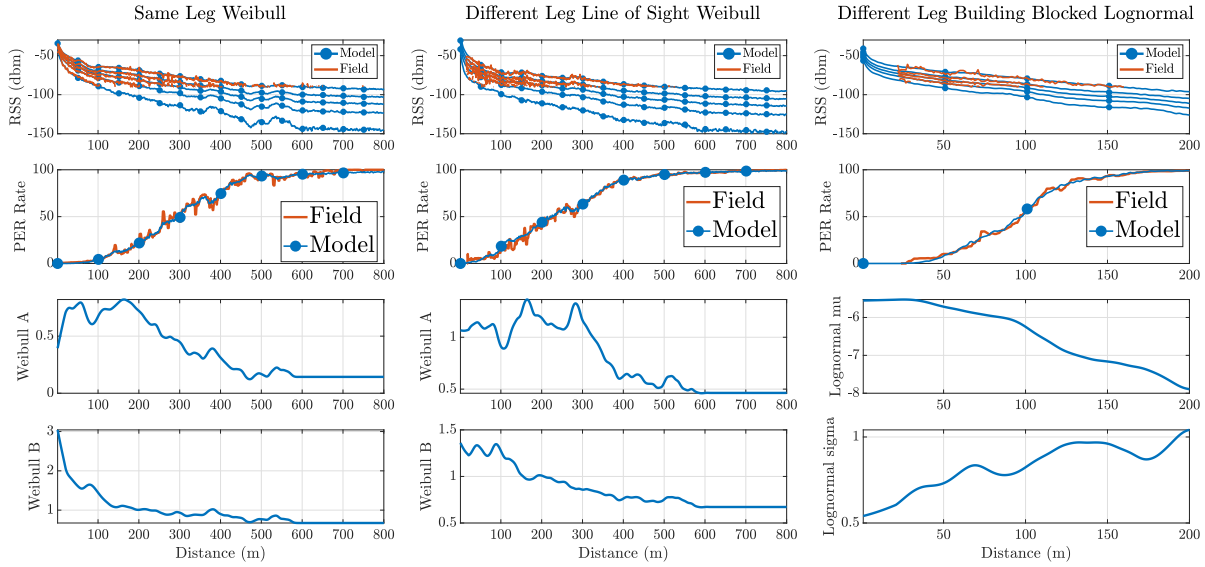

(a) (b) (c)

Figure 2.17: Intersection channel modeling results using log-normal distribution. From left to right, columns show results of the Same Leg LOS, Different Leg LOS and Different Leg Building Blocked (NLOS) channel modeling, respectively. The first two rows are the comparison of RSS percentiles and packet error rate, respectively. The last two rows are parameters of log-normal distribution with respect to transmitter-receiver distance.

CHAPTER 3: SCALABLE V2V COMMUNICATION THROUGH DSRC BASED CHANNEL CONGESTION CONTROL

This chapter evaluates the SAE J2945/1 congestion control [58] algorithm using realistic vehicle mobility and channel propagation models. While some previous research efforts evaluate the overall stability and fairness of the algorithm, this work focuses more on the end goal of scalable communication among entities in a vehicular context. To that end, we present performance evaluation metrics for cases where reliable communication is most needed. The second major contribution is to further analyze the BSM generation rate and transmit power settings to reveal any potential room for improvement in the default parameter settings of the algorithm.

3.1 Overview of the SAE J2945/1 Congestion Control Algorithm

The SAE J2945/1 outlines a feedback loop based adaptive channel congestion control (CC) algorithm that regulates BSM scheduling interval and BSM transmit power. This section provides a brief overview of the CC mechanism including the algorithm inputs, BSM scheduling criteria and the transmit power control logic.

3.1.1 Algorithm Prerequisites

The SAE J2945/1 BSM scheduling protocol requires a set of input parameters to be updated at a predefined interval to adaptively change the inter-transmit interval and transmit power. These parameters are consulted at every BSM scheduling interval ($t_{txCtrlIntvl}$) to make a transmission decision.

- **Vehicle Density (VD):** Each ego-vehicle or host vehicle (HV) keeps track of its surrounding vehicle density by aggregating information from the received BSMs. This quantity is denoted as N_s and essentially computes the number of unique V2V entities within a predefined range (r_{PER}), regardless of their travel direction. At least one BSM needs to be received from each node to be considered in the density calculation. This parameter assists the CC algorithm to have a coarse estimation of the number of transmitting vehicles contributing to the channel load.

- **Channel Busy Percentage (CBP):** Expressed as a percentage, this network layer metric measures the ratio of the time during which the wireless channel is busy (i.e., the energy level is higher than the carrier sensing threshold) to the period of time ($t_{cbpIntvl}$) over which CBP is being measured. If t_{busy} is the measured total busy duration, then CBP can be calculated as follows :

$$CBP = 100 * \frac{t_{busy}}{t_{cbpIntvl}} \tag{3.1}$$

  CBP is considered a local feedback measurement available at every node in the network at any time.

- **Packet Error Ratio (PER):** This metric essentially quantifies the communication channel quality as the time-window based packet loss ratio by determining the number of missed packets at a receiver from a transmitter and the total number of sent packets by that transmitter. The number of the total sent packet is determined from the sequence number of received BSMs.

3.1.2 BSM Scheduling

The SAE J2945/1 states that the host vehicle shall decide at every t_{txCtrl}, time indexed as k, if a BSM update is required to be broadcast based on the following criteria.

- If the vehicle is currently experiencing any critical event such as hard-braking, a BSM is definitely transmitted with the latest vehicle status update.

- Otherwise, the vehicle shall determine the estimated tracking error perceived by the remote vehicles by extrapolating the last sent BSM considering the BSM loss probability as indicated by the channel quality. Depending on the estimated error, a BSM is transmitted probabilistically using the following equation.

$$p(k) = \begin{cases} 1 - e^{-\alpha * |err(k) - T|^2}, & \text{if } T \leq err(k) < S \\ 1, & \text{if } err(k) \geq S \\ 0, & \text{Otherwise} \end{cases} \tag{3.2}$$

where $err(k)$ is the estimated tracking error of the host vehicle perceived by the remote vehicles at $k-th$ BSM schedule interval. T and S are the minimum and maximum bounds for tracking errors, respectively.

- Otherwise, the vehicle shall schedule a BSM based on determined vehicle density N_s within r_{PER}, as follows.

$$ITT(k) = \begin{cases} 100, & \text{if } N_s(k) \leq \beta \\ 100 * \frac{N_s(k)}{\beta}, & \text{if } \beta < N_s(k) < \frac{itt_{max}}{100} * \beta \\ itt_{max}, & \text{if } \frac{itt_{max}}{100} * \beta \leq N_s(k) \end{cases} \tag{3.3}$$

Where β is the vehicle density coefficient that determines the starting point of rate control and defines the slope of rate change. The constraint of itt_{max} ensures that for highly dense traffic conditions, the vehicles will disseminate BSMs to maintain the minimum safety requirement of inter-packet gap.

3.1.3 Transmit Power Control

The SAE J2945/1 BSM scheduling protocol uses transmit power control as a function of channel busy percentage. The system calculates the transmit power based on the latest available CBP (referred to as U in the equation). Raw radiated power (RP) is calculated as follows.

$$f(U) = \begin{cases} RP_{max}, & \text{if } U \leq U_{min} \\ RP_{max} - \\ \frac{RP_{max} - RP_{min})}{U_{max} - U_{min}} * (U - U_{min}), & \text{if } U_{min} < U < U_{max} \\ RP_{min}, & \text{if } U_{max} \leq U \end{cases} \tag{3.4}$$

where U is the current CBP measurement, U_{min} and U_{max} are used to constrain the transmit power to keep channel load within the optimal channel utilization range. Radiated power (RP) is then calculated as follows.

$$RP = RP_{Previous} + SUPRAGain * (f(U) - RP_{Previous}) \tag{3.5}$$

And final transmit power is then determined by accounting for the antenna gain G and cable loss $loss_{cable}$.

$$TxPower = RP - G + loss_{cable} \tag{3.6}$$

3.2 Evaluating the SAE J2945/1 Congestion Control Algorithm

We performed extensive simulations to evaluate the performance of the CC algorithm in a variety of vehicular environments for different levels of traffic density. Communication link performance in inherently dynamic vehicular environments varies significantly. Therefore, it is important to realize the characteristics of the propagation channel for performance evaluation of V2V communication protocols. Capturing realistic vehicle movements are equally important for the legitimate evaluation of performance metrics such as tracking error. A high fidelity simulation platform is thus desired to validate the safety benefits of the standardized CC algorithm.

3.2.1 Simulation Setup

The degree of dependability in VANET simulation experiments relies on the realism of modeled components such as vehicle trajectory, wireless propagation model and the radio model. To that end, we enhanced ns-3 [68], a discrete event network simulator, by incorporating various simulation components derived from an empirical dataset. Received signal strength (RSS) samples from a large-scale field test are obtained to model realistic radio signal propagation in a vehicular context. The RSS measurements are from a carefully chosen freeway region-of-interest on the I-405 in Orange County, CA and a typical sub-urban 4-way intersection, also located in Orange County, CA. Collected RSS samples from the freeway region of interest were broadly classified into three different densities based on available loop-sensor data provided by CalTrans PeMS dataset [72].

Derived channel propagation models further consider the relative direction of the sender-receiver pair, as a significant difference in link quality is observed for the same direction and opposite direction traffic. The large-scale path loss is modeled using two-ray ground reflection [74] with different loss exponents for different traffic density levels in freeway scenarios. In intersection channel models, the path loss exponents vary based on the relative positioning of the sender-receiver pair. While all Tx-Rx links in the freeway (same and opposite direction) and same roads in intersection scenarios are modeled as a function of 2D Euclidean distance between Rx-Tx, the model for intersecting Tx-Rx considers the pair's relative distance from the intersection center. This distinction was made to further realize the effects of the intersection landscape on signal propagation [77], as vehicle pairs on intersecting legs typically have an NLOS or partial LOS. We aimed to validate the CC algorithm using the same physical environments the channel characteristics measurements were collected from. Therefore, vehicle mobility traces were generated for the same road stretches, utilizing a microscopic traffic simulation model calibrated using CalTrans PeMS data. The mobility generation tool is specifically geared to capture the traffic levels at different times of the day, and it enabled us to narrow in to time-period specific vehicle trajectories that match the densities observed during RSS measurement. A high fidelity DSRC PHY model is used in the simulation experiments which was validated against a large-scale field dataset as reported in [78] [79]. The simulation platform used in the validation of the CC algorithm is detailed in Chapter 2. Congestion control settings used in the simulated environments are tabulated in Table 3.1.

Table 3.1: Simulation settings for SAE J2945/1 BSM congestion control

Parameter	Value	Parameter	Value
β	25	itt_{max}	600 ms
RP_{min}	10 dBm	RP_{max}	20 dBm
U_{min}	50%	U_{max}	80%
T	0.2 m	S	0.5 m
α	75	$SUPRAGain$	0.5
G	0 dB	$loss_{cable}$	0 dB
$t_{txCtrlIntvl}$	100 ms	r_{PER}	100 m

3.2.2 Performance Metrics

We evaluate the performance of the standardized CC algorithm in terms of an evaluation metric called information age (IA), and a performance metric called tracking error (TE). These metrics are defined as follows.

3.2.2.1 Tracking Error

At a given time t, the tracking error (TE) at the receiver HV for a particular transmitting remote vehicle RV is the 2D distance difference between the current position estimate of the transmitting RV at HV and the true position of that RV obtained from GPS logs. Since TE sampling is dependent

on the availability of actual position updates, it can be done at most at the sampling rate of GPS updates, which is 10 Hz in our simulation experiments. Vehicle dimension and GPS error are not considered in the simulations, and therefore, TE is only affected by the communication link quality and vehicle dynamics. If t is the GPS time at a certain RV and t' is the last received BSM timestamp from that RV at HV, then the estimated position of the RV at t can be extrapolated over $\Delta t = t' - t$ using the received BSM information as follows:

$$\begin{cases} \hat{x} = \tilde{x} + \Delta t * \tilde{v} * cos(\tilde{\theta}) \\ \\ \hat{y} = \tilde{y} + \Delta t * \tilde{v} * sin(\tilde{\theta}) \end{cases} \tag{3.7}$$

where $(\hat{x}, \hat{y})$ is the estimate of the current position of RV at HV, assuming Cartesian coordinate system and constant velocity model, and $(\tilde{x}, \tilde{y})$ is the latest received BSM position from RV with a speed value of $\tilde{v}$. The tracking error TE can then be calculated as

$$TE_{HV,RV}(t) = d((\hat{x}, \hat{y}), (x, y)) \tag{3.8}$$

where $d(.,.)$ is the 2D Euclidean distance, in meters.

3.2.2.2 Information Age

The information age (IA) at a given time t, at a given HV, is the difference between the timestamp corresponding to the data contained in the most recently received information k_t from a given

transmitting RV and can be expressed as follows.

$$IA_{HV,RV}(t) = t - t_{RV,HV(k_t)} \tag{3.9}$$

where k_t is the index of the most recent data received up to time t, $t_{RV,HV(k_t)}$ is the timestamp corresponding to the data of sample indexed k_t, received from RV at the HV. Figure 3.1 illustrates how IA is calculated over time as BSMs from a certain remote vehicle are being received.

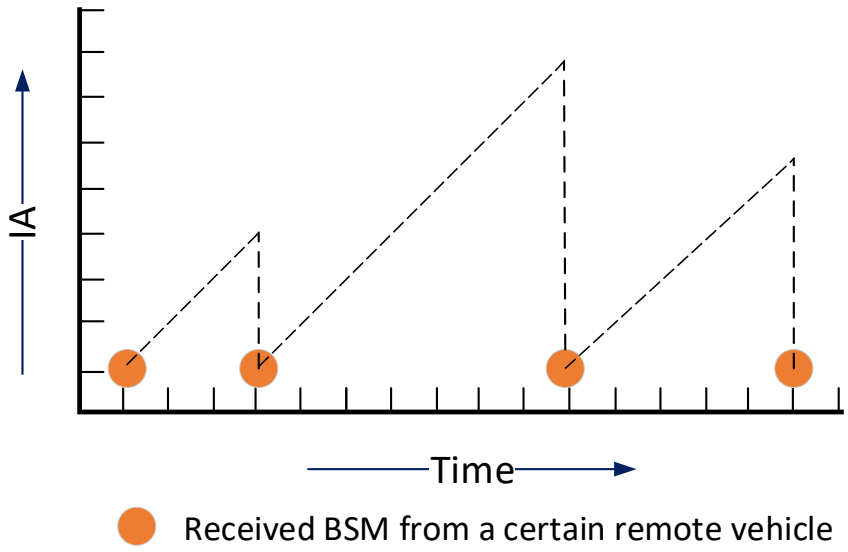

Figure 3.1: IA calculation over time. IA grows from the point a BSM is received from a particular RV, until the next BSM is received form it. Each tick on both axes represents unit time.

3.2.3 Evaluating CC Algorithm in Freeway Scenarios

To evaluate the performance of CC algorithm in freeway scenarios, we simulated a 3.5-kilometer section of the I-405 freeway in Orange County, California, stretched between the I-405/I-605/SR-

22 and I-405/SR-22 junctions (Figure 3.2). This part of the freeway has 16 lanes of traffic consisting of 8 lanes in each direction (including two High Occupancy Vehicle (HOV) lanes in each direction). Realistic vehicle mobility traces are generated using a calibrated micro-simulation mobility tool. The mobility generation tool also enabled us to accurately timestamp the hard-braking events as well as the lane-change maneuvers. The simulated vehicular environments are broadly categorized in light, medium and heavy traffic density and have average vehicle densities of 10, 25 and 50 vehicles/mile/lane, respectively.

Figure 3.2: Highlighted stretch of the I-405 Freeway in Orange County, CA is chosen as our region of interest for freeway RSS measurement, and subsequently used for the validation of the SAE J2945/1 CC algorithm. Source: Google Inc ©

Figure 3.3(a) shows the CBP and transmit power measured at the subject vehicle. It suggests that the transmit power is adjusted adaptively based on the measured channel load. And thus, channel load is kept within the optimal operating range. Figure 3.3(b) shows how the rate is adaptively adjusted based on vehicle density, to regulate the offered load to the channel.

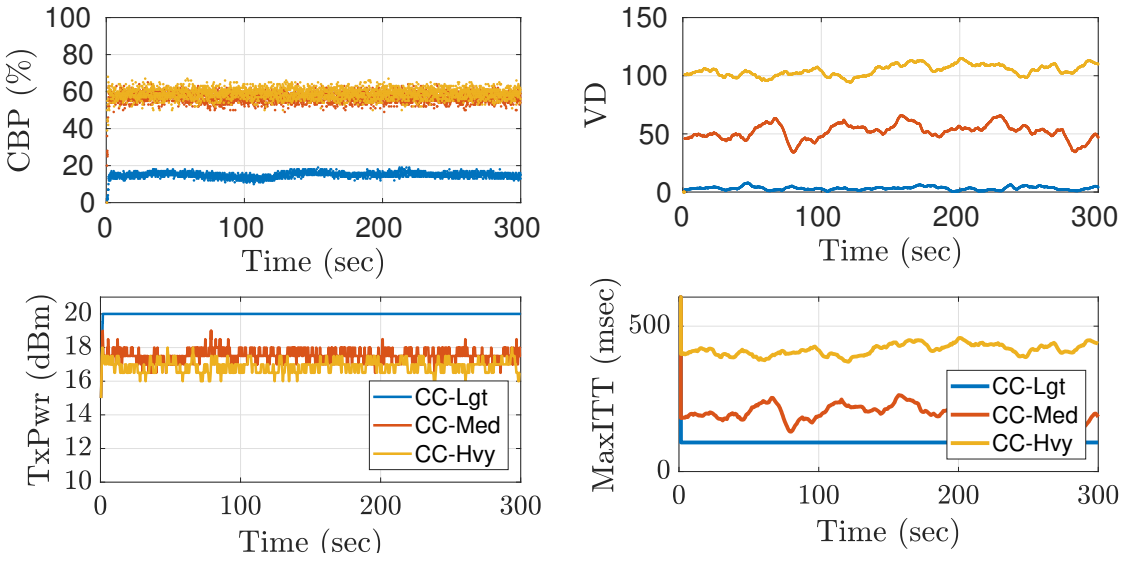

(a) CBP and Transmit Power

(b) VD and Max ITT

Figure 3.3: CBP, Transmit Power, Vehicle Density (VD) in 100 m radius and Max ITT for different traffic density cases.

The collection of performance measures from the simulation logs, as depicted in Figure 3.4, show IA and TE comparisons of the baseline (No CC) and CC algorithm. IA for light and medium densities are similar for both baseline and CC algorithms. When the channel is loaded below the optimal level, the baseline can achieve the same performance as the CC algorithm. When the channel gets congested with BSMs from an increased number of transmitting vehicles, as is the case for the heavy traffic scenario we simulated, IA for CC transmit protocol outperforms baseline. Higher density translates to a higher number of BSM transmission which essentially increases the probability of packet collision over the air. As a result, BSMs from farther ranges have a greater loss ratio compared to the BSMs from closer ranges. This is because the BSMs from a farther distance will attenuate more, resulting in a relatively lower received power at the HV side. CC algorithm keeps the interference level at a minimal level by reducing the BSM scheduling frequency as density increases. In addition, it further adapts the transmit power to limit the interference range. The combined effect of rate and power adaptation results in an improved information age at farther ranges. While IA has a direct relationship with the BSM reception ratio, TE of an RV depends on the corresponding IA and vehicle dynamics. Figure 3.4(b) shows how tracking accuracy of CC compares with baseline. It is observed that, while both the baseline and CC transmit protocols performed well on tracking accuracy, the CC algorithm achieves slightly better accuracy. The performance gain once again has a wider margin at farther ranges.

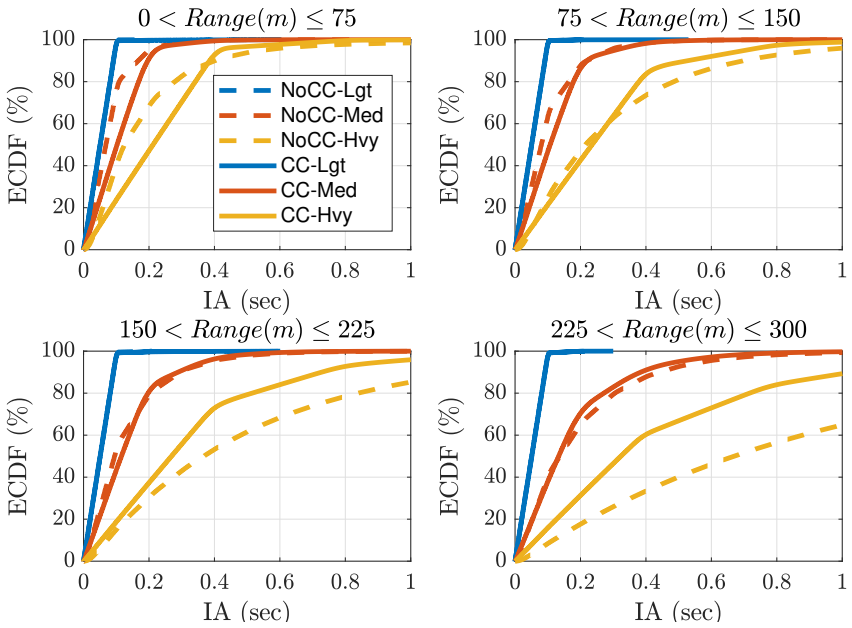

(a) Information Age (IA)

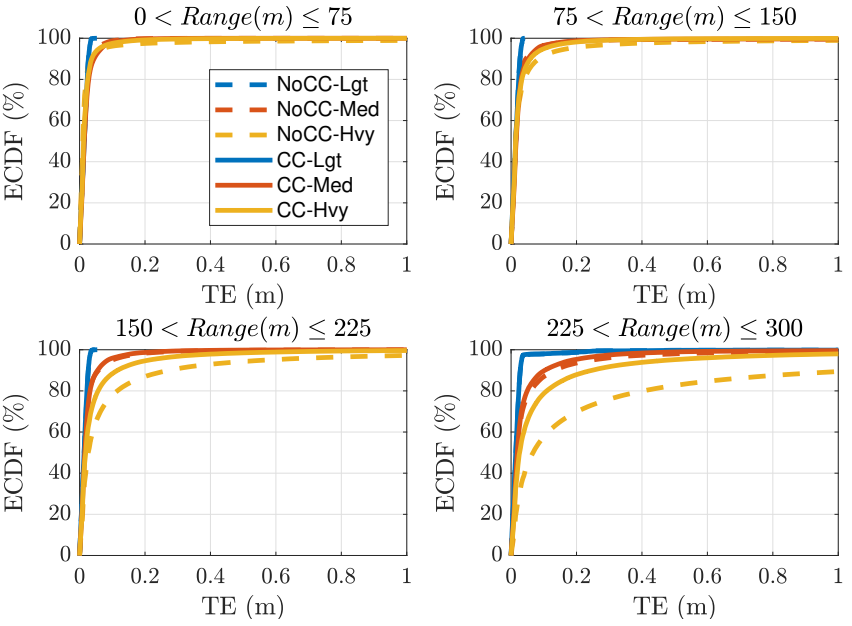

(b) Tracking Error (TE)

Figure 3.4: Performance evaluation of No CC vs. CC in freeway scenarios. Empirical CDFs are calculated for samples pertaining to same direction traffic. The samples are aggregated regardless of the remote vehicle maneuvers.

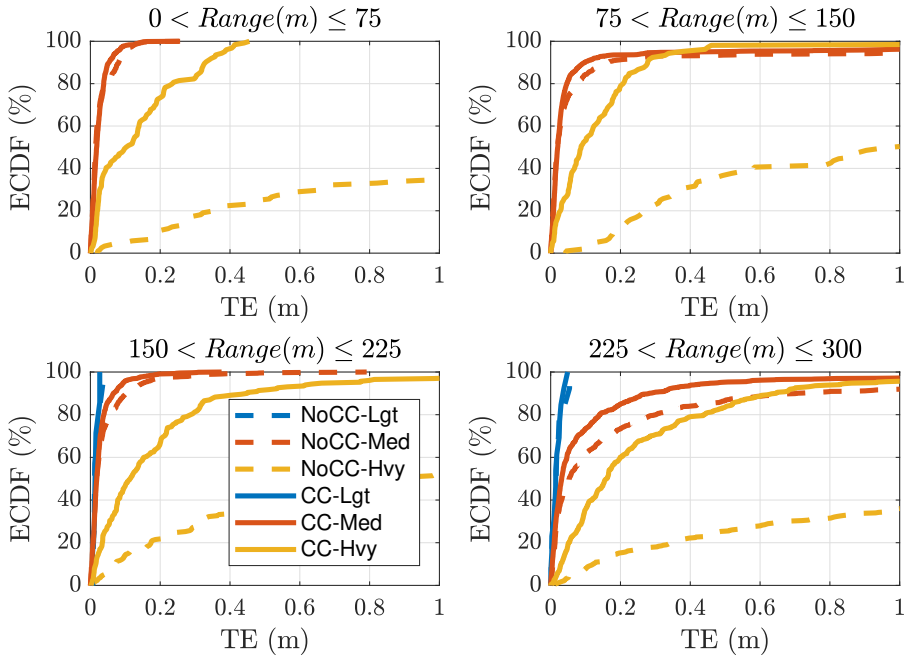

(a) Hard Brake TE

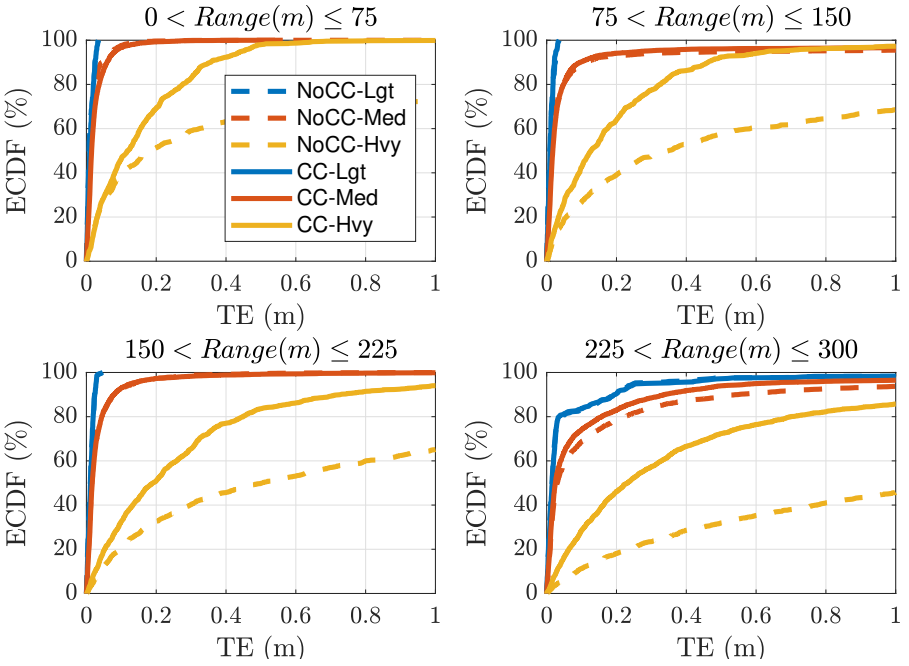

(b) Lane Change TE

Figure 3.5: Tracking errors during hard-braking and lane change maneuvers of remote vehicles.

As mentioned in Section 3.1, the CC algorithm transmits event- and dynamics-driven BSMs to further the situational awareness. A lower generation rate for the guard BSMs ensures that the critical BSMs can get through in a timely manner. Guard BSMs are those BSMs that are transmitted based on the HV node's perceived vehicle density within a predefined range. The microscopic traffic simulation tool we used for generating realistic vehicle trajectories enabled us to timestamp the span of critical events for each vehicle. Using that information we can filter the IA and TE samples for critical event instances. Likewise, lane change maneuvers were also timestamped to further investigate the efficacy of the CC algorithm in improving situational awareness. The tracking performance of the CC algorithm during lane-change and critical event conditions, as shown in Figure 3.5, outperforms the No-CC transmit approach. This substantial gain in tracking accuracy can be attributed to the lower interference levels the critical BSMs experience. Typically, at a given time a small subset of the total participating transmitting nodes engage in hard-brake or lane-change maneuvers. Therefore, the inter-transmit times of this subset go low, while the rest are communicating at higher intervals (guard intervals). The net interference level, therefore, for the time-critical BSMs are low, and that leads to a higher successful receive ratio and eventually, higher tracking accuracy.

3.2.4 Evaluating CC Algorithm in Intersection Scenarios

As mentioned earlier, a representative of the typical suburban 4-way intersections (the intersection of Beach Boulevard and Westminster Avenue in Orange County, CA illustrated in Figure 3.6)

was selected as our evaluation environment. The intersection is characterized by building blocks on each corner, effectively creating a non-line of sight condition for communication vehicle pairs on perpendicular roads. Vehicles on the same leg or the same road generally have line-of-sight, ignoring blockage by vehicle bodies. Due to very different communication link characteristics, we look into performance measures by filtering IA and TE samples based on the relative position of the sender-receiver pair. We also bounded our analysis region of interest (ROI) to 100m from the center of the intersection, as most of the vehicles in this environment are concentrated around the intersection. The ROI-filtered samples are then binned based on the 2D distance of the Tx-Rx pair.

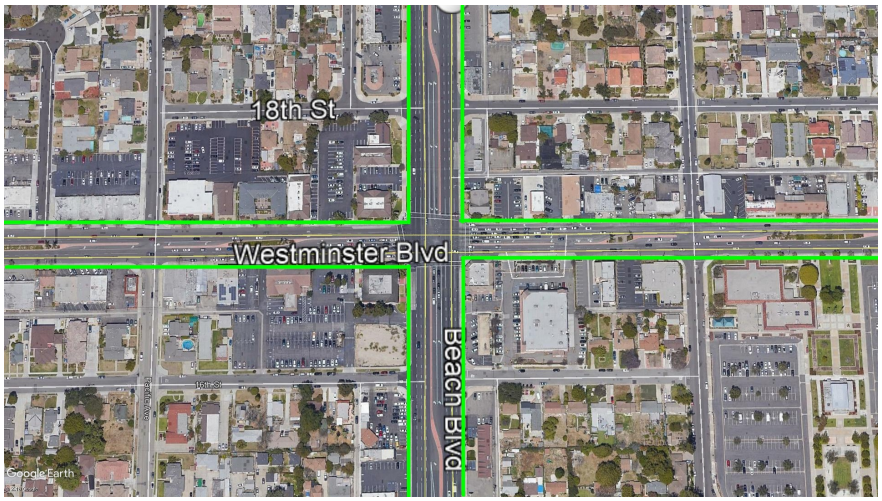

Figure 3.6: 4-way Intersection of Beach Boulevard and Westminster Avenue in Orange County, CA. Source: Google Inc ©

Table 3.2 captures the IA and TE measures for CC and No-CC cases. Note that the range bin size and maximum range are different than the results shown in freeway scenarios. Relative vehicle density in intersection scenarios is relatively low and from a safety application perspective, a maximum ROI range of 150m is deemed to be sufficient in such environments. From Table 3.2,

we observe that, while at closer ranges the No-CC performs slightly better, the obvious benefits of CC are noticeable at farther ranges. It is worth noting that the CC algorithm, by design, allows the perceived tracking error to grow to some extent, by increasing the inter-transmit time as density grows. This helps reduce the interference level and enables BSMs from farther ranges to be received.

Table 3.2: 90-th Percentile IA and TE for intersection scenarios. Results are filtered based on relative positions of sender-receiver pairs on same road and intersecting roads.

Density	Road Type	Range	No-CC IA (s)	CC IA (s)	No-CC TE (m)	CC TE (m)
Light	Same	0m - 50m	0.092	0.131	0.013	0.015
		50m - 100m	0.096	0.157	0.020	0.021
		100m - 150m	0.150	0.187	0.028	0.044
	Intersecting	0m - 50m	0.094	0.135	0.009	0.010
		50m - 100m	0.153	0.218	0.011	0.014
		100m - 150m	0.298	0.365	0.087	0.083
Heavy	Same	0m - 50m	0.218	0.459	0.020	0.064
		50m - 100m	0.445	0.513	0.134	0.184
		100m - 150m	0.929	0.848	0.313	0.276
	Intersecting	0m - 50m	0.253	0.420	0.041	0.139
		50m - 100m	0.758	0.643	0.217	0.206
		100m - 150m	1.775	0.854	3.243	0.589

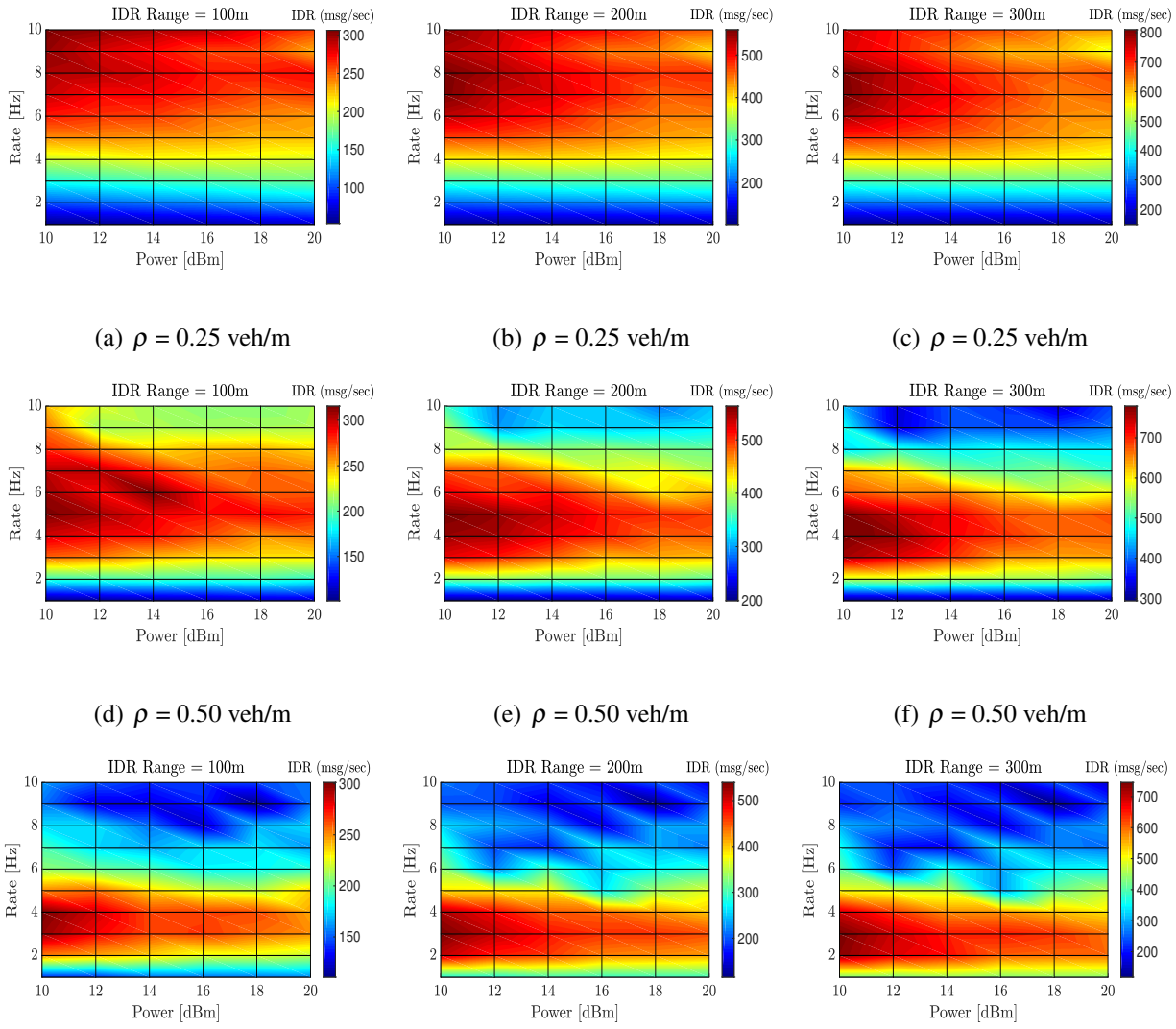

(a) $\rho = 0.25$ veh/m (b) $\rho = 0.25$ veh/m (c) $\rho = 0.25$ veh/m

(d) $\rho = 0.50$ veh/m (e) $\rho = 0.50$ veh/m (f) $\rho = 0.50$ veh/m

(g) $\rho = 0.75$ veh/m (h) $\rho = 0.75$ veh/m (i) $\rho = 0.75$ veh/m

Figure 3.7: IDR vs. Message Rate and Transmit Power (EDT = -82 dBm)

3.3 Optimizing Information Dissemination Rate

In this section, we seek to confirm the adequacy of the default CC parameter settings with respect to the realistic channel propagation model we used in simulation experiments. Since, from the cooperative vehicle communication viewpoint, maximizing the amount of delivered information to the neighboring vehicles is a desired feature, we look into the performance measure referred to as Information Dissemination Rate (IDR) in [66]. This metric is an indication of how well neighboring vehicles can hear each other and quantifies, in vehicular communication context, the number of successfully received basic safety messages (BSMs) by a set of receiving vehicles from a certain transmitter. Typically, V2V applications tend to track a small subset of the vehicles in close proximity, and therefore, IDR measures at a set of target safety ranges are more meaningful. If there are N nodes in the communication range or within the range of interest of a transmitter, IDR can be calculated as follows.

$$IDR = \sum_{i=N/2}^{N/2} SRR(i) \tag{3.10}$$

where $SRR(.)$ is the successful reception rate at the receivers that are located within communication range of the subject transmitter.

Since all transmitting nodes in the DSRC channel use CSMA/CA mechanism for medium access, and assuming similar hidden nodes situation for all nodes, IDR will be similar for all nodes in a homogeneous traffic density scenario. Thus, IDR can be calculated from receiving node's perspective as well, meaning the quantity in (3.10) equates to the number of successfully received

messages by a receiving vehicle in per unit time, from all the transmitting vehicles in range (whole communication range or a range of interest).

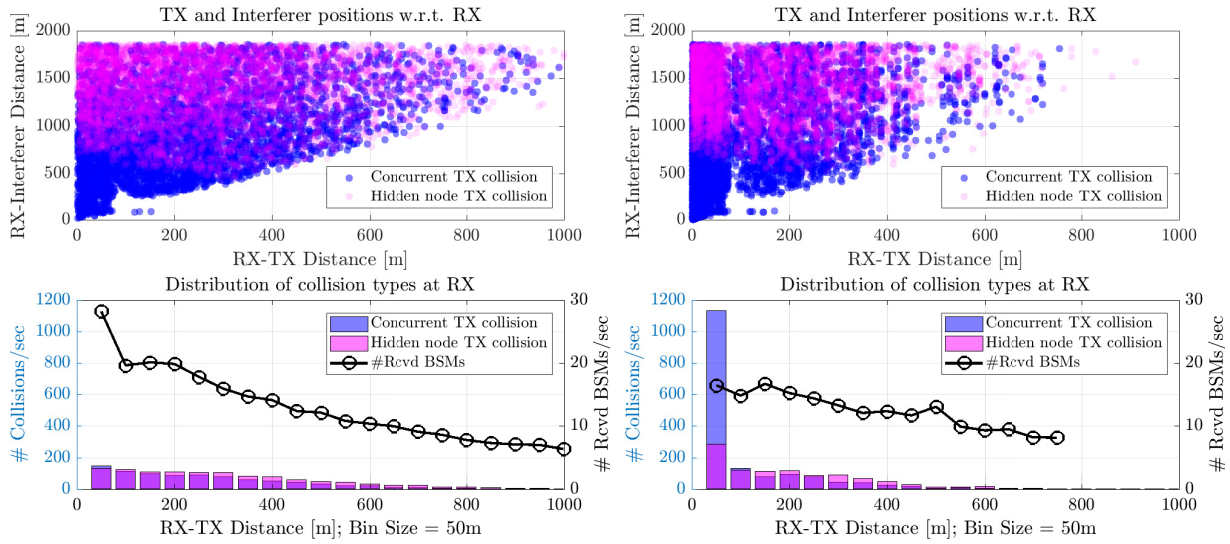

(a) Rate = 2 Hz, Power = 20 dBm

(b) Rate = 10 Hz, Power = 20 dBm

Figure 3.8: Packet collision statistics of all the received packets (from all neighbors in communication range) at the subject vehicle for vehicle density of 0.75 veh/m. Distance of SOI node and interfering nodes are calculated with respect to the receiver node. The right Y-axis shows the number of received BSMs per second at the receiver from different ranges.

Participating vehicles in cooperative safety communications employ broadcast transmit mode which does not have any handshake protocol in place. The only available carrier sensing in broadcast is physical carrier sensing. Therefore, the energy detection threshold (EDT) of the V2V radio devices becomes a determining factor of IDR. Typically, EDT is not configurable at run-time, and mostly depends on the chipset manufacturer, and may vary across chip makers. Furthermore, IDR can be defined over the entire communication range as well as over a range of interest. From vehi-

cle safety perspective IDR needs to be maximized over an application-specific critical range rather than the entire communication range. As a result, the impact of transmit rate and power is required to be analyzed for designing optimal channel congestion management schemes.

The application-layer metric *IDR* depends on the choices of rate and transmit power, thus, has the following relationship:

$$IDR \stackrel{\text{def}}{=} f_{idr}(R,P) \tag{3.11}$$

where R is the set of rate values and P is the set of transmit power values. The end goal of the CC algorithm is to find the optimal combination of these parameters that maximizes the IDR. Thus, we can formulate the objective function of the CC algorithm as:

$$\begin{aligned} &\underset{R,P}{\text{maximize}} \quad IDR \\ &\text{subject to} \quad R_{min} \leq R \leq R_{max},\ P_{min} \leq P \leq P_{max}. \end{aligned} \tag{3.12}$$

where message rate R is bounded between R_{min} and R_{max}, and transmit power P is bounded between P_{min} and P_{max}.

3.3.1 Simulation Study

We analyze different aspects of the IDR metric through simulation experiments. We set up a simulation environment with an 8 kilometer long 1-D roadway. Transmitting nodes are placed with uniform spacing in-between. In the experiments, we vary node density ρ to determine the impact of PHY and MAC layer on IDR. Furthermore, channel load U for a given density is varied

by varying message generation rate R and transmit power P. We set EDT to -82 dBm as found by the hardware test reported in [73]. In this study, we use the channel model derived for heavy traffic condition in freeway scenario, as mentioned in Section 3.2.

3.3.2 BSM Rate, Transmit Power and IDR

To determine how BSM rate (inter-transmit interval), transmit power and IDR are related, we perform simulations for different rate and power settings for varying node density levels. Figure 3.7 shows that a higher BSM rate generally achieves higher IDR when vehicle density is lower. As vehicle density increases, maximum IDRs tend to be achieved at lower message rates. Another observation we made is that for a fixed density, lower message rates improve IDRs at higher ranges. This observation can be explained using the interference characteristics of transmitting nodes.

Handshake RTS/CTS mechanism is not available in CSMA/CA-based cooperative vehicle communication systems as such networks use broadcast transmit protocol. All contending nodes use the same contention window (CW) (assuming similar IP traffic) for channel access in a broadcast which potentially increases the possibility of multiple nodes count down to zero after their respective back-off procedures. This allows multiple transmitting nodes to collide concurrently. This is very commonplace for VANETs as smaller CW_{min} is preferable due to latency requirements of V2X safety applications. Furthermore, the transmitters involved in concurrent packet collisions are usually closely located to the origin of the signal of interest (SOI), which results in a lower SINR for the SOI at the receiver end. Another factor affecting the packet collision rate is the

presence of hidden nodes. This particularly affects VANETs due to high fading and shadowing channels. Typically, nodes that are geographically far apart tend to appear as hidden nodes to each other. The spatial relationship between the SOI and interference signals explains the IDR gain at lower message rates in the congested scenario. SOI is the incoming signal that the receiver is eventually tuned to after preamble detection and frame capture (if any). When the last bit of the SOI arrives at the receiver antenna, it decides whether the total frame can be declared successfully decoded. In our simulator, this is determined using an empirical error rate model which is a function of SINR of the SOI [73]. Figure 3.8 graphs the distances of the interferer nodes to the RX that are deemed hidden to each other. It also shows the distances of interfering nodes that count down to zero at the same time as the SOI node to gain access to the channel. Note that we graph only those interfering node positions, signals from which are above the noise floor (-98 dBm). Packet collisions due to multiple nodes being counted down to zero are referred to as the concurrent collision in this paper. Figure 3.8 shows that when BSM transmit interval is sparse, the number of concurrent collision and collision due to hidden nodes are significantly low. An increase in the BSM rate increases packet collisions of both kinds. Increased concurrent collisions are particularly detrimental for successful packet reception, as transmitting nodes contributing to concurrent collisions are geographically located at close proximity of each other and the SOI node, and therefore, severely impacts the SINR of SOI. In contrast, distances between SOI and hidden nodes are greater, which naturally have a lower impact on the SINR of SOI. The rate control component of the CC algorithm helps reduce the concurrent collisions significantly, which essentially

benefits the upper layer performance metrics in dense traffic conditions. With a lower number of overall BSMs, the number of hidden node collisions is also get reduced.

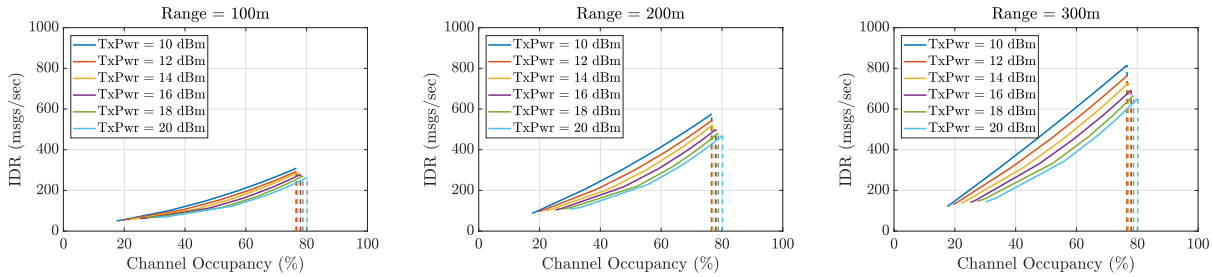

(a) $\rho = 0.25$ veh/m (b) $\rho = 0.25$ veh/m (c) $\rho = 0.25$ veh/m

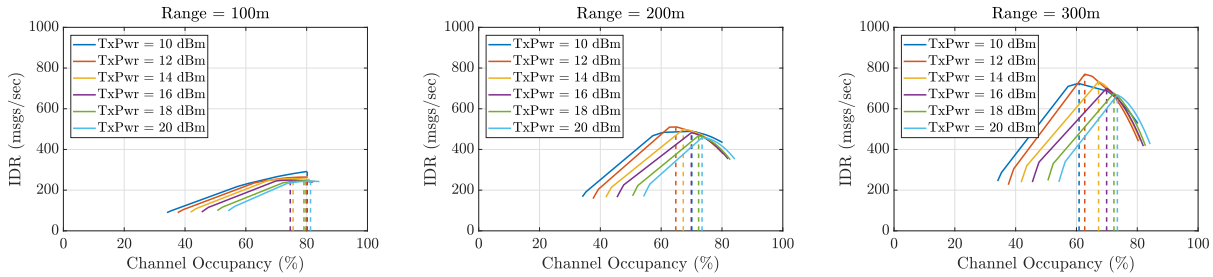

(d) $\rho = 0.50$ veh/m (e) $\rho = 0.50$ veh/m (f) $\rho = 0.50$ veh/m

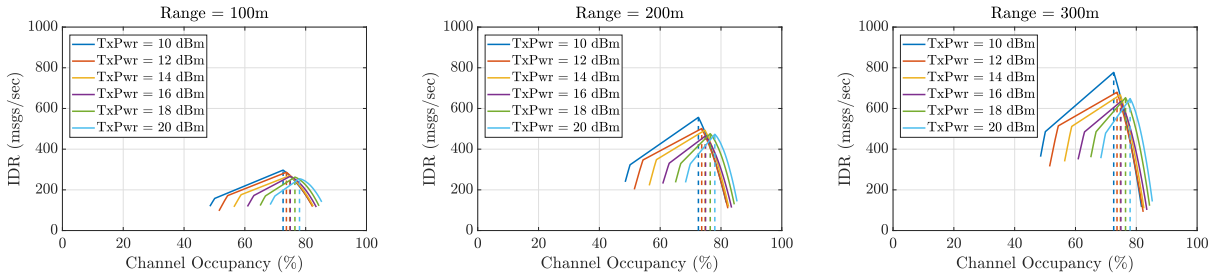

(g) $\rho = 0.75$ veh/m (h) $\rho = 0.75$ veh/m (i) $\rho = 0.75$ veh/m

Figure 3.9: IDR versus Channel Occupancy for different TxPower levels. The vertical lines correspond to each of the TxPower-IDR curve.

3.3.3 Channel Occupancy and IDR

Figure 3.9 shows the IDR measures for different channel occupancy levels for varying vehicle densities of 0.25, 0.50 and 0.75 veh/m. Note the channel occupancy levels corresponding to the maximum achievable IDR. When the channel is under-utilized or saturated, the CBP values associated with optimal IDRs remain similar for individual power levels at different ranges. It is observed that the optimal CBP varies for different IDR ranges, and generally remains within 60%-80%, which suggests that the current settings of minimum and maximum channel utilization in CC algorithm are in good agreement with realistic propagation models derived from field RSS dataset. The current minimum and maximum channel utilization parameters are set at 50% and 80%, respectively.

3.4 Optimizing SAE J2945/1 Congestion Control Parameters

From the simulation experiments using mobility traces obtained from calibrated microscopic traffic simulation tool, we observe that the frequency of BSM transmissions due to higher-order vehicle dynamics or hard-braking events are relatively lower compared to the guard interval triggered BSM exchange. Therefore, most of the channel load is offered by the density-triggered guard messages as defined in (3.3). The CC algorithm set default itt_{max} to 600 milliseconds. However, based on extensive simulation results for different channel conditions, it is observed that the BSM generation rate of 2-3 Hz yields optimal IDR in a highly congested scenario. This observation

calls for further tuning of the rate control component in the CC algorithm. One potential parameter change could set the itt_{max} to the optimal BSM rate value observed; however, doing so will limit the flexibility of accommodating an increasing number of nodes. Therefore, a favorable improvement option would be to adjust the slope of inter-transmit time as defined in (3.3) which defines how the inter-transmit time changes over different density values considering the configured vehicle density coefficient (β) value. A lower β value means a more aggressive inter-transmit time (ITT) changes as the density changes. Figure 3.10 shows the ITT changes for different β values. We performed simulations for a range of β values to see how the tracking accuracy compare over different ranges of interest, as illustrated in Figure 3.11 and Figure 3.12. We observed that a higher density coefficient sacrifices some of the tracking gains at higher ranges while affording better tracking accuracy at closer distances.

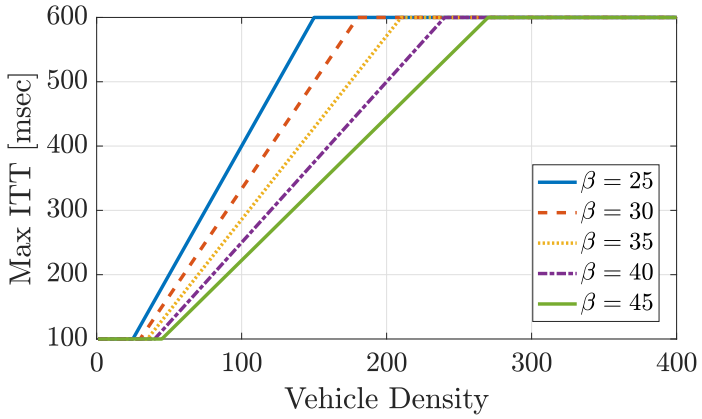

Figure 3.10: Max ITT for different density coefficients (β).

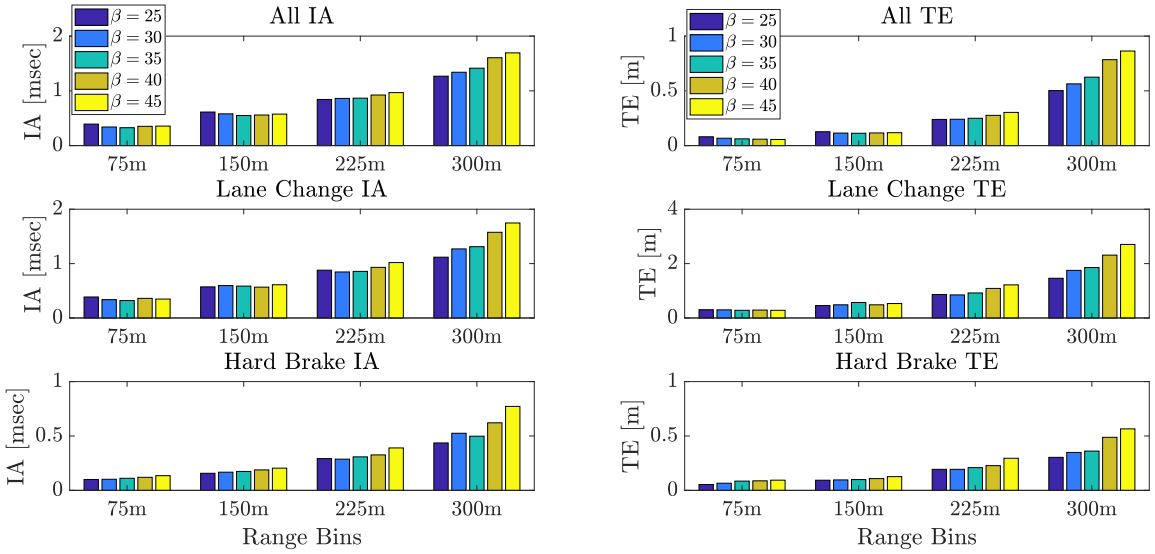

(a) IA

(b) TE

Figure 3.11: 90-th Percentile IA and TE for different choices of vehicle density coefficient (β) in freeway scenarios with heavy traffic.

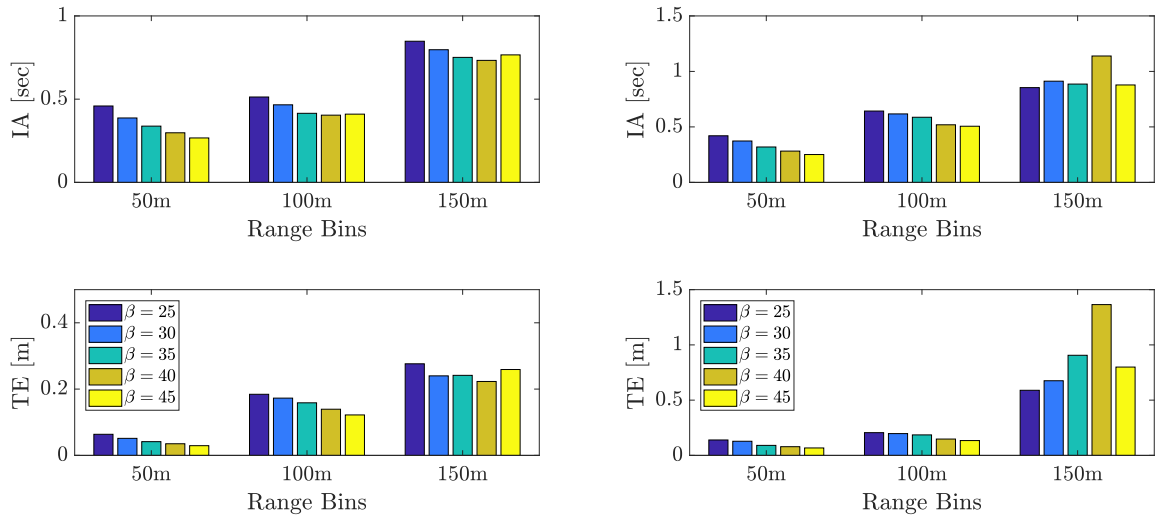

(a) Same Road

(b) Intersecting Road

Figure 3.12: 90-th Percentile IA and TE for different choices of vehicle density coefficient (β) in intersection scenarios.

CHAPTER 4: CONTENT ADAPTIVE V2X COMMUNICATION ARCHITECTURE FOR CONNECTED AUTOMATED DRIVING

[1]This chapter discusses a content-adaptive communication architecture for CAV driving systems where disseminated content information consists of multi-sensor data from onboard sensor suite. The first main contribution of this chapter is a thorough investigation of different message content control approaches in CAV driving systems based on the distances of the mapped objects to the sender vehicle. We demonstrate that including information about vehicles located near the edge of the sensor range is more beneficial to map accuracy than exchanging information about closer vehicles. We believe that this is the first work that investigates into the distance aspect of sharable map objects in a cooperative automated driving system. We also believe that the findings of this work will serve as a guideline for designing map sharing algorithms in cooperative driving systems. The second main contribution of our work is that we study different channel congestion control algorithms based on the adaptation of message length, transmit rate, and a combination of both of these parameters. We determine, by examining the trade-off between message length and transmission rate, that a joint rate-length congestion control offers improvement in terms of the network throughput and the position tracking capability in cooperative vehicle safety systems. We

[1]The work presented in this chapter is based on the following publication: S M Osman Gani, Yaser P. Fallah, Gaurav Bansal, Takayuki Shimizu, *A Study of the Effectiveness of Message Content, Length and Rate Control for Improving Map Accuracy in Automated Driving Systems*, IEEE Transactions on Intelligent Transportation Systems, 2018

evaluate the proposed content control approaches for a variety of traffic densities using a realistic channel propagation model derived from a large-scale field test data.

4.1 System Architecture

The basic components of a relay-based cooperative vehicle communication system are illustrated in Figure 4.1. Each vehicle is equipped with sensing devices such as LIDAR, radar, GNSS receiver, and cameras. Data collected by the sensor suite is fed to a data fusion module that is used to create the situational awareness map (object map) of the vehicle. The map information available at each vehicle can then be exchanged aiming at extending the situational awareness range. This exchange of map information is particularly beneficial to higher-layer applications in making timely decisions. Combining the communicated information with the locally available sensor data enhances the local map even further.

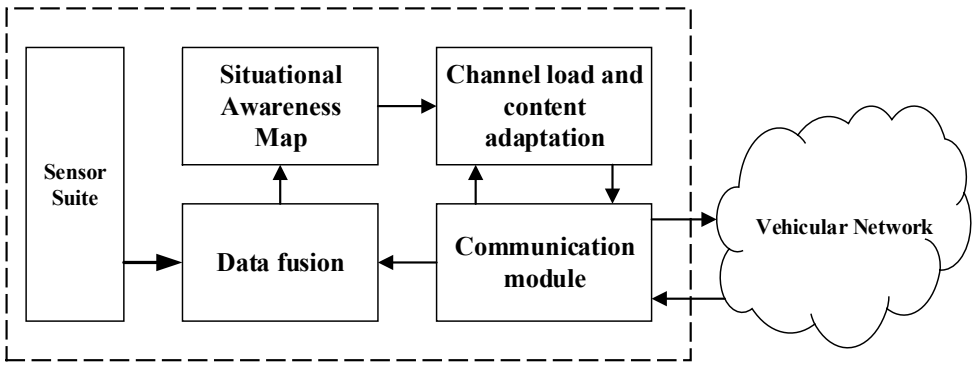

Figure 4.1: Functional diagram of cooperative vehicle communication system.

While sharing the local map data with neighboring vehicles can increase the overall tracking accuracy, the capacity of the communication channel limits the amount of sharable information. To make the communication scalable, aggregated offered load to the channel needs to be controlled using feedback from the network-layer performance metrics such as CBP, PER, and IDR. TABLE I provides definitions of these performance metrics along with others that we use throughout this paper. Generally, any network-layer performance measure Γ in cooperative vehicle safety communications depends on transmission rate, power (or range), and the size of messages broadcast by the vehicles forming the network, and can be defined as a multi-variable function:

$$\Gamma \stackrel{\text{def}}{=} f(R, L, P) \tag{4.1}$$

where $R \stackrel{\text{def}}{=} [r_1, r_2, ..., r_v]^T$ is the vector of transmit rates of v vehicles forming the network of automated vehicles, $P \stackrel{\text{def}}{=} [p_1, p_2, ..., p_v]^T$ is the vector of transmit powers and $L \stackrel{\text{def}}{=} [l_1, l_2, ..., l_v]^T$ is the vector of the transmitted message lengths.

After determining a suitable performance measure as the feedback parameter for controlling the network load, the next direction towards ensuring the effectiveness of the communication protocol is to look at it from the application-layer perspective. In automated driving systems, tracking neighboring objects with high accuracy is of the utmost importance. However, network-layer performance measures may not always be a true indicator of application-layer performance. For example, optimal network performance in terms of throughput can be achieved through a combination of transmit rate, message length and transmit power adaptation, but optimal network performance may not altogether ensure optimal application-layer performance. If we consider position tracking error (PTE) as a performance metric, for example, it not only depends on network performance

but also depends on the exchanged contents, which are not taken into accounts by network layer metrics like CBP, IDR, and PER.

In this work, we adopt *CBP* as the network-layer performance metric for controlling the channel load, and PTE as the application-layer performance metric to evaluate the effectiveness of different scalability approaches. *CBP* is readily available at the DSRC onboard units (OBUs) and this metric provides a fairly good estimation about the channel congestion level. Therefore, *CBP* can be used as a feedback metric in any congestion control approaches that employ message length, transmission rate or power adaptation. On the other hand, the application-layer metric PTE quantifies how good the neighboring vehicles are being tracked by a subject vehicle, which is essentially the single most important metric of interest for vehicular safety applications. Since we focus on the performance evaluation of channel congestion control schemes based on message length and transmission rate adaptation, we keep transmit power fixed, and thus, PTE can be defined as follows:

$$PTE \stackrel{\text{def}}{=} e(\Gamma, C) = h(R, L, C) \tag{4.2}$$

where $C \stackrel{\text{def}}{=} \{C_1, C_2, \ldots, C_v\}$ is the set of the map objects included in the broadcast messages. The dependence of PTE on the content of the exchanged messages cannot usually be quantifiable, and is therefore, proposed in this paper rather heuristically. Once a message content selection scheme is chosen, our next goal is to study the effect of different rate and length control schemes, and

to find out the optimal combination of these parameters that minimizes the PTE. Thus, we can formulate the objective function as:

$$\begin{aligned} &\underset{R,L}{\text{minimize}} \quad PTE \\ &\text{subject to} \quad R_{min} \leq R \leq R_{max},\ L_{min} \leq L \leq L_{max}. \end{aligned} \tag{4.3}$$

where message rate R is bounded between R_{min} and R_{max}, message length L is bounded between L_{min} and L_{max}.

4.2 Channel Congestion Control

In this section, we describe the transmit parameters that a cooperative vehicle communication system can control to achieve scalability. As mentioned earlier, we use *CBP* as the feedback measure to determine the channel condition. Let $CBP = U(R,L)$ denote the channel utilization measured by a vehicle when the message generation rate is R, the message length is L, and the transmit power is assumed to be fixed. Therefore, a specific level of channel utilization can be achieved by controlling message length and rate separately, or by a joint rate/length control. We denote the optimal channel occupancy level, CBP^* which is used by both rate and length control algorithms for convergence. The optimal value for CBP^* used by the algorithms in this paper is ideally around 68% as found in [66].

4.2.1 Message Length Control

Message size is adapted at each iteration t using a descent-based message size-control algorithm proposed in [66] as follows:

$$L_{OPT}^{t} = L_{OPT}^{t-1} + \eta * (CBP^{*} - CBP^{t-1}) \tag{4.4}$$

where L_{OPT}^{t} denotes the message size at iteration t, CBP^{t-1} is the observed channel busy ratio at the end of iteration $t-1$, CBP^{*} is the desired channel busy value that ensures maximum throughput and η is a tunable gain that can be adjusted to ensure convergence of the length control algorithm. The value of η must be selected in a way such that the system does not end up achieving low IDR values. Since the granularity of the message length in the map sharing model is on the scale of an object, and each object consists of several bytes, we simplify (4.4) as follows. If the measured channel occupancy is below CBP^{*}, the number of message items is incremented by one from the last iteration; otherwise, one less item will be included in the next transmission cycle. We also constrain the number of message items to be bounded between L_{min} and L_{max}. Note that L_{OPT}^{t} is the number of map items to be included in the message in addition to a sender's status update. Therefore, if a vehicle requires C bytes to include the self-status update and k bytes for each additional map item, then the size of the message generated at iteration t would be $C + L_{OPT}^{t} * k$ bytes.

4.2.2 Message Rate Control

This subsection describes an adaptive message transmission approach which, instead of using a fixed transmit rate (TX cycle), sends safety messages based on the observed channel load. At each vehicle, *CBP* is measured at the end of a fixed channel monitoring interval τ. To reduce the measurement noise, calculated *CBP* is smoothed out at each iteration t using a first-order auto-regressive, AR (1) technique:

$$CBP^t = \alpha * CBP^t + (1-\alpha) * CBP^{t-1} \tag{4.5}$$

where α is the smoothing factor, and $0 < \alpha < 1$. At the end of each τ interval, a new message rate is calculated for the next iteration using the following control function.

$$R^t = \begin{cases} R^{t-1} * (1-a_D), & \text{if } CBP^t \geq CBP^* \\ R^{t-1} + a_I, & \text{otherwise} \end{cases} \tag{4.6}$$

where a_D and a_I are decrease factor and increase parameter, respectively, and R^t is bounded between some predefined values of R_{min} and R_{max}.

4.3 Message Content Selection

Relay based vehicle communication system is different from basic DSRC communications in that it not only exchanges information containing a status update of individual vehicles, but it also forwards information collected through different sources such as local sensors and communicated

messages. Therefore, in this architecture, any application layer performance metric such as map accuracy or PTE depends largely on the content of the exchanged messages. Message contents can be selected using a multitude of approaches, and since the optimality of a certain approach is difficult to prove in this paradigm, we rely on heuristics. In cooperative ITS, a vehicle can receive messages from all the neighboring vehicles in its communication range; however; from the perspective of safety applications, a subset of these neighboring entities makes up the area of interest for the subject vehicle. This area of interest can be defined in terms of a map radius that the subject vehicle concerns about and therefore, tracks only those of the neighboring vehicles that are in the map radius. Figure 4.2 shows an example orientation of map objects from the viewpoint of a subject vehicle. It also illustrates the sensor range and the map radius form the subject vehicle's point of view. In this illustration, we see that some map objects are located within local sensor range, and therefore, position updates of these objects are available either from the local sensors or from the communicated messages or both of these sources. The position updates of the map objects which are located beyond the sensor range but within the map radius can be obtained from communicated messages only. In this way, map objects can be categorized into two broad classes: a) sensor-sensed and/or communicated objects, and b) only communicated objects.

In this work, we seek to demonstrate how the distances of the included map objects impact the tracking accuracy. With this goal in mind, we consider three different content control schemes, as illustrated simplistically in Figure 4.3. The inclusion weight function g_1 assigns equal weights to all objects in the map radius. For objects located in the sensor range, g_2 prefers closer ones, while g_3 assigns higher inclusion weights to farther objects. In this subsection we provide formal

description of the content control strategies depicted in Figure 4.3. For analysis simplicity, we consider the deterministic variants of g_2 and g_3. This means that instead of computing probabilistic inclusion weights, map objects are sorted according to their distance to the sender.

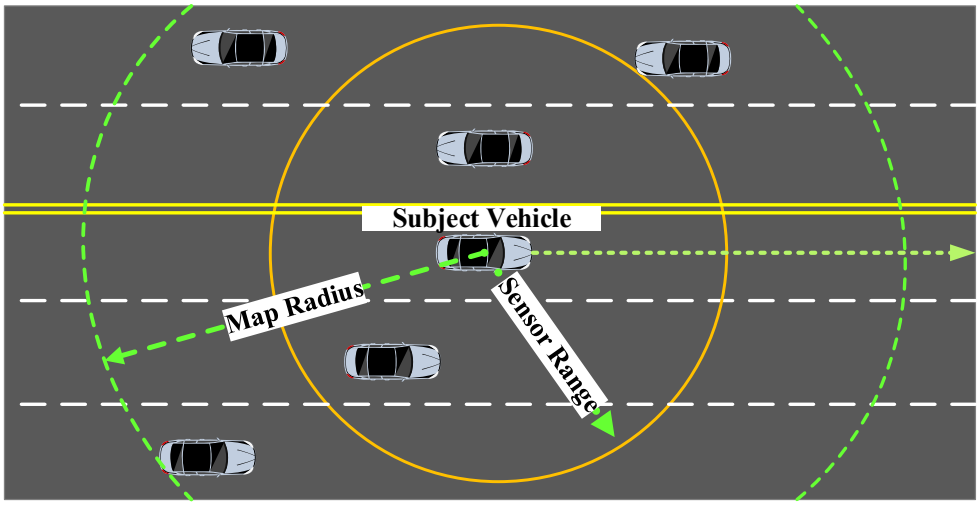

Figure 4.2: Example orientation of map objects with respect to the subject vehicle.

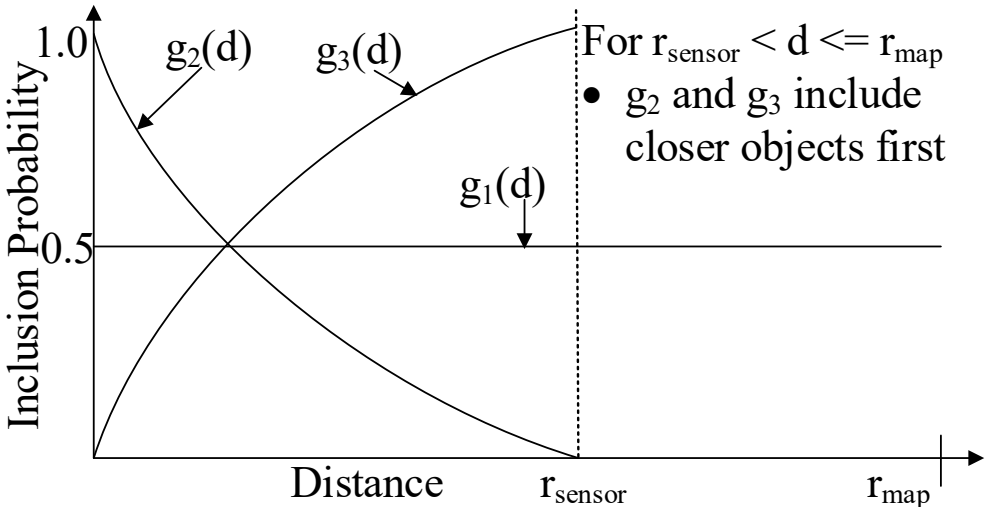

Figure 4.3: Content control options based on the distance of mapped object to the sender.

Algorithm 1 Baseline Content Selection

Require: Number of objects to fill Msg (N_{Msg}), Object map (map)

Ensure: Fill Msg with N_{Msg} objects from the map

1: **if** $N_{Msg} > size(map)$ **then**
2: Include all the map objects into Msg
3: **else**
4: Randomly shuffle objects of the map
5: **for** $i = 0 \rightarrow N_{Msg}$ **do**
6: Include object i from the shuffled map into Msg
7: **end for**
8: **end if**

4.3.1 Baseline

The map object inclusion scheme which we name baseline is depicted as the function g_1 in Figure 4.3. In this scheme, all objects located in the map radius of the sender are given equal priority, and thus, objects are selected uniformly w.r.t. their distance. The baseline content selection approach is motivated to determine whether distinguishing map objects based on their distance affects tracking accuracy. Baseline content selection is detailed in Algorithm 1. The algorithm requires the number of message objects N_{Msg} which is determined by the length adaptation procedure outlined in Section 4.2. In lines 1-2, the algorithm checks the map size against N_{Msg}. If N_{Msg} is smaller than the map size, the algorithm trivially includes all map objects into the message. If

N_{Msg} is greater than the map size, map objects are randomly shuffled in line 3, and then N_{Msg} count of objects are included in the message iterating over the shuffled map list (lines 5-7).

Algorithm 2 Closer Objects First (COF) Content Selection

Require: Number of objects to fill Msg (N_{Msg}), Object map (map)

Ensure: Fill Msg with N_{Msg} objects from the map

1: **if** $N_{Msg} > size(map)$ **then**
2: Include all the map objects into Msg
3: **else**
4: Sort the subset "1" of map objects that are within the sensor range in ascending order according to their distance to the sender vehicle
5: **for** each object obj in subset "1" and in sensor range & $size(Msg) < N_{Msg}$ **do**
6: Include obj into Msg
7: **end for**
8: Sort the subset "2" of map objects that are beyond the sensor range in ascending order according to their distance to the sender vehicle
9: **for** $i = 0 \rightarrow N_{Msg} - size(Msg)$ **do**
10: Include object i from the sorted map subset "2" into Msg
11: **end for**
12: **end if**

4.3.2 Closer-Objects First (COF)

The weight function for including map objects graphed as g_2 in Figure 4.3 is a non-increasing function of distance which can be described as follows:

$$Pr_{inclusion}(d) = e^{-k*d} \tag{4.7}$$

where d is the object's distance to the sender and $k > 0$. A content selection approach of this form includes "closer objects first" into the outgoing messages, and hence, we name this approach closer objects first (COF). This algorithm is motivated by the objective to determine whether the tracking capability is increased by the inclusion of closer objects that have a higher degree of certainty in terms of position updates at the subject vehicle. Position updates from closer objects are available from local sensors as well as the communicated messages. Furthermore, communication links for these entities are highly reliable because of their close proximity to the subject vehicle.

Algorithm 2 details the object selection strategy of COF which, similar to the baseline algorithm, requires N_{Msg} as input. In lines 1-2, COF trivially includes all map objects if the map size is smaller than N_{Msg}. Otherwise, line 4 sorts the map elements in the sensor range in increasing order of distance from the vehicle. In lines 5-7, the algorithm iterates over the sorted list to include object into the message as long as there is room. After iterating over all the objects in the sensor range, if the number of included objects is still smaller than N_{Msg}, the algorithm, in line 8, sorts the list of map objects located beyond the sensor range in increasing order of distance. In lines 9-11, the algorithm fills up the remaining empty spots in the message by iterating over this sorted list.

4.3.3 Farther-Objects First (FOF)

In "farther objects first" or FOF approach shown in Figure 4.3 as g_3, map objects located near the edge of the sensor range are assigned higher priorities during inclusion into the message, and can generally be formulated as a non-decreasing function of distance, as follows:

$$Pr_{inclusion}(d) = 1 - e{-}k * d \tag{4.8}$$

where d is the object's distance to the sender and $k > 0$. In a typical vehicular communication scenario, the message loss ratio for farther vehicles is higher than that of the closer vehicles. Generally, a higher message loss ratio contributes to the decrease in tracking capability. If objects located near the edge of the sensor range are included in the outgoing messages, some of the recipients of those messages will find the information useful as the included objects are farther from the sender vehicle. Therefore, the included map objects for FOF are those physically located even farther away from a receiver subset. Because of the fact mentioned above, the FOF approach selects objects from the edge of sensor range first. If there is still room for more map objects in the message, after including all objects located in the sensor range, the algorithm employs a closer-objects-first policy for the objects beyond the sensor range. Algorithm 3 describes the FOF approach in detail. The selection procedure of map objects is similar to COF except for the sorting order of map items located in sensor range. While COF sorts the object list in increasing order of distance, FOF sorts them in decreasing order to allow farther objects to be included first.

Algorithm 3 Farther Objects First (FOF) Content Selection

Require: Number of objects to fill Msg (N_{Msg}), Object map (map)

Ensure: Fill Msg with N_{Msg} objects from the map

1: **if** $N_{Msg} > size(map)$ **then**
2: Include all the map objects into Msg
3: **else**
4: Sort the subset "1" of map objects that are within the sensor range in descending order according to their distance to the sender vehicle
5: **for** each object obj in subset "1" and in sensor range & $size(Msg) < N_{Msg}$ **do**
6: Include obj into Msg
7: **end for**
8: Sort the subset "2" of map objects that are beyond the sensor range in ascending order according to their distance to the sender vehicle
9: **for** $i = 0 \rightarrow N_{Msg} - size(Msg)$ **do**
10: Include object i from the sorted map subset "2" into Msg
11: **end for**
12: **end if**

4.4 Experiment and Evaluation

To evaluate the performance of the content control schemes, we use ns-3 [68], a discrete-event network simulator. ns-3 enables the simulation of both the communication and the application aspects of cooperative driving systems. The presented content control schemes are evaluated based on actual position tracking error (PTE) which is defined as the 2D Euclidian distance between the estimated position and the actual position of a simulated vehicle. The estimated position of a vehicle at each PTE calculation cycle (every 100 milliseconds) is determined by extrapolating its position from the local situational awareness map data which consists of the sensor and communicated information. The actual instantaneous position is obtained from the mobility model of the simulated vehicles. In the DSRC-enabled communication architecture used in this paper, we assume that all vehicles are equipped with the GNSS receiver (as required by upcoming V2X standards). The positioning information (position, speed, heading, time) of the subject vehicle is derived from the GNSS receiver information and included in the exchanged BSMs. Whenever a BSM is received from a neighboring vehicle, the situational awareness map updates the corresponding neighboring vehicle information with the positioning information contained in the received BSM. The BSM information, in turn, is used for estimating the vehicle position in the simulation. We use 95-th percentile PTE as the evaluation metric, which is the value below which 95% of the tracking error observations are found. 20-meter distance bins and 5-second time bins are used in the figures. Also, measurements collected during the first 5 seconds were not considered in the computation of

any performance metrics as we allowed the congestion control algorithms to converge first. As a result, all the distance-plots start from 20 meters while the time-plots start from 10 seconds.

4.4.1 Simulation Setup

Two road topologies are used in the simulations as shown in Figure 4.4. The first one is a circular roadway, as illustrated in Figure 4.4(a), which has three lanes in each direction with the outermost lane having a 650-meter radius. In this road topology, the simulated vehicles have constant heading change over time, which makes it a good road scenario to evaluate the tracking performance of the presented algorithms. The second road topology used in the simulation is a 4-kilometer long highway, as depicted in Figure 4.4(b), which has three lanes in each direction and a winding segment in the middle with a 40-meter radius of curvature. The vehicle trajectories for this highway scenario are produced by using the traffic simulator Simulation of Urban Mobility (SUMO) [80] with the modifications detailed in [81]. The extracted vehicle trajectories from SUMO for this road topology consist of realistic lane change maneuvers in a typical highway scenario. Furthermore, the sharp curvature of the road poses a real challenge for vehicle safety applications that require precise tracking estimations. Therefore, we also deem this road topology an ideal traffic scenario for evaluating the tracking performance of the discussed content control schemes. In both road topologies, the average speeds of the vehicles are 17 m/s, 18 m/s, and 19 m/s from the slowest (rightmost) to the fastest (leftmost) lane, respectively.

(a) (b)

Figure 4.4: Road topologies used in the ns-3 simulations; (a) Circular Roadway, (b) Winding Roadway

In order to evaluate the content control approaches, a propagation loss model is derived from a large-scale field test conducted by the Crash Avoidance Metrics Partnership (CAMP) Vehicle Safety Communications 3 (VSC-3) Consortium, in partnership with the United States Department of Transportation (USDOT). This data collection campaign was a part of the V2V safety communications scalability activity of the Interoperability Issues of Vehicle-to-Vehicle Based Safety Systems (V2VInteroperability) Project. In this derived propagation model, the two-ray interference model [74] is used for modeling the deterministic, large-scale path loss component. This pathloss model has recently been validated for vehicular networks and takes into account the interference caused by a single ground reflection ray at the receiver. Similar to most studies in the literature, the random, small-scale fading component of the wireless channel is modeled assuming a Nakagami-m distribution (for fading amplitude in linear units) [38]. The Nakagami distribution can model a wide range of small-scale fading scenarios from the strong line-of-sight (LOS) and Rician-distributed fading ($m > 1$), to non-LOS and Rayleigh-distributed fading ($m \leq 1$). The MAC protocol used in the simulations is carrier-sense multiple access with collision avoidance (CSMA/CA) with the quality of service (QoS) based contention mechanism called enhanced dis-

tributed channel access (EDCA). A higher fidelity DSRC receiver model proposed in [78] is used as the physical layer (PHY) model which provides an implementation of packet preamble decoding and frame capture features available in modern network chipsets. The derived channel propagation model and the receiver model have been validated in [78] against the large-scale data set collected by CAMP in the data collection campaign mentioned above.

The DSRC-enabled vehicles in the simulations are configured as follows. The core content of a BSM containing the self-status update of a vehicle requires 204 bytes, while each map entry requires an additional 68 bytes. The packet fragmentation threshold is set to 2346 bytes as per the IEEE 802.11 standard [69]. The maximum number of message items L_{max} is set to 29 which amounts to a total message length of 2242 byte including the core BSM contents and the headers for transport, internet, and data link protocols. The value of L_{max} is chosen such that the total message length remains smaller than the fragmentation threshold. To isolate the effect of communication loss on the tracking accuracy of the simulated vehicles, we make the simplifying assumption that each vehicle is equipped with such a sensor that can detect all objects located within its sensing radius, meaning that no real-life events are considered like occlusion, badly set thresholds or other sources of typical sensing errors. In this way, the possibility of any error sources from local sensors contributing to the calculated tracking error is restricted. We assume that this hypothetical sensor can detect objects in the range of up to 120 meters. We recognize that a sensor does not necessarily pinpoint an object at a distance close to its detection range; however, the hypothetical assumption we made about detecting all objects within the sensor range does not affect the content selection schemes presented in this paper, because the sensor range is used as a configurable parameter in

the algorithms, and the content control part of the algorithms selects map objects that are assumed detected. Furthermore, the main objective of this work is to determine the impact of inter-vehicle communication on map accuracy. For further details on map information representation, an interested reader is referred to [65]. In the simulations, we use a map radius of 300 meters which is sufficient for the anticipated vehicle safety applications [58, 82, 83]. Other simulation parameters are summarized in Table 4.1.

Table 4.1: System parameters used in ns-3 simulations

Parameter	Value	Parameter	Value
Carrier Sense Threshold	-94 dBm	Contention Window (min)	15
CBP^*	68%	MAC Queue Size	1
Transmit Power	15 dBm	L_{min}, L_{max}	0,29
Minimum Message Rate (R_{min})	1 Hz	Max Allowed Message Rate (R_{max})	10 Hz
Rate Decrease Factor	0.15	Rate Increase Constant	0.3

We performed simulation tests for three different vehicle densities: 25, 125 and 250 veh/ km. The first two vehicle densities were simulated for 100 seconds, while the third one was simulated for 60 seconds as we deemed these simulation durations sufficient enough to gather meaningful statistics about the tracking aspects of the experimented road topologies. Generally, for a higher vehicle density like 250 veh/km, a shorter simulation time than that of the lower vehicle density scenarios (25 veh/km or 125 veh/km) can gather a reasonable amount of statistics since the total number of exchanged BSMs are higher due to higher vehicle density. Since we evaluate the

performance of different congestion control schemes in terms of map accuracy, and the map accuracy depends on the content of the exchanged messages, we start with investigating the impact of content control approaches on PTE.

4.4.2 Effect of Message Content Control

To analyze the impact of the content selection schemes on the tracking accuracy, we performed tests for all three content-adaptive approaches outlined in Section 4.2.2. Message length adaptation was enabled during these tests to keep the channel utilization at the optimal level. Note that enabling the length adaptation does not skew the performance of the content control schemes because it runs independently, and determines the same message length values for all content control schemes. Figure 4.5 - Figure 4.7 show the 95-th percentile PTE for different traffic densities. The first observation from the figures is that both COF and FOF show a lower tracking error, compared to the baseline scheme. The consistent poor tracking accuracy of the baseline scheme is due to its indifference to the proximity of included objects, and therefore, this scheme includes objects from the communicated information with the same level of priority as sensor-sensed objects. Furthermore, in the baseline scheme, objects are selected randomly from the local map which can lead to situations where some objects would not be included in the outgoing messages by any vehicles in an arbitrary road topography. In contrast, COF and FOF select objects, depending on the distribution of vehicles, in such a way that information of all vehicles in any given area are relayed. To illustrate how information in a road scenario propagates, we consider a one-dimensional road

topology as shown in Figure 4.8, where a sender picks objects from either side of its current location to include in the message. Let the x- position of the vehicles on that road be stretched from -20 to 20, and hypothesize that there is a vehicle at each discrete x-position; the sensor range is hypothesized to be 5 and each message has room for 2 objects. Fiugre 4.9 shows the x-position of included objects and the number of times each vehicle positioned at x is chosen by neighboring vehicles to be included in their outgoing messages. As can be seen, both COF and FOF ensure that all objects are included at least once. In contrast, information about some map objects is not shared at all in the baseline scheme, which is why it shows a lower map accuracy than COF and FOF. This issue about the baseline scheme is compounded when messages are exchanged at lower rates. Figure 4.5 shows the 95-th percentile PTE for a vehicle density of 25 veh/ km with a maximum allowed message rate of 10 Hz for circular and winding roadways. Since vehicle density is low in this traffic setting, the channel is likely to be less congested and allows for more successful reception, which in turn increases the tracking accuracy. Furthermore, channel load remains within the optimal channel utilization range when the network is lightly loaded, and all exchanged messages include L_{max} objects. Therefore, the difference in tracking performance depends solely on the content control scheme. In fact, in low vehicle density, both COF and FOF show similar performance when $N_{Msg} \gg N_{Rng}$, where N_{Msg} is the number of objects in the communicated messages, and N_{Rng} is the number of objects within the sensor range. This observation can be explained using the ratio (β) of message length to the available objects in the sensor range.

$$\beta = \frac{N_{Msg}}{N_{Rng}} \tag{4.9}$$

where N_{Msg} is the number of objects in message and N_{Rng} is the number of objects within r_{sensor}.

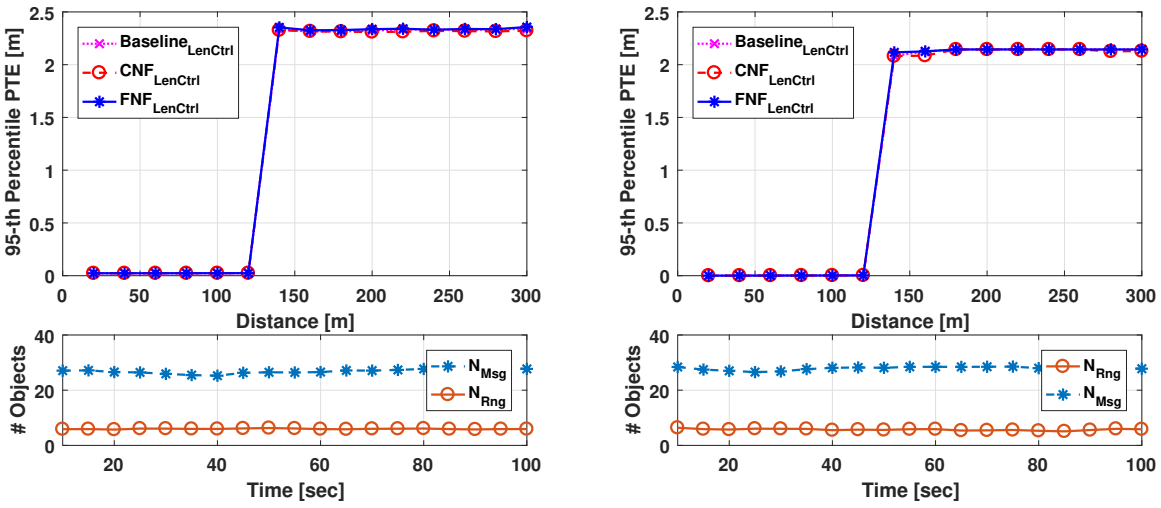

(a) (b)

Figure 4.5: 95-percentile PTE and (bottom) N_{Msg} and N_{Rng} for $\rho = 25veh/km; R_{max} = 10Hz$: (a) Circular Roadway, and (b) Winding Roadway

Both COF and FOF include the same set of objects when $\beta \geq 1$, and as expected, both the algorithms show similar tracking accuracy in light traffic scenario. Figure 4.6 depicts the 95-th percentile PTE curves for $\rho = 125veh/km$ and $r = R_{max} = 10Hz$. It is evident that as message length remains the same for both the content selection approaches and $\beta < 1$, the better tracking performance of FOF can be attributed to its object selection approach where farther objects get a higher priority during the inclusion process. β becomes even smaller when the channel load increases either because of an increase in the number of vehicles or an increase in the message rate and thus, the difference in the performance of COF and FOF becomes more prominent. In the $\rho = 250veh/km$ scenario, for both COF and FOF, message length adaptation helps to curb

the channel congestion, and as shown in Figure 4.7, FOF outperforms COF again because of its content selection approach.

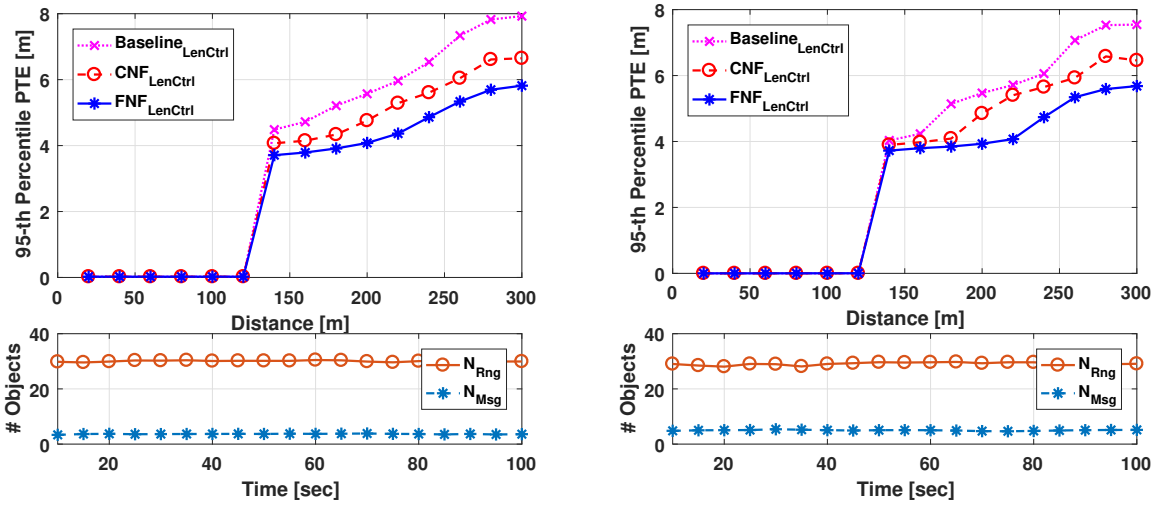

(a) (b)

Figure 4.6: 95-percentile PTE and (bottom) N_{Msg} and N_{Rng} for $\rho = 125veh/km; R_{max} = 10Hz$: (a) Circular Roadway, and (b) Winding Roadway

To get more insight into the performance of the distance-based content selection, we consider a simplified one-dimensional road topology where the sender is located at the center, as shown in Figure 4.10. Let d be the distance of the objects that are included in the generated message by the sender, r_{sensor} is the detection range of the sensing device, and r_{comm} is the communication range. We assume uniform vehicle density and all distances are normalized with respect to r_{comm}. Let n be the number of receivers in the communication range of the sender, and k be the number of included objects in the message. Now, from Figure 4.10 (a) we see that in COF, the included objects do not

offer any new information to the receivers that are located within the range of $2 * r_{sensor} - 2 * d$ due to the fact that the included objects are already in the sensor range of the receivers.

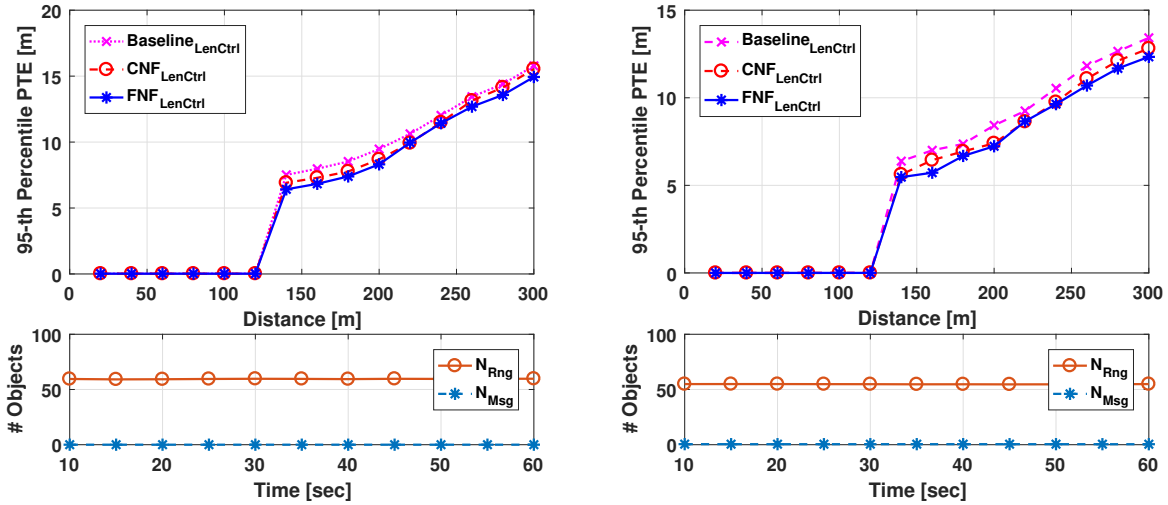

(a) (b)

Figure 4.7: 95-percentile PTE and (bottom) N_{Msg} and N_{Rng} for $\rho = 250veh/km; R_{max} = 10Hz$: (a) Circular Roadway, and (b) Winding Roadway

For FOF, Figure 4.10 (b) shows that $k/2$ of the included objects are useful to receivers located in each half of the sensor range of the sender. This is because the objects that are selected from one side of the sender are not in the sensor range of the receiver vehicles on the other side of it. Now we define a function g that describes how useful the included object (located at distance d from the sender) is for the intended recipients located at distance x.

$$g(x) = \begin{cases} 0, & \text{if } |x-d| \leq r_{sensor} \\ 1, & \text{otherwise} \end{cases} \tag{4.10}$$

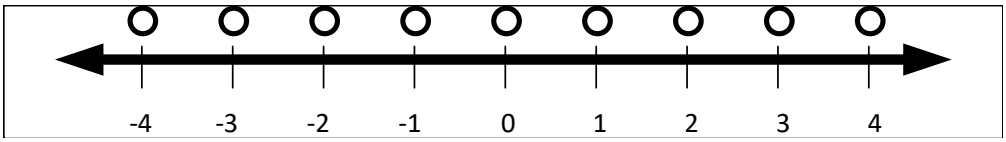

Figure 4.8: One-dimensional road topology where it is assumed that a vehicle (depicted as a circle) is located at each discrete x-position

The total number of recipients u within the communication range r_{comm} that find the included information useful can be computed as follows

$$u = \sum_{i}^{n} g(x_i, d) \tag{4.11}$$

Both COF and FOF provides similar useful information to recipients when no loss in the communication channel is assumed. However, by factoring in the packet error ratio (PER), which quantifies the message loss ratio for a sender-receiver pair, we can see what is helping FOF to achieve higher tracking accuracy than COF. PER has a direct relationship with distance; the greater the distance, the higher the PER. Now, for example, assume that the sender-receiver distance is r and the distance of the included object to the sender is d, meaning that the distance of the included objects to the intended receiver is $(r+d)$, assuming the recipient is located on the opposite side of the road of the included object. In COF, closer neighbors are included first, and thus, as $d \rightarrow 0$, $PER(r) \approx PER(r+d)$. Therefore, it is likely that receivers will have the same probability of receiving packets from both the sender and its neighbors that are included in the sender's message. On the other hand, FOF prefers objects near the sensor range boundary. Clearly, when $d \rightarrow r_{sensor}$, $PER(r+r_{sensor}) > PER(r)$, and therefore, FOF shows better tracking accuracy because it provides

the receivers with the information about farther objects, transmitted messages from which would have a higher loss ratio at the intended receivers.

4.4.3 Effect of Message Length Control

As discussed in Section 4.2, channel congestion can be controlled by adapting message length and transmission rate separately, or through joint adaptation of both parameters. The effectiveness of message length adaptation can be shown analytically. For a given bit error rate p_b, the packet loss probability p for L bit long packet can be expressed as,

$$p = 1 - (1 - p_b)^L \tag{4.12}$$

Now, very large messages of length L may lead to channel saturation quickly where high packet loss ratio limits the throughput. Because p is an increasing function of L, if we seek to achieve the optimal packet length, L_{OPT}, p needs to be reduced exponentially from $p = 1 - (1 - p_b)^L$ to $p = 1 - (1 - p_b)^{L_{OPT}}$. This packet loss probability p has a significant impact on the overall broadcast throughput when the number of vehicles increases in the network, or the channel becomes congested because of large packets transmitted at high rates. Shorter packets are desirable in those situations as they are more robust against channel errors, and since the length adaptation approach tries to adapt the length of transmitted messages to maintain the optimal channel load, better tracking accuracy is expected with L_{OPT}.

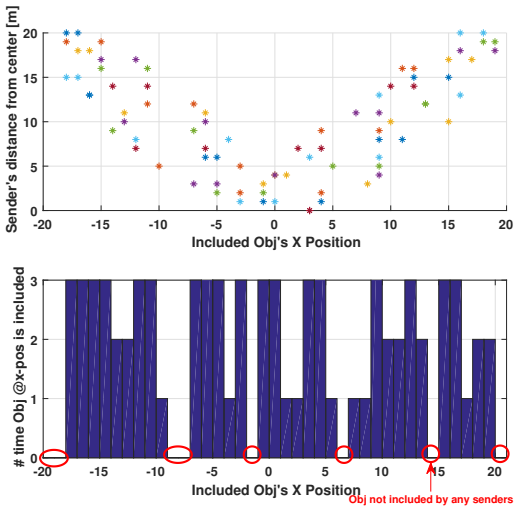

(a)

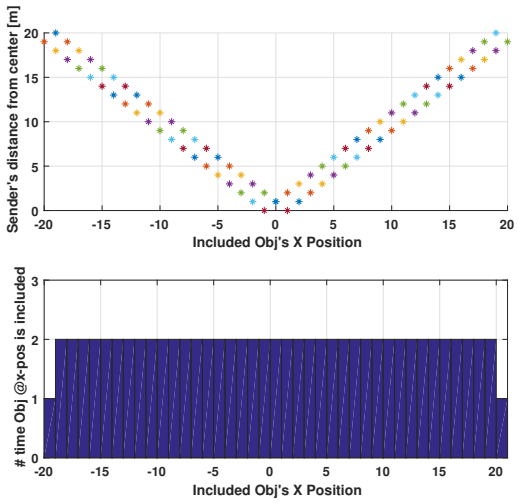

(b)

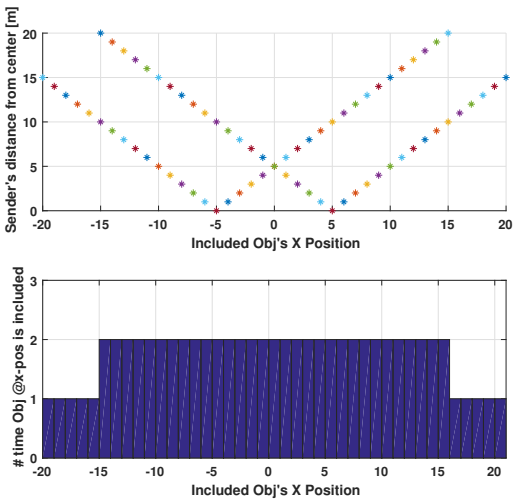

(c)

Figure 4.9: Object inclusion by the vehicles in a one-directional roadway: (a) Baseline, (b) COF, and (c) FOF

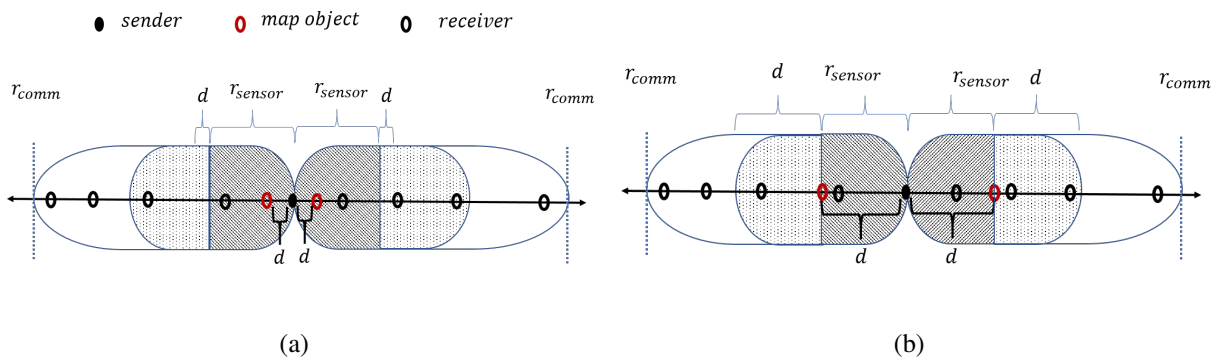

Figure 4.10: Included object's distance to the sender: (a) COF and (b) FOF approaches

4.4.4 Effect of Message Rate Control

Message transmit rate adaptation or joint rate-length adaptation can improve the network throughput by selecting the right combination of message rate and length values. To evaluate which approach performs better, we compare all three options through simulations. Figure 4.11 – Figure 4.12 show tracking improvement when message rate control is employed in conjunction with or without message length adaptation for vehicle densities of 125 and 250 veh/ km, respectively. Message rates and lengths over the simulation time are also shown in the figures which show that lower transmission rates allow the exchange of larger messages. If both length and rate parameters are adapted together, they work in tandem and seek to achieve a combination of rate and length values that keeps the channel load close to CBP^*. But when the length adaptation is disabled, the rate must be very low as it is the sole congestion control parameter in this setting to maintain the channel load close to CBP^*. Transmit rate values are depicted in the middle plots of Figure 4.11 and Figure 4.12. It is apparent from the figures that as the traffic density increases when the message rate control is disabled, the communication channel gets congested even if vehicles share messages

containing only core BSM contents and no additional information about map objects. Therefore, in high traffic densities, message length control alone cannot keep the channel load at its optimal operating point, and thus, enabling message rate control achieves better tracking accuracy in these density settings. Notice that the PTE curves show a higher tracking accuracy when "only" rate control is enabled. To explain the performance gain of rate control, we take the traffic scenario where $\rho = 125veh/km$ and $R_{max} = 10Hz$. (r,d) pairs from Figure 4.11(b) for different channel load adaptation approaches are shown in Table 4.2. In CSMA/CA-based DSRC communications, we can represent emission throughput of the network as

$$T_{emission} \stackrel{\text{def}}{=} f_{emission}(r,l) = r * l \tag{4.13}$$

And reception throughput can be defined as

$$T_{reception} \stackrel{\text{def}}{=} f_{reception}(r,l,PER) \tag{4.14}$$

where packet error ratio at distance d is defined as $PER = f_{per}(d,r,l)$. From (4.14) it is obvious that at a given distance d, $T_{reception}$ depends on the rate and the length choices of the transmitted messages. Since the offered load on the communication channel remains close to the optimal level in all three (r,l) choices tabularized in Table 4.2, and as the PER curves show similar trends, the network throughput remains almost the same, for these rate-length combinations. However, the goodput, which quantifies the useful data bits exchanged over the communication channel, for individual approaches may vary. Each L unit long packet is comprised of a K unit long overhead and a $(L-K)$ unit long actual payload data. In IEEE 802.11p, the headers for user datagram protocol (UDP), internet protocol (IP), logical link control (LLC) and MAC protocol are 8, 20,

8 and 26 bytes long, respectively. Also, the frame check sequence (FCS) is 4 bytes long. All these headers and the FCS amount to a total of K = 66 Bytes in the simulations. For analysis simplicity and without any loss of generality, we assume $T_{emission} = T_{reception} = T$ as PER remains almost the same in all three cases. Now, computing the goodput G as $G \approx R * (L - K)$, we get $G_{LengthCtrl} \approx 5440 bytes/sec$, $G_{Length+RateCtrl} \approx 5502 bytes/sec$ and $G_{RateCtrl} \approx 5658 bytes/sec$. Therefore, exchanging larger packets at lower rates yield better goodput because of the less overhead. And it is evident that rate control offers more information dissemination irrespective of the usage of length adaptation. In terms of the tracking accuracy of the example cases tabularized in Table 4.2, message rate control achieves higher accuracy than the joint length-rate control schemes. This observation brings in the following question: Does transmitting larger messages at low rates (minimum possible) always allow to achieve a higher map accuracy? To answer this question, we shed more light on the interaction of message length and transmit rate with respect to the performance metrics CBP and PTE.

We ran simulations for different fixed message length and rate settings. For $L^t_{OPT} = \{2,4,6,8,10,12,14,16,18,20,22,24,26,28\}$, simulations were run for each of the message rate value in the range of 1 to 10 Hz. To plot the CBP curves in Figure 4.13(b), we use the mean of all CBP values calculated at each vehicle. The PTE metric is measured by averaging (weighted by a function W) over all the vehicles in the map radius $r_{map} = 300\ meters$, as follows.

$$PTE_{avg} = \frac{1}{N} * \sum_{i \in N} W(i) * PTE(i) \tag{4.15}$$

Assuming equal weight W for all N vehicles in map radius, PTE is plotted in Figure 4.13(a). The optimal message rates for different message lengths can be found from the intersecting points

of the CBP curves and the optimal CBP^*. Figure 4.13(c) shows the optimal CBP control line, which suggests that any (r,l) pair from this line can achieve optimal channel utilization. It is evident from the PTE curves that neither the maximum-sized messages at the minimum rate nor the minimum-sized messages at the maximum rate can ensure the optimal PTE performance. The optimal operating point is something in between. Of course, there is an exception for low-density traffic scenarios where the maximum message rate is expected to achieve the best performance as the message lengths are typically smaller there because of the smaller map size. For moderate to heavy traffic density scenarios, the non-linear relationship between channel load and tracking performance demands further investigation. Certainly, better network goodput is a desirable property in vehicle safety applications to achieve optimal or near-optimal tracking performance. However, the goodput analysis explains the effectiveness of different channel control schemes to some extent, but not completely. Increases in the network goodput may not always result in improvement in tracking accuracy because of the data quality. This is because cooperative safety communication systems not only require better network goodput but also demand freshness of the exchanged information which can be quantified using the metric Information Age (IA). In CSMA/CA, when senders transmit fixed-length messages containing only their own status updates, information age depends on the throughput and the MAC layer delay. Aging of information due to delay in the MAC layer is mostly dominated by the configured maximum MAC queue size in the network device. In low-density traffic scenarios where the network is lightly loaded, the MAC queue remains almost empty and does not affect IA. However, in higher traffic densities, longer MAC queue size increases the information age significantly. In vehicular safety applications where we care about

sharing the latest status update of the vehicles, having outdated information stored in the MAC queues does not help. Therefore, in the simulations, we configured the queue size to be 1. Furthermore, when a new packet is generated at the application layer, we discarded the outdated packet in the MAC queue to replace it with the newly generated one. In this way, the information age due to MAC queue delay is reduced. Although MAC delay cannot completely be eliminated in this way, we keep the delay to the least amount possible without making any changes in the MAC mechanism, and by simply reconfiguring the MAC queue size and the queue drop policy. Since the queue delay factor of information aging is minimized and kept constant for all simulation scenarios, the throughput of the network decides the IA performance. In all of the channel congestion control strategies presented in this work, the same optimal CBP value is used for convergence, therefore, the overall throughput remains similar. Hence, in relay-based communication architecture where variable-length messages are exchanged, IA depends on both the choices of (r,l) and the content of the messages. Now that the factors that directly impact mapping accuracy are identified, we seek to relate them. CBP, map accuracy and IA for different choices of message rate and length values are illustrated in Figure 4.14 - Figure 4.16 for $\rho = 25, 125$ *and* 250 veh/km. Map accuracy is calculated as follows.

$$Map\ Accuracy = \frac{1}{N} * \sum_{i \in N} \frac{Error_{threshold}}{PTE(i)} \tag{4.16}$$

where $Error_{threshold}$ defines the tracking error tolerance value below which all estimated position measurements are considered accurate. One advantage of using map accuracy as a performance metric is that this quantity is not affected by the objects that cannot be tracked due to the lack of communicated or sensor data. Generally, vehicles that are not tracked are assigned a very large

tracking error. Therefore, (4.16) will compute zero as the map accuracy for these vehicles. Also, this quantity is normalized between 0 and 1 with respect to the $Error_{threshold}$ and can be adopted as an efficiency measure for networked systems of different sizes. We set $Error_{threshold} = 0.5m$ in our map accuracy calculation, meaning that the PTE measurements below 0.5m are considered to have 100% map accuracy in the computation.

Table 4.2: (r,l) Pairs for Different Channel Load Adaptation Approaches when $\rho = 125veh/km$ and $R_{max} = 10Hz$

Adapted Parameters	Rate (Hz)	Length (Bytes)
Length	10	~ 610
Length + Rate	~ 3	~ 1900
Rate	~ 2.6	2242

Generally, all feedback control systems use a threshold value for comparing the feedback metric. In the congestion control algorithms presented in this paper, CBP is used as the feedback metric and the chosen threshold value $CBP^* = 68\%$. Comparing the CBP plots and their corresponding map accuracy for $\rho = 125 and 250veh/km$, it is observed that an acceptable range of map accuracy can be achieved for CBP values in the range between 40% and 80%. This observation is in good agreement with the observations about CBP in [66]. For $\rho = 25veh/km$, CBP does not exceed the optimal level, and good map accuracy is observed when CBP is higher than 30%. Comparing the map accuracy and the IA plots, we see that information age can be directly related to tracking accuracy because a lower IA is an indication of a lower end-to-end delay of the exchanged

information. Note that finding the absolute optimal tracking accuracy in real-time is impractical in map sharing based vehicular networks. However, through our observations based on actual PTE, we see that the congestion control algorithm based on a target CBP keeps the tracking accuracy close to the optimal value. Notice that the results from transmit rate control in the simulations consistently show a better tracking performance than the approach that employs a combination of message length and transmit rate control. We identify that the decrease factor of the transmit rate parameter is the key component here that affects the tracking accuracy in joint length-rate control. When there is no length adaptation for the messages, the transmit rate will eventually settle at some value to keep the channel utilization close to CBP^*. The time required for the transmit rate to converge depends on the choices of the rate decrease factor. An aggressive decrease factor makes the transmit rate converge faster than that of a conservative decrease factor. However, both the aggressive and the conservative decrease factor yield the same steady-state transmit rate when only the message rate is adapted. In the case where both length and rate adaptations are enabled, the choices of the decrease factor have a significant impact on the steady-state transmit rate. Since both message length and transmit rate use the same feedback metric CBP for convergence, the rates at which the parameters adapt matters. As can be seen in Figure 4.13(c), several combinations of the message rate and length can achieve the optimal channel utilization. However, not all combinations may result in the same tracking accuracy as can be seen in Figure 4.13(a). Now, from Figure 4.15 we see that for $\rho = 250 veh/km$, there is a large patch of length values for a certain range of rate values allow the system to achieve optimal or near-optimal tracking accuracy. This observation suggests that, depending on the adaptation rate of the message length and rate parameter, the joint

rate-length adaptation may end up in some sub-optimal regions of the map accuracy space. Now we assume that the joint rate-length control algorithm starts with L_{max} and R_{max}. If the message rate is adapted at a higher proportion than the length parameter to settle on a smaller rate value, the algorithm will allow using a large message length value. And this combination of the message rate and length would have a higher likelihood to match one of the rate-length combinations that achieve near-optimal tracking accuracy as depicted in Figure 4.15. To see how the choices of message rate decrease factor affect the tracking accuracy, we tested two different rate decrease factors, 0.15 and 0.40. Figure 4.17 shows how a larger decrease factor increases the tracking accuracy for joint length-rate adaptation and achieves almost similar performance as the "rate only" adaptation. Based on the above observation we conclude that even though "rate-only" and joint length-rate adaptations demonstrate similar tracking performance, the latter is preferable because it can scale in very dense traffic scenarios as with joint length-rate adaptation, the algorithm has two parameters at disposal for maintaining the channel load at the desired level. In contrast, by adapting only the rate parameter, the transmission of fixed-length messages of size L_{max} at the lowest possible rate R_{min} may still lead to channel saturation in high traffic conditions.

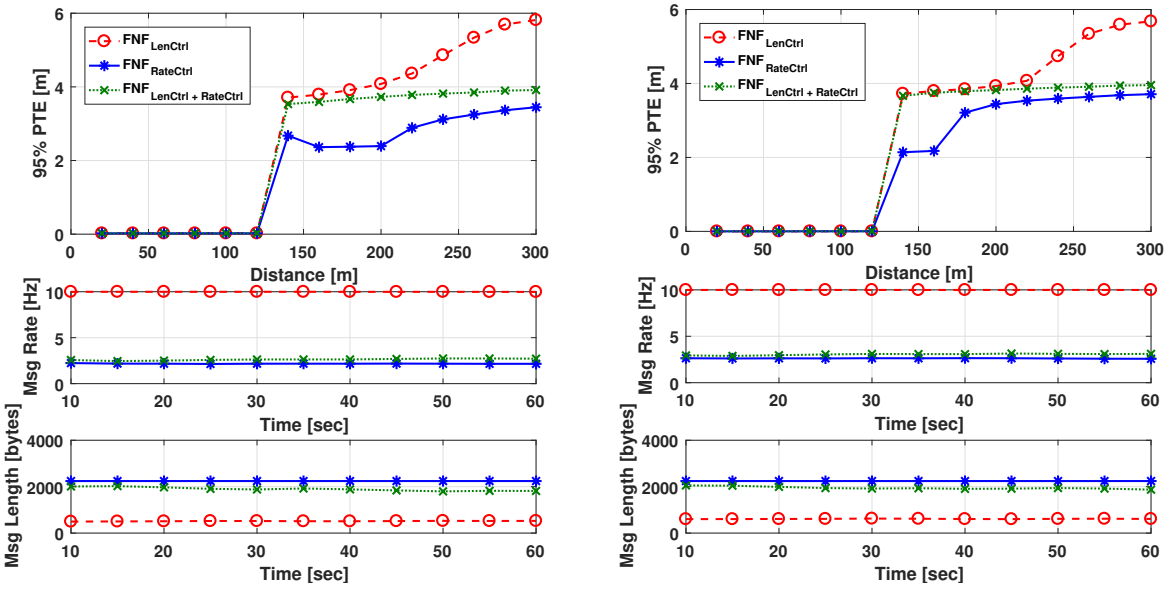

(a) (b)

Figure 4.11: top) 95-percentile PTE, (middle) Average message rate, (bottom) Average message length for $\rho = 125 veh/km$; $R_{max} = 10 Hz$: (a) Circular, (b) Winding roadway

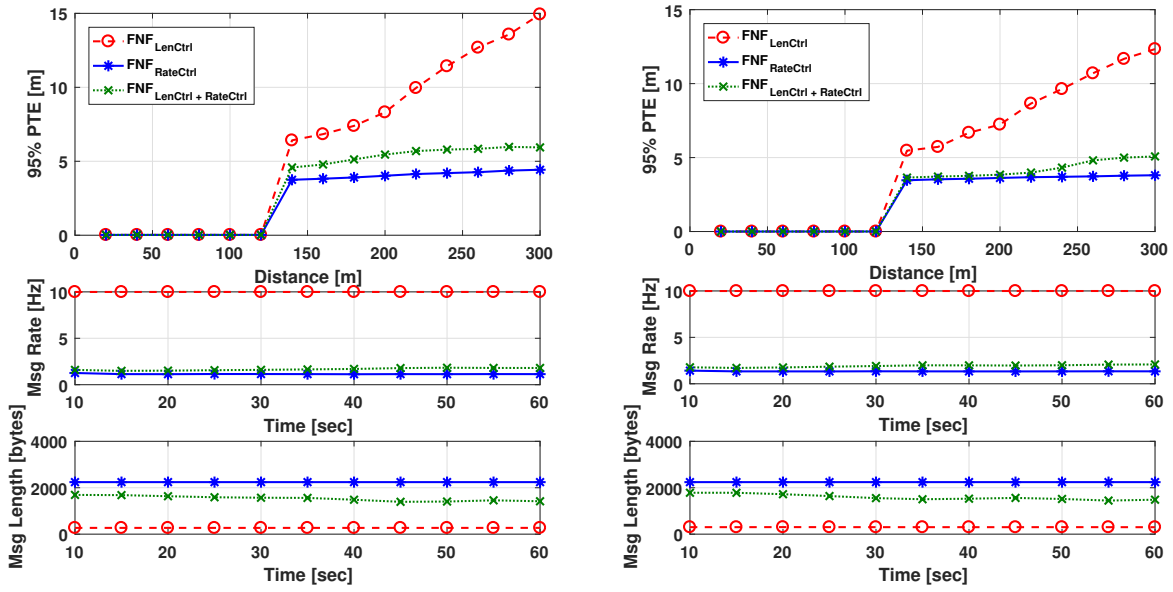

(a) (b)

Figure 4.12: top) 95-percentile PTE, (middle) Average message rate, (bottom) Average message length for $\rho = 250 veh/km$; $R_{max} = 10 Hz$: (a) Circular, (b) Winding roadway

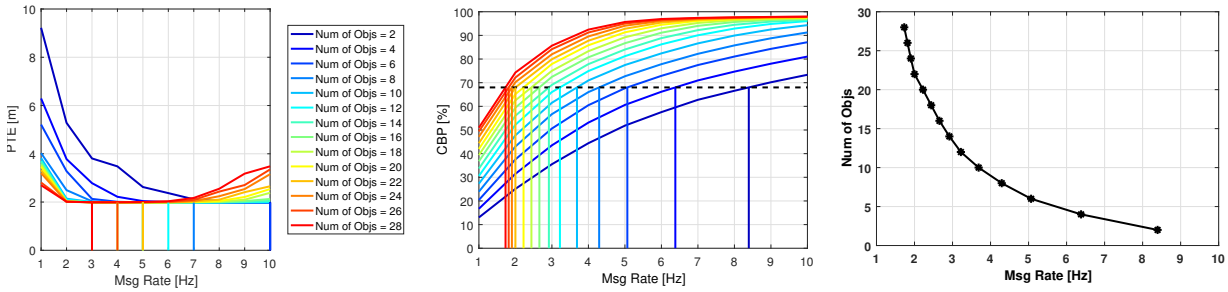

(a) (b) (c)

Figure 4.13: (a) 95% PTE; the perpendicular lines show the minimum points for each PTE curve, (a) CBP, and (c) Optimal CBP control Line for different rate and length setting for $\rho = 250 veh/km$

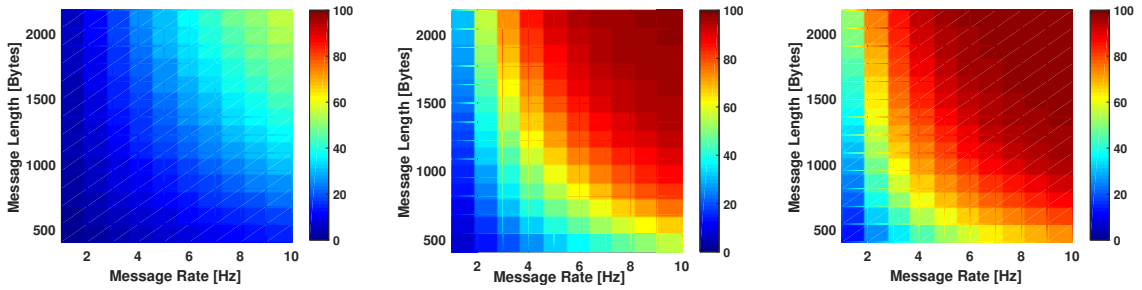

(a) (b) (c)

Figure 4.14: Mean CBP (%) for different (rate, length) choices: (a) $\rho = 25$, (b) $\rho = 125$ and (c) $\rho = 250 veh/km$

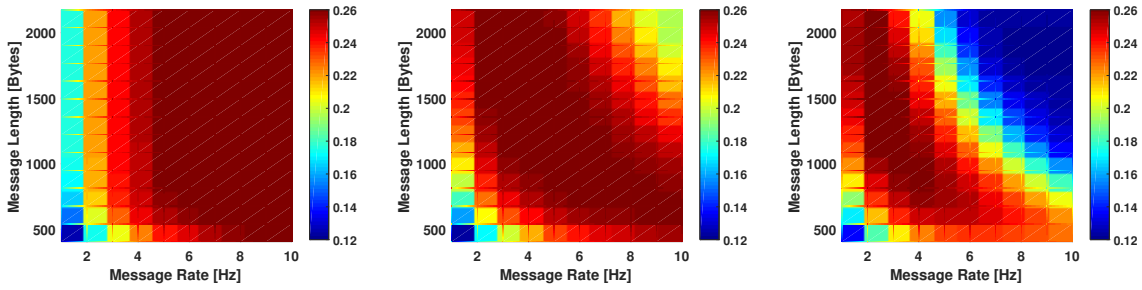

(a) (b) (c)

Figure 4.15: Map Accuracy for different (rate, length) choices: (a) $\rho = 25$, (b) $\rho = 125$ and (c) $\rho = 250 veh/km$

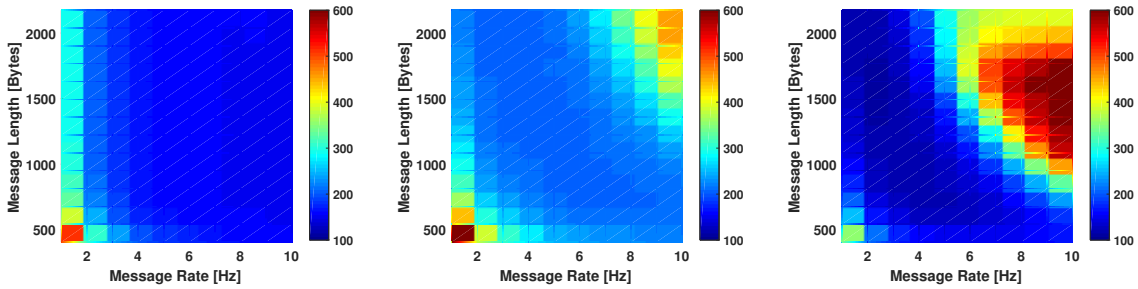

(a) (b) (c)

Figure 4.16: Information Age (IA) in milliseconds for different (rate, length) choices: (a) $\rho = 25$, (b) $\rho = 125$ and (c) $\rho = 250 veh/km$

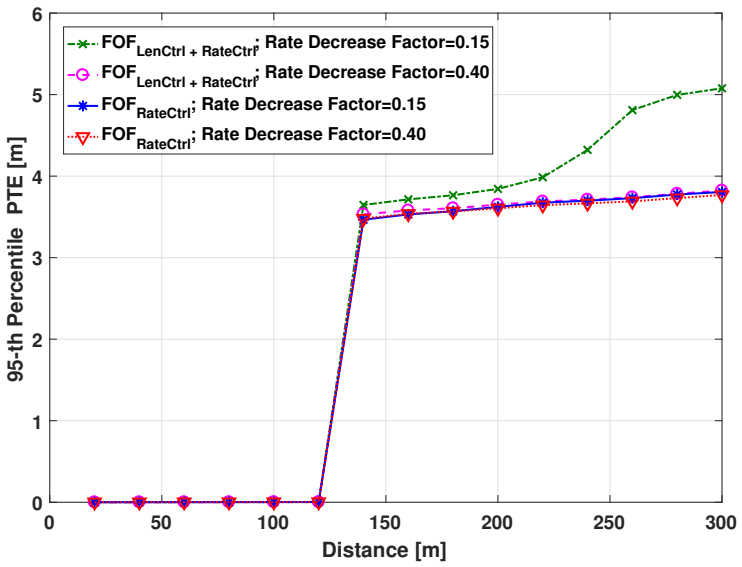

Figure 4.17: 95-percentile PTE for different decrease factors; density = 250 vehicles/ km; max message rate = 10 Hz (Winding roadway)

CHAPTER 5: CONCLUSIONS

We provided an overview of the DSRC simulation process, describing specific components of simulation which include node and propagation modeling. Node behavior modeling has been presented with a focus on the most commonly used approach of a frame or sub-frame-based simulation. We described methods used by popular discrete event simulators such as ns-3 and presented several corrections and enhancements that were made to achieve higher fidelity of simulation for DSRC. Channel modeling approaches were also briefly discussed, and the steps of RSS-based channel model implementation has been presented in detail. To describe the channel propagation model, a specific model developed from large scale field test data has been explained. The overall simulation model for the channel and node behavior was validated and shown to be more accurate than the frame-level simulator.

We presented a performance evaluation of the SAE J2945/1 congestion control algorithm by presenting extensive simulation experiments using realistic vehicle trajectories. To validate the performance of the congestion control algorithm, a large-scale field RSS dataset is used to derive a realistic channel propagation model and vehicle trajectories from a microscopic traffic simulation tool are obtained for the same road stretch the channel measurements were collected from. Presented results show that the congestion control algorithm achieves significant performance gain in terms of the information age and tracking accuracy in dense traffic scenarios. Further analysis of

the relationship of message rate and power with information dissemination rate reveals a potential area of improvement to optimize the vehicle density coefficient parameter of the congestion control algorithm. Simulation experiments were performed to find an optimal value for this parameter and results indicate that the choice of this parameter value comes with a trade-off for safety benefits at different range of interests. A less aggressive rate control approach achieves slightly better tracking gain at lower ranges, trading off greater safety benefits at higher distances.

We also presented an overview of different message rate, length and content control schemes, and evaluated their performance in terms of position tracking accuracy, in a map information sharing based cooperative V2X communication architecture. It was shown that including information about objects that are located near the edge of local sensors' detection range is more beneficial to map accuracy. We also investigated the effect of message length and rate control on mapping accuracy. Our study found that tracking accuracy in cooperative vehicle communications can be improved through the use of channel congestion control based on message length, rate and/or joint rate-length adaptation. By examining the trade-off between message length and transmission rate, we determined that a joint rate-length congestion control offers more flexibility than controlling the parameters separately.

LIST OF REFERENCES

[1] J. B. Kenney, "Dedicated Short-Range Communications (DSRC) Standards in the United States," *Proceedings of the IEEE*, vol. 99, no. 7, pp. 1162–1182, July 2011.

[2] M. R. Hafner, D. Cunningham, L. Caminiti, and D. Del Vecchio, "Cooperative Collision Avoidance at Intersections: Algorithms and Experiments," *IEEE Transactions on Intelligent Transportation Systems*, vol. 14, no. 3, pp. 1162–1175, Sep. 2013.

[3] L. Makarem and D. Gillet, "Model predictive coordination of autonomous vehicles crossing intersections," in *16th International IEEE Conference on Intelligent Transportation Systems (ITSC 2013)*, Oct 2013, pp. 1799–1804.

[4] S. Boskovich and M. Barth, "Vehicular network rerouting autonomy with a V2V, I2V, and V2I communication matrix classification," in *16th International IEEE Conference on Intelligent Transportation Systems (ITSC 2013)*, Oct 2013, pp. 172–177.

[5] "Dedicated Short Range Communications (DSRC) Message Set Dictionary, Std. J2735," *SAE*, Nov 2009.

[6] "Intelligent Transport Systems (ITS); Vehicular communications; Basic Set of Applications; Part 2: Specification of Cooperative Awareness Basic Service," *ETSI EN 302 637-2, V1.3.2*, 2014.

[7] R. Sengupta, S. Rezaei, S. E. Shladover, D. Cody, S. Dickey, and H. Krishnan, "Cooperative Collision Warning Systems: Concept Definition and Experimental Implementation," *Journal of Intelligent Transportation Systems*, vol. 11, no. 3, pp. 143–155, 2007. [Online]. Available: https://doi.org/10.1080/15472450701410452

[8] K. Dar, M. Bakhouya, J. Gaber, M. Wack, and P. Lorenz, "Wireless communication technologies for ITS applications [Topics in Automotive Networking]," *IEEE Communications Magazine*, vol. 48, no. 5, pp. 156–162, May 2010.

[9] F. Bai and H. Krishnan, "Reliability Analysis of DSRC Wireless Communication for Vehicle Safety Applications," in *2006 IEEE Intelligent Transportation Systems Conference*, Sep. 2006, pp. 355–362.

[10] Q. Chen, D. Jiang, V. Taliwal, and L. Delgrossi, "IEEE 802.11 Based Vehicular Communication Simulation Design for NS-2," in *Proceedings of the 3rd International*

Workshop on Vehicular Ad Hoc Networks, ser. VANET '06. New York, NY, USA: ACM, 2006, pp. 50–56. [Online]. Available: http://doi.acm.org/10.1145/1161064.1161073

[11] Q. Chen, F. Schmidt-Eisenlohr, D. Jiang, M. Torrent-Moreno, L. Delgrossi, and H. Hartenstein, "Overhaul of IEEE 802.11 Modeling and Simulation in Ns-2," in *Proceedings of the 10th ACM Symposium on Modeling, Analysis, and Simulation of Wireless and Mobile Systems*, ser. MSWiM '07. New York, NY, USA: ACM, 2007, pp. 159–168. [Online]. Available: http://doi.acm.org/10.1145/1298126.1298155

[12] J. Lee, W. Kim, S.-J. Lee, D. Jo, J. Ryu, T. Kwon, and Y. Choi, "An Experimental Study on the Capture Effect in 802.11a Networks," in *Proceedings of the Second ACM International Workshop on Wireless Network Testbeds, Experimental Evaluation and Characterization*, ser. WinTECH '07. New York, NY, USA: ACM, 2007, pp. 19–26. [Online]. Available: httpdoi.acm.org10.11451287767.1287772

[13] J. Ryu, J. Lee, S.-J. Lee, and T. Kwon, "Revamping the IEEE 802.11a PHY Simulation Models," in *Proceedings of the 11th International Symposium on Modeling, Analysis and Simulation of Wireless and Mobile Systems*, ser. MSWiM '08. New York, NY, USA: ACM, 2008, pp. 28–36. [Online]. Available: http://doi.acm.org/10.1145/1454503.1454513

[14] J. Lee, J. Ryu, S.-J. Lee, and T. T. Kwon, "Improved Modeling of IEEE 802.11a PHY Through Fine-grained Measurements," *Comput. Netw.*, vol. 54, no. 4, pp. 641–657, Mar. 2010. [Online]. Available: http://dx.doi.org/10.1016/j.comnet.2009.08.003

[15] (2018) QualNet Network Simulator. [Online]. Available: http://www.scalable-networks.com

[16] S. Papanastasiou, J. Mittag, E. G. Strom, and H. Hartenstein, "Bridging the Gap between Physical Layer Emulation and Network Simulation," in *2010 IEEE Wireless Communication and Networking Conference*, April 2010, pp. 1–6.

[17] J. Mittag, S. Papanastasiou, H. Hartenstein, and E. G. Strom, "Enabling Accurate Cross-Layer PHY/MAC/NET Simulation Studies of Vehicular Communication Networks," *Proceedings of the IEEE*, vol. 99, no. 7, pp. 1311–1326, July 2011.

[18] A. Goldsmith, *Wireless Communications*. Cambridge University Press, 2005.

[19] J. S. Seybold, *Introduction to RF Propagation*. John Wiley & Sons, Sep 2005.

[20] J. Kunisch and J. Pamp, "Wideband Car-to-Car Radio Channel Measurements and Model at 5.9 GHz," in *2008 IEEE 68th Vehicular Technology Conference*, Sep. 2008, pp. 1–5.

[21] J. Karedal, N. Czink, A. Paier, F. Tufvesson, and A. F. Molisch, "Path Loss Modeling for Vehicle-to-Vehicle Communications," *IEEE Transactions on Vehicular Technology*, vol. 60, no. 1, pp. 323–328, Jan 2011.

[22] A. Paier, J. Karedal, N. Czink, C. Dumard, T. Zemen, F. Tufvesson, A. F. Molisch, and C. F. Mecklenbräuker, "Characterization of Vehicle-to-Vehicle Radio Channels from Measurements at 5.2 GHz," *Wireless Personal Communications*, vol. 50, no. 1, pp. 19–32, Jul 2009. [Online]. Available: https://doi.org/10.1007/s11277-008-9546-6

[23] A. Paier, J. Karedal, N. Czink, H. Hofstetter, C. Dumard, T. Zemen, F. Tufvesson, A. F. Molisch, and C. F. Mecklenbrauker, "Car-to-car radio channel measurements at 5 GHz: Pathloss, power-delay profile, and delay-Doppler spectrum," in *2007 4th International Symposium on Wireless Communication Systems*, Oct 2007, pp. 224–228.

[24] A. Paier, J. Karedal, N. Czink, H. Hofstetter, C. Dumard, T. Zemen, F. Tufvesson, C. F. Mecklenbrauker, and A. F. Molisch, "First Results from Car-to-Car and Car-to-Infrastructure Radio Channel Measurements at 5.2 GHz," in *2007 IEEE 18th International Symposium on Personal, Indoor and Mobile Radio Communications*, Sep. 2007, pp. 1–5.

[25] O. Renaudin, V. Kolmonen, P. Vainikainen, and C. Oestges, "Car-to-car channel models based on wideband MIMO measurements at 5.3 GHz," in *2009 3rd European Conference on Antennas and Propagation*, March 2009, pp. 635–639.

[26] J. K. Taimoor Abbas, Katrin Sjöberg and F. Tufvesson, "A Measurement Based Shadow Fading Model for Vehicle-to-Vehicle Network Simulations," *International Journal of Antennas and Propagation,*, vol. 2015, no. Article ID 190607, 2015. [Online]. Available: https://doi.org/10.1155/2015/190607

[27] X. Cheng, Q. Yao, C. Wang, B. Ai, G. L. Stuber, D. Yuan, and B. Jiao, "An Improved Parameter Computation Method for a MIMO V2V Rayleigh Fading Channel Simulator Under Non-Isotropic Scattering Environments," *IEEE Communications Letters*, vol. 17, no. 2, pp. 265–268, February 2013.

[28] X. Cheng, C. Wang, B. Ai, and H. Aggoune, "Envelope Level Crossing Rate and Average Fade Duration of Nonisotropic Vehicle-to-Vehicle Ricean Fading Channels," *IEEE Transactions on Intelligent Transportation Systems*, vol. 15, no. 1, pp. 62–72, Feb 2014.

[29] X. Cheng, Q. Yao, M. Wen, C. Wang, L. Song, and B. Jiao, "Wideband Channel Modeling and Intercarrier Interference Cancellation for Vehicle-to-Vehicle Communication Systems," *IEEE Journal on Selected Areas in Communications*, vol. 31, no. 9, pp. 434–448, Sep. 2013.

[30] J. Maurer, T. Fugen, and W. Wiesbeck, "Narrow-band measurement and analysis of the inter-vehicle transmission channel at 5.2 GHz," in *Vehicular Technology Conference. IEEE 55th Vehicular Technology Conference. VTC Spring 2002 (Cat. No.02CH37367)*, vol. 3, May 2002, pp. 1274–1278 vol.3.

[31] G. Acosta-marum and M. A. Ingram, " Doubly selective vehicle-to-vehicle channel measurements and modeling at 5.9 GHz ," in *PROC. INT. SYMP. WIRELESS PERSONAL MULTIMEDIA COMMUN*, 2006.

[32] G. Acosta, K. Tokuda, and M. A. Ingram, "Measured joint Doppler-delay power profiles for vehicle-to-vehicle communications at 2.4 GHz," in *IEEE Global Telecommunications Conference, 2004. GLOBECOM '04.*, vol. 6, Nov 2004, pp. 3813–3817 Vol.6.

[33] J. Yin, G. Holland, T. ElBatt, F. Bai, and H. Krishnan, "DSRC Channel Fading Analysis from Empirical Measurement," in *2006 First International Conference on Communications and Networking in China*, Oct 2006, pp. 1–5.

[34] M. Boban, W. Viriyasitavat, and O. K. Tonguz, "Modeling Vehicle-to-vehicle Line of Sight Channels and Its Impact on Application-layer Performance," in *Proceeding of the Tenth ACM International Workshop on Vehicular Inter-networking, Systems, and Applications*, ser. VANET '13. New York, NY, USA: ACM, 2013, pp. 91–94. [Online]. Available: http://doi.acm.org/10.1145/2482967.2482980

[35] M. Boban, R. Meireles, J. Barros, O. Tonguz, and P. Steenkiste, "Exploiting the height of vehicles in vehicular communication," in *2011 IEEE Vehicular Networking Conference (VNC)*, Nov 2011, pp. 163–170.

[36] M. Boban, T. T. V. Vinhoza, M. Ferreira, J. Barros, and O. K. Tonguz, "Impact of Vehicles as Obstacles in Vehicular Ad Hoc Networks," *IEEE Journal on Selected Areas in Communications*, vol. 29, no. 1, pp. 15–28, January 2011.

[37] R. Meireles, M. Boban, P. Steenkiste, O. Tonguz, and J. Barros, "Experimental study on the impact of vehicular obstructions in VANETs," in *2010 IEEE Vehicular Networking Conference*, Dec 2010, pp. 338–345.

[38] L. Cheng, B. E. Henty, D. D. Stancil, F. Bai, and P. Mudalige, "Mobile Vehicle-to-Vehicle Narrow-Band Channel Measurement and Characterization of the 5.9 GHz Dedicated Short Range Communication (DSRC) Frequency Band," *IEEE Journal on Selected Areas in Communications*, vol. 25, no. 8, pp. 1501–1516, Oct 2007.

[39] L. Cheng, B. E. Henty, F. Bai, and D. D. Stancil, "Highway and rural propagation channel modeling for vehicle-to-vehicle communications at 5.9 GHz," in *2008 IEEE Antennas and Propagation Society International Symposium*, July 2008, pp. 1–4.

[40] G. P. Grau, D. Pusceddu, S. Rea, O. Brickley, M. Koubek, and D. Pesch, "Vehicle-2-vehicle communication channel evaluation using the CVIS platform," in *2010 7th International Symposium on Communication Systems, Networks Digital Signal Processing (CSNDSP 2010)*, July 2010, pp. 449–453.

[41] V. Taliwal, D. Jiang, H. Mangold, C. Chen, and R. Sengupta, "Empirical Determination of Channel Characteristics for DSRC Vehicle-to-vehicle Communication," in *Proceedings of the 1st ACM International Workshop on Vehicular Ad Hoc Networks*, ser. VANET '04. New York, NY, USA: ACM, 2004, pp. 88–88. [Online]. Available: http://doi.acm.org/10.1145/1023875.1023890

[42] T. Islam, Y. Hu, E. Onur, B. Boltjes, and J. F. C. M. de Jongh, "Realistic simulation of IEEE 802.11p channel in mobile Vehicle to Vehicle communication," in *2013 Conference on Microwave Techniques (COMITE)*, April 2013, pp. 156–161.

[43] D. Vlastaras, T. Abbas, M. Nilsson, R. Whiton, M. Olbäck, and F. Tufvesson, "Impact of a truck as an obstacle on vehicle-to-vehicle communications in rural and highway scenarios," in *2014 IEEE 6th International Symposium on Wireless Vehicular Communications (WiVeC 2014)*, Sept 2014, pp. 1–6.

[44] M. Segata, B. Bloessl, S. Joerer, C. Sommer, R. L. Cigno, and F. Dressler, "Short paper Vehicle shadowing distribution depends on vehicle type Results of an experimental study," in *2013 IEEE Vehicular Networking Conference*, Dec 2013, pp. 242–245.

[45] N. Akhtar, S. C. Ergen, and O. Ozkasap, "Vehicle Mobility and Communication Channel Models for Realistic and Efficient Highway VANET Simulation," *IEEE Transactions on Vehicular Technology*, vol. 64, no. 1, pp. 248–262, Jan 2015.

[46] H. N. Mahjoub, A. Tahmasbi-Sarvestani, S. M. O. Gani, and Y. P. Fallah, "Composite α - μ Based DSRC Channel Model Using Large Data Set of RSSI Measurements," *IEEE Transactions on Intelligent Transportation Systems*, pp. 1–13, 2018.

[47] H. Hartenstein and L. Laberteaux, "A tutorial survey on vehicular ad hoc networks," *IEEE Communications magazine*, vol. 46, no. 6, 2008.

[48] C. Campolo and A. Molinaro, "Multichannel communications in vehicular ad hoc networks: a survey," *IEEE Communications Magazine*, vol. 51, no. 5, pp. 158–169, 2013.

[49] C. Huang, Y. P. Fallah, R. Sengupta, and H. Krishnan, "Adaptive intervehicle communication control for cooperative safety systems," *IEEE Network*, vol. 24, no. 1, pp. 6–13, Jan 2010.

[50] G. Bansal, J. B. Kenney, and C. E. Rohrs, "LIMERIC: A Linear Adaptive Message Rate Algorithm for DSRC Congestion Control," *IEEE Transactions on Vehicular Technology*, vol. 62, no. 9, pp. 4182–4197, Nov 2013.

[51] H. Lu, G. Bansal, and J. Kenney, "A joint rate-power control algorithm for vehicular safety communications," in *ITS world congress*, 2015.

[52] A. Weinfied, J. Kenney, and G. Bansal, "An adaptive DSRC message transmission interval control algorithm," in *ITS world congress*, October 2011.

[53] M. Torrent-Moreno, J. Mittag, P. Santi, and H. Hartenstein, "Vehicle-to-Vehicle Communication: Fair Transmit Power Control for Safety-Critical Information," *IEEE Transactions on Vehicular Technology*, vol. 58, no. 7, pp. 3684–3703, Sept 2009.

[54] S. Kumar, L. Shi, N. Ahmed, S. Gil, D. Katabi, and D. Rus, "Carspeak: a content-centric network for autonomous driving," in *Proceedings of the ACM SIGCOMM 2012 conference on Applications, technologies, architectures, and protocols for computer communication*. ACM, 2012, pp. 259–270.

[55] B. Kloiber, J. Härri, T. Strang, S. Sand, and C. R. García, "Random Transmit Power Control for DSRC and its Application to Cooperative Safety," *IEEE Transactions on Dependable and Secure Computing*, vol. 13, no. 1, pp. 18–31, Jan 2016.

[56] J. T. Willis, A. Jaekel, and I. Saini, "Decentralized congestion control algorithm for vehicular networks using oscillating transmission power," in *2017 Wireless Telecommunications Symposium (WTS)*, April 2017, pp. 1–5.

[57] N. Taherkhani and S. Pierre, "Centralized and Localized Data Congestion Control Strategy for Vehicular Ad Hoc Networks Using a Machine Learning Clustering Algorithm," *IEEE Transactions on Intelligent Transportation Systems*, vol. 17, no. 11, pp. 3275–3285, Nov 2016.

[58] "SAE International," *Surface Vehicle Standard – On-Board System Requirements for V2V Safety Communications, J2945^{TM}/1*, March 2016.

[59] "Intelligent Transport Systems (ITS); Decentralized Congestion Control Mechanisms for Intelligent Transport Systems Operating in the 5 GHz Range; Access Layer Part," *ETSI TC ITS, Technical Specification 102 687*, July 2011.

[60] X. Shen, X. Cheng, R. Zhang, B. Jiao, and Y. Yang, "Distributed Congestion Control Approaches for the IEEE 802.11p Vehicular Networks," *IEEE Intelligent Transportation Systems Magazine*, vol. 5, no. 4, pp. 50–61, winter 2013.

[61] Y. Cao, H. Zhang, X. Zhou, and D. Yuan, "A Scalable and Cooperative MAC Protocol for Control Channel Access in VANETs," *IEEE Access*, vol. 5, pp. 9682–9690, 2017.

[62] S. A. A. Shah, E. Ahmed, F. Xia, A. Karim, M. Shiraz, and R. M. Noor, "Adaptive Beaconing Approaches for Vehicular Ad Hoc Networks: A Survey," *IEEE Systems Journal*, vol. 12, no. 2, pp. 1263–1277, June 2018.

[63] "Intelligent transport systems - Cooperative systems - Definition of a global concept for Local Dynamic Maps," *ISO/TS 18750:2015*, 2015.

[64] "Intelligent Transport Systems (ITS); Vehicular Communications; Basic Set of Applications; Local Dynamic Map (LDM)," *ETSI EN 302 895 (V1.1.0)*, 2014.

[65] M. Fanaei, A. Tahmasbi-Sarvestani, Y. P. Fallah, G. Bansal, M. C. Valenti, and J. B. Kenney, "Adaptive content control for communication amongst cooperative automated vehicles," in *2014 IEEE 6th International Symposium on Wireless Vehicular Communications (WiVeC 2014)*, Sept 2014, pp. 1–7.

[66] Y. P. Fallah, C. Huang, R. Sengupta, and H. Krishnan, "Analysis of Information Dissemination in Vehicular Ad-Hoc Networks With Application to Cooperative Vehicle Safety Systems," *IEEE Transactions on Vehicular Technology*, vol. 60, no. 1, pp. 233–247, Jan 2011.

[67] Y. Fallah, C. Huang, R. Sengupta, and H. Krishnan, "Congestion Control Based on Channel Occupancy in Vehicular Broadcast Networks," in *2010 IEEE 72nd Vehicular Technology Conference - Fall*, Sept 2010, pp. 1–5.

[68] (2018) The ns-3 Network Simulator. [Online]. Available: http://www.nsnam.org

[69] "IEEE Standard for Information technology–Telecommunications and information exchange between systems Local and metropolitan area networks–Specific requirements Part 11: Wireless LAN Medium Access Control (MAC) and Physical Layer (PHY) Specifications," *IEEE Std 802.11-2012 (Revision of IEEE Std 802.11-2007)*, pp. 1–2793, March 2012.

[70] "Interoperability Issues of Vehicle-to-Vehicle Based Safety System Project (V2V-Interoperability) Phase 2 Final Report Volume 1 – Communications Scalability for V2V Safety Development," *CAMP Vehicle Safety Communications 3*, February 2012.

[71] J. Lee, W. Kim, S.-J. Lee, D. Jo, J. Ryu, T. Kwon, and Y. Choi, "An Experimental Study on the Capture Effect in 802.11a Networks," in *Proceedings of the Second ACM International Workshop on Wireless Network Testbeds, Experimental Evaluation and Characterization*, ser. WinTECH '07. New York, NY, USA: ACM, 2007, pp. 19–26. [Online]. Available: http://doi.acm.org/10.1145/1287767.1287772

[72] " Caltrans Performance Measurement System," http://pems.dot.ca.gov/, accessed: 2018-09-10.

[73] "Interoperability Issues of Vehicle-to-Vehicle Based Safety System Project (V2V-Interoperability) Phase 2 Final Report Volume 1 – Communications Scalability for V2V Safety Development," *CAMP Vehicle Safety Communications 3*, February 2012.

[74] C. Sommer, S. Joerer, and F. Dressler, "On the applicability of Two-Ray path loss models for vehicular network simulation," in *2012 IEEE Vehicular Networking Conference (VNC)*, Nov 2012, pp. 64–69.

[75] C. Sommer and F. Dressler, "Using the right two-ray model? A measurement based evaluation of PHY models in VANETs," in *2011 ACM MobiCom*, 2011.

[76] L. G. Kraft, "A device for quantizing, grouping, and coding amplitude-modulated pulses," Ph.D. dissertation, Massachusetts Institute of Technology. Dept. of Electrical Engineering, 1949.

[77] S. M. O. Gani, Y. P. Fallah, and S. A. Ahmad, "Identifying DSRC Channel Loss Factors of Urban Intersections using RSS Datasets," in *2018 IEEE Connected Automated Vehicles Symposium*, August 2018, (in press).

[78] S. M. O. Gani, A. Tahmasbi-Sarvestani, M. Fanaei, and Y. P. Fallah, "High fidelity DSRC receiver model for ns-3 simulation using large-scale field data," in *2016 IEEE Wireless Communications and Networking Conference*, April 2016, pp. 1–6.

[79] Y. P. Fallah and S. M. Osman Gani, *Efficient and High Fidelity DSRC Simulation*. Cham: Springer International Publishing, 2019, pp. 217–243. [Online]. Available: https://doi.org/10.1007/978-3-319-94785-3_9

[80] D. Krajzewicz, J. Erdmann, M. Behrisch, and L. Bieker, "Recent Development and Applications of SUMO - Simulation of Urban MObility," *International Journal On Advances in Systems and Measurements*, vol. 5, no. 3&4, pp. 128–138, December 2012.

[81] G. Bansal, H. Lu, J. B. Kenney, and C. Poellabauer, "EMBARC: Error Model Based Adaptive Rate Control for Vehicle-to-vehicle Communications," in *Proceeding of the Tenth ACM International Workshop on Vehicular Inter-networking, Systems, and Applications*, ser. VANET '13. New York, NY, USA: ACM, 2013, pp. 41–50. [Online]. Available: http://doi.acm.org/10.1145/2482967.2482972

[82] J. Harding, G. Powell, R. Yoon, J. Fikentscher, C. Doyle, D. Sade, M. Lukuc, J. Simons, and J. Wang, "Vehicle-to-vehicle communications: Readiness of V2V technology for application. (Report No. DOT HS 812 014)," *National Highway Traffic Safety Administration*, August 2014.

[83] J. Chang, "Summary of NHTSA Heavy-Vehicle Vehicle-to-Vehicle Safety Communications Research (Report No. DOT HS 812 300)," *National Highway Traffic Safety Administration*, July 2016.